2014 R&D 100

Oak Ridge National Laboratory

CIRFT
Cyclic Integrated Reversible-Bending Fatigue Tester

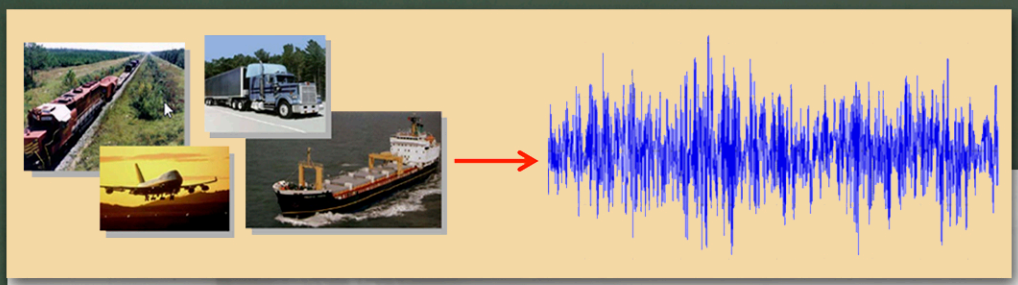

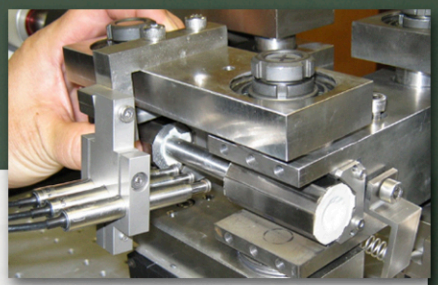

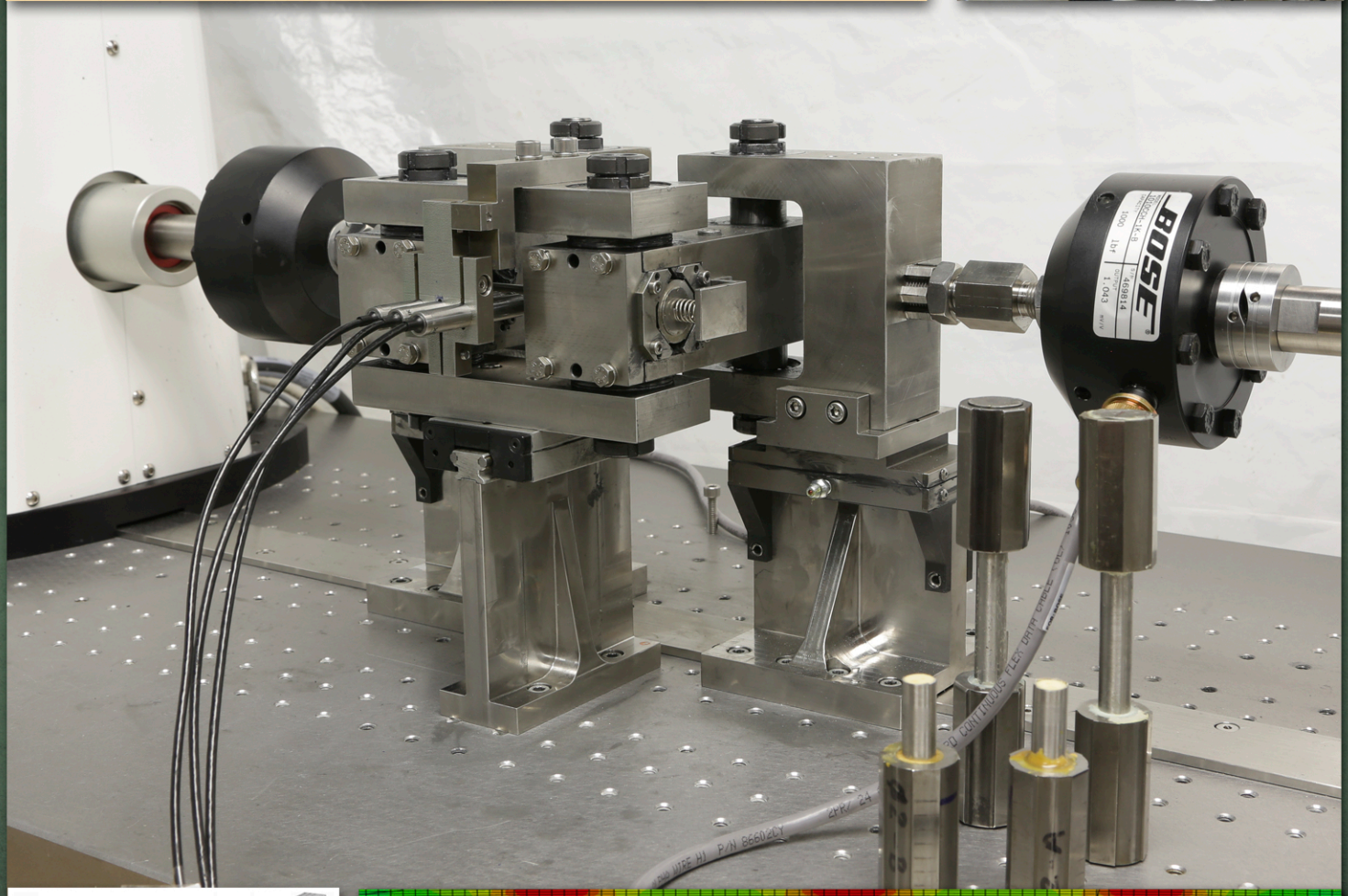

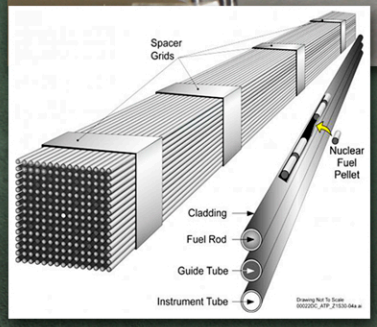

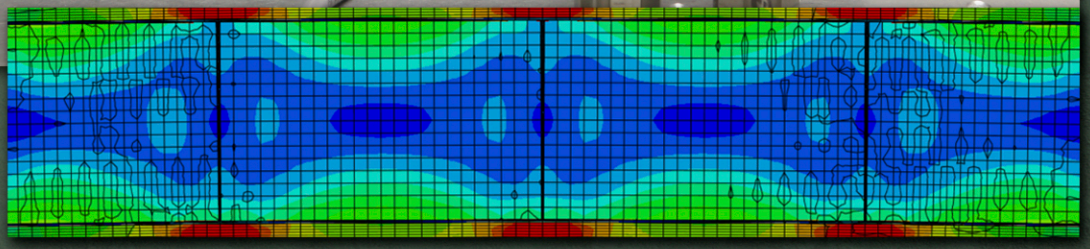

BOSE®

Oak Ridge National Laboratory

ORNL 2014-G00189/tcc

2014 R&D 100 AWARDS ENTRY FORM
OAK RIDGE NATIONAL LABORATORY

1. ORGANIZATION CONTACT INFORMATION

A. Submitter Information

Organization:	**Oak Ridge National Laboratory***
Contact:	**Thom Mason, Director**
Address:	P.O. Box 2008
City/State:	Oak Ridge, TN
Zip Code:	37831-6255
Country:	USA
Phone:	865-576-2900
Fax:	865-241-2967
Email:	masont@ornl.gov
Web URL:	http://www.ornl.gov

Relationship to product being submitted: **Product developer**

(Marketing and media contacts are listed in Appendix B.)

B. Developer Organization Information

Organization:	**Oak Ridge National Laboratory (ORNL)**
Role:	Principal developer organization
Address:	P.O. Box 2008
City:	Oak Ridge
State:	TN
Zip/Postal:	37831-6255
Country:	USA
Web URL:	http://www.ornl.gov
Contact Name:	**Thom Mason, Director**
Phone:	865-576-2900
Fax:	865-241-2967
Email:	masont@ornl.gov

*Research sponsored by the U.S. Department of Energy and performed at Oak Ridge National Laboratory, managed by UT-Battelle, LLC, for the U.S. Department of Energy under contract DE-AC05-00OR22725. The submitted manuscript has been authored by a contractor of the U.S. government under contract No. DE-AC05-00OR22725. Accordingly, the U.S. government retains a nonexclusive, royalty-free license to publish or reproduce the published form of this contribution, or allow others to do so, for U.S. government purposes.

Organization:	**Bose Corporation, ElectroForce Systems Group**
Role:	Supporting developer organization
Address:	10250 Valley View Road, Suite 113
City:	Eden Prairie
State:	MN
Zip/Postal:	55344
Country:	USA
Web URL:	www.bose-electroforce.com
Contact Name:	**Ed Moriarty, General Manager**
Phone:	952-278-3042
Fax:	952-278-3071
Email:	ed_moriarty@bose.com

C. Principal/primary investigator, developer, inventor, or team leader

Name:	**Jy-An John Wang**
Title:	**Distinguished R&D Staff**
Organization:	**Oak Ridge National Laboratory**
Address:	1 Bethel Valley Road
City/State:	Oak Ridge, TN
Zip/Postal:	37831-6069
Country:	USA
Phone:	865-574-2274
Fax:	865-574-6098
Email:	wangja@ornl.gov

(All team members are listed in Appendix A.)

2. PRODUCT INFORMATION

A. Product brand name

Cyclic Integrated Reversible-Bending Fatigue Tester (CIRFT)

B. Generic description of product

The Cyclic Integrated Reversible-Bending Fatigue Tester (CIRFT) can be used for investigating the vibration integrity of spent nuclear fuel during transportation.

C. Product photos

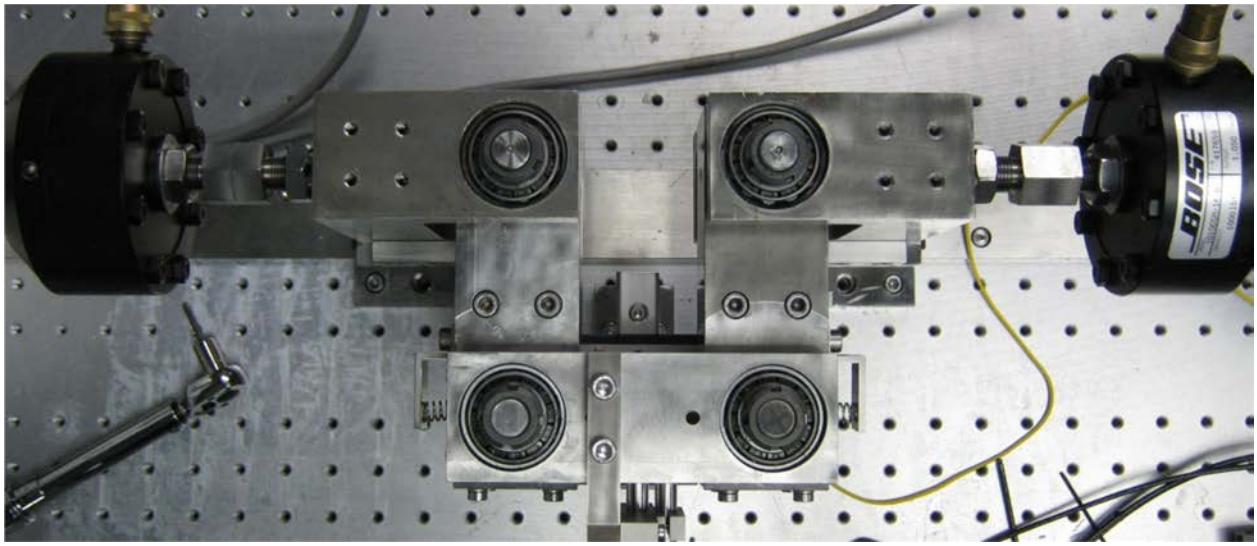

Top view of the CIRFT system's U-frame setup.

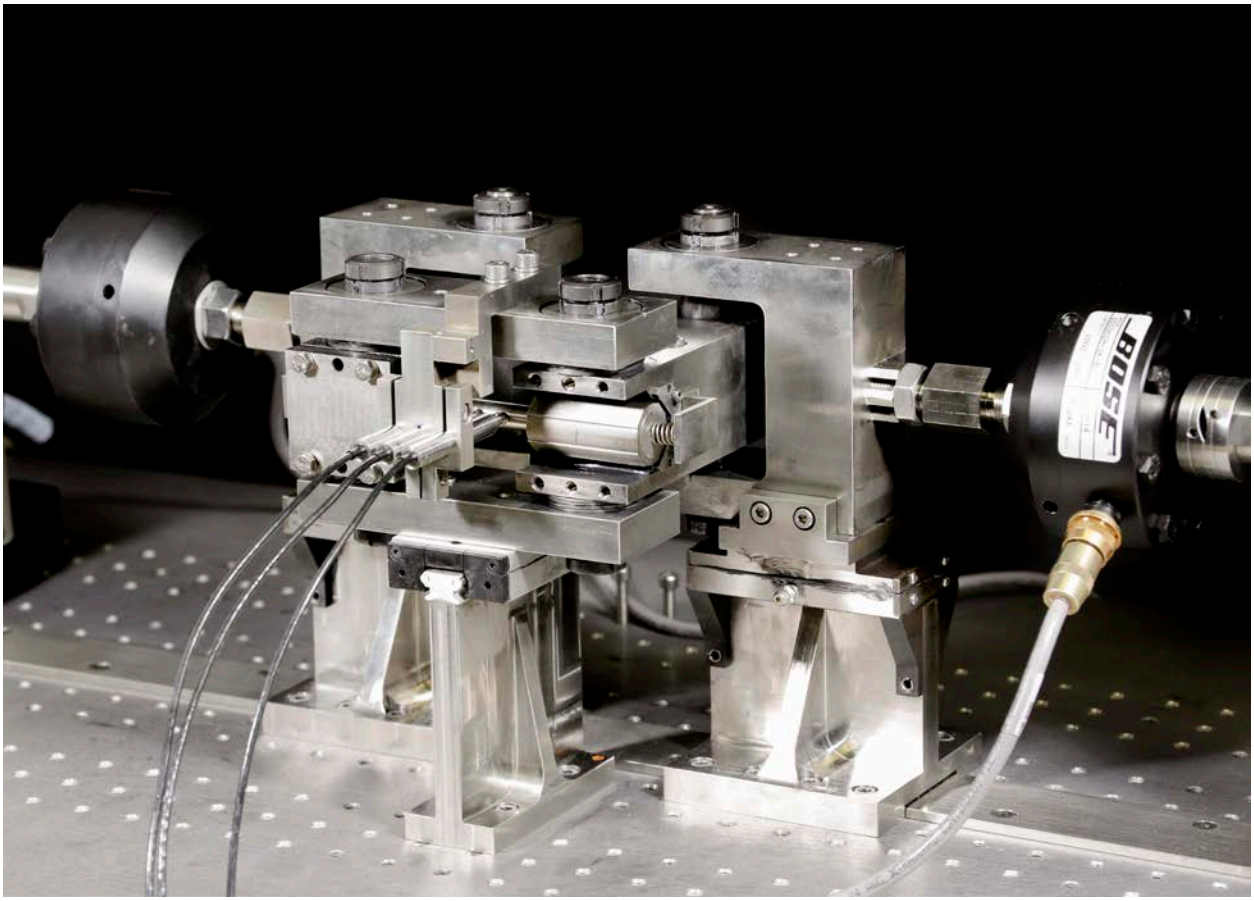

Frontal view of the CIRFT system.

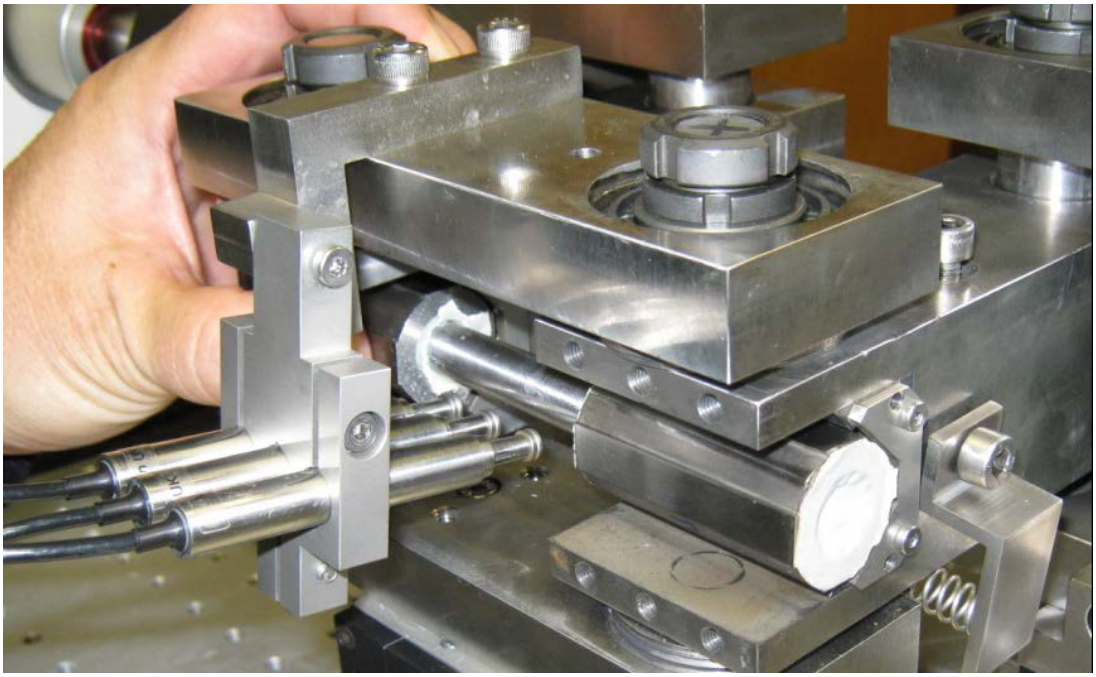

Frontal view of the end-grip section of CIRFT showing a rod sample equipped with a rigid sleeve and three linear variable displacement transducers (LVDTs) for measuring rod deflection at three points.

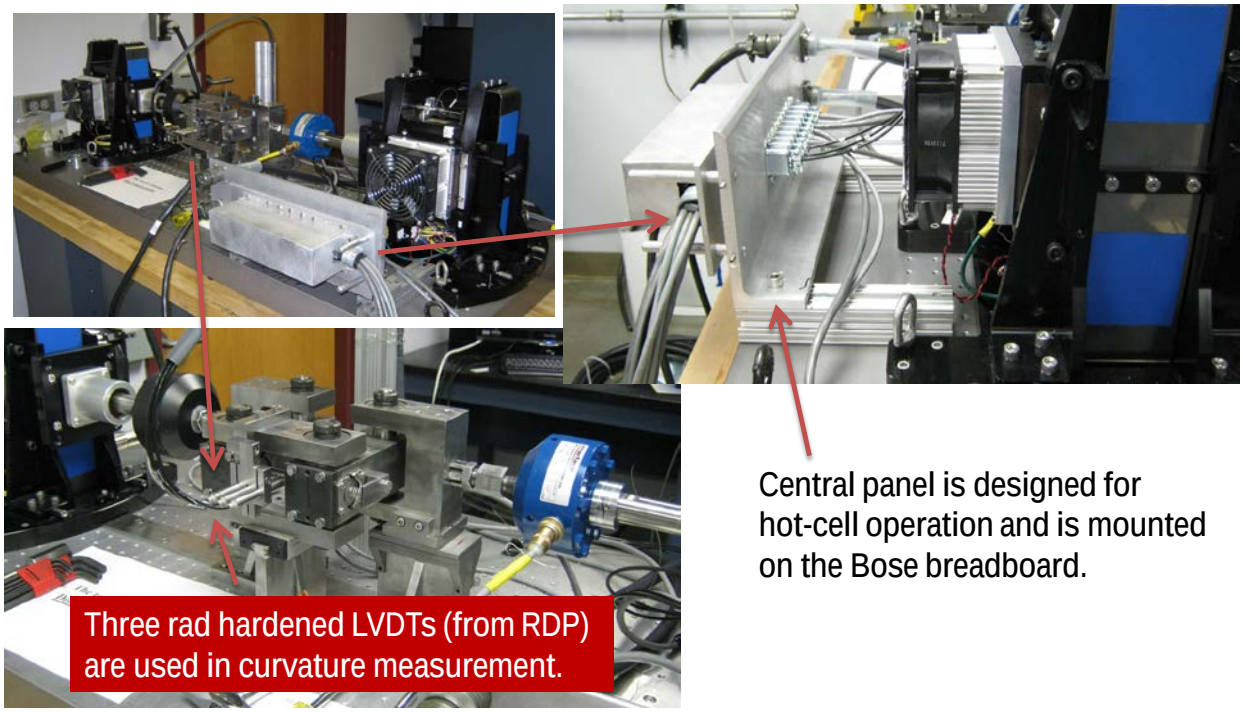

(Upper left) **CIRFT with a Bose dual linear motor, U-frame setup, and central panel installed on a test bench.** ***(Upper right)*** **A rear view of the central panel.** ***(Lower left)*** **Enlargement of the U-frame setup showing LVDTs (RDP Electrosense, Pottstown, PA).**

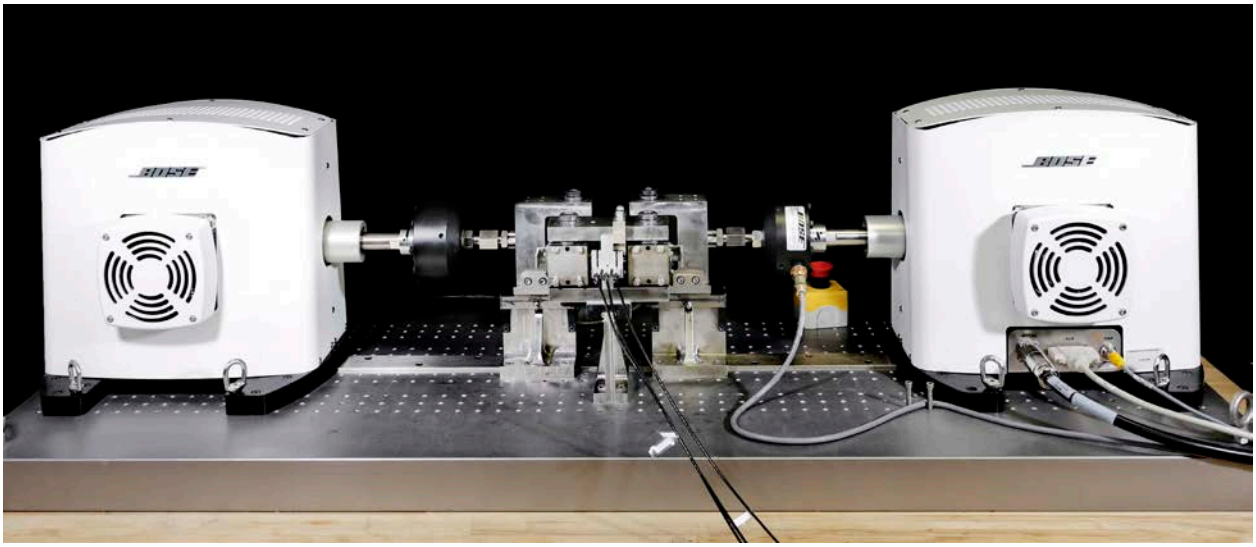

Integrated CIRFT system before installation into the hot cell.

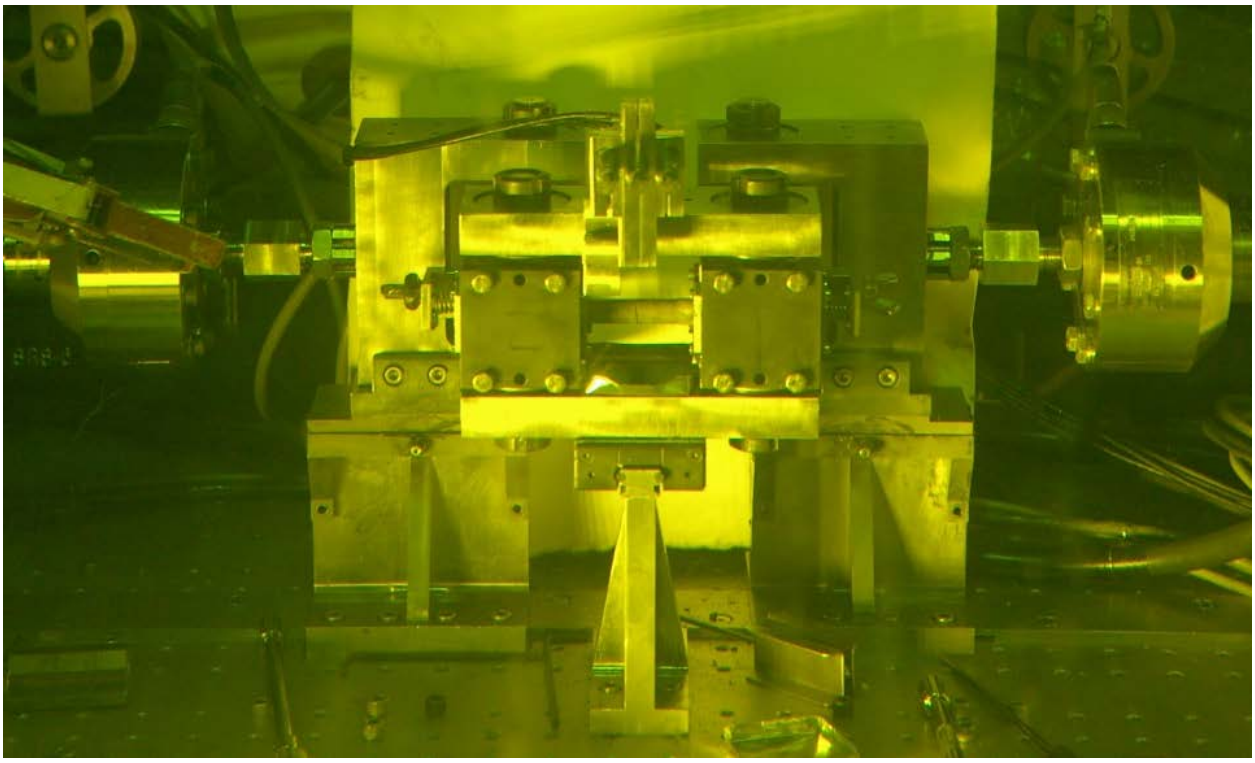

Frontal view of CIRFT with an installed nuclear fuel rod in the ORNL hot cell.

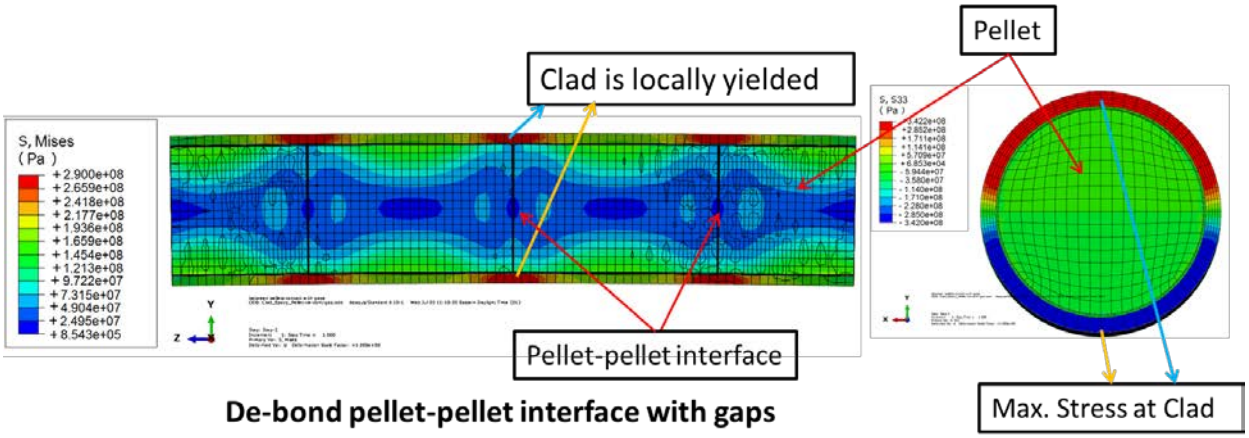

De-bond pellet-pellet interface with gaps

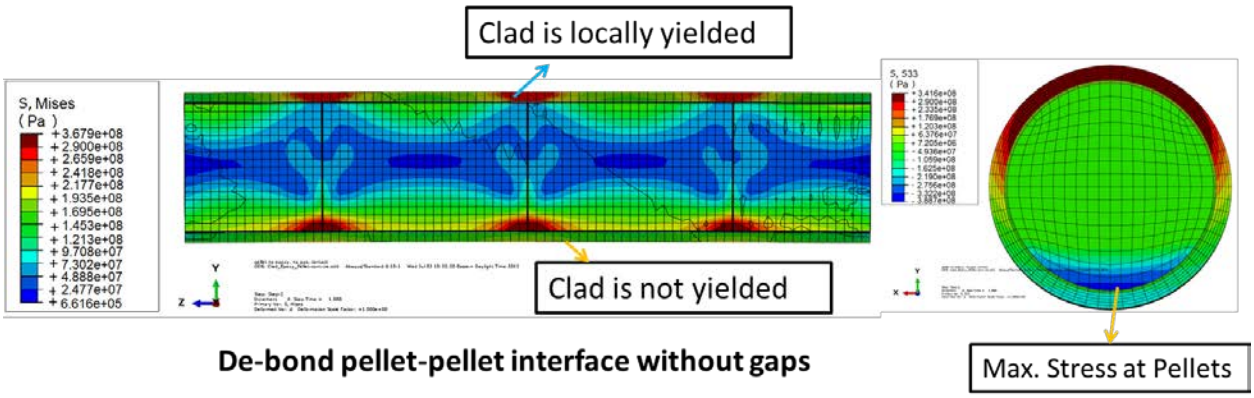

De-bond pellet-pellet interface without gaps

The importance of pellet–pellet interface bonding efficiency to pellet–clad system vibration integrity was discovered by CIRFT testing. An in-house developed finite element code, CIRFT-PCBE, was used to further quantify the flexural rigidity variation because of pellet–pellet–clad interface bonding efficiency. The bending stress distribution profiles in a pellet–clad composite system obtained from CIRFT-PCBE code were demonstrated in the above two figures.

Three views of the uniquely designed grip-end for use in a hot cell.

3. EXECUTIVE SUMMARY

CIRFT enables the vibration integrity of spent nuclear fuel (SNF) during transportation to be investigated. The first CIRFT system was installed and operated in an ORNL hot cell in August 2013. The tester includes a U-shaped loading frame developed by ORNL and a dual linear-motor Bose® ElectroForce® TestBench Test Instrument. The SNF rod specimen is installed and integrated into the U-frame through specially designed specimen grips; a setup of three displacement transducers measures rod deformation or curvature. This invention can test SNF rods and other materials under reversible bending in both static and dynamic loading conditions. For the first time, the nuclear industry and nuclear regulatory bodies can test and evaluate the mechanical properties of SNF rods in a simulated transportation environment. Such information is vital to the nuclear industry's success in dealing with issues related to the back end of the nuclear fuel cycle and high-radiation-level waste management.

4. INTRODUCTION DATE

The first CIRFT was delivered to the ORNL hot cell on August 19, 2013.

5. PREVIOUS R&D 100 ENTRY

No.

6. PRICE

Product price in US dollars: $300K.

7. PATENTS

A patent for a “Reversal Bending Fatigue Testing” was filed on February 14, 2012, and the application number is 13/396,413. One of the draft patent figures is shown below.

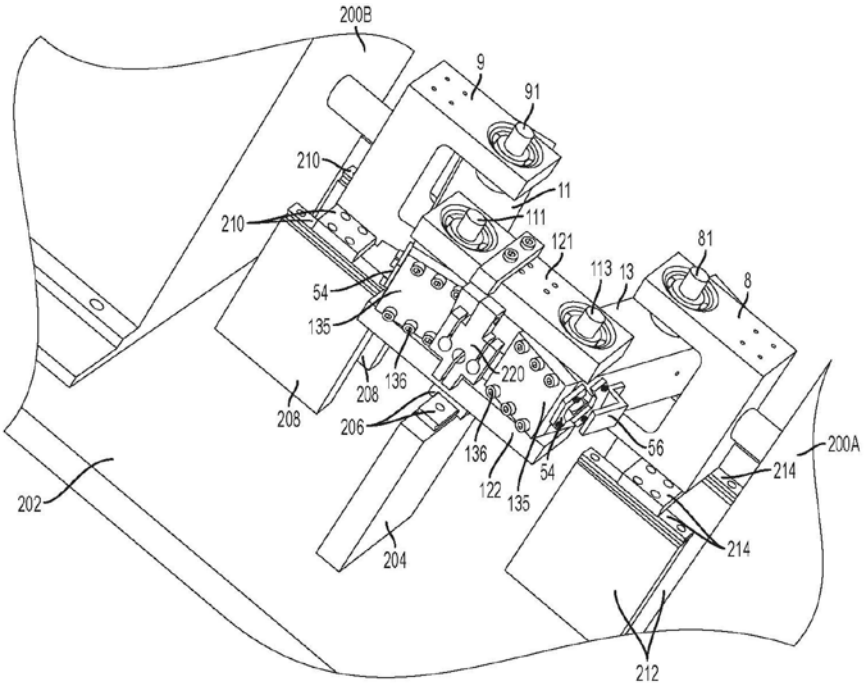

8. PRODUCT DESCRIPTION

A. What it does

No test system has existed to evaluate fatigue in SNF during expected normal conditions of transportation (NCT), although international efforts to develop a system have been ongoing. Using a design that bears no resemblance to conventional methods, CIRFT provides a unique,

robust approach to enable the free-fixed boundary conditions that allow for unconstrained axial movement of fueled specimens during fatigue testing, resulting in a realistic SNF vibration simulation. Because the entire SNF system is used, vital fuel and clad interaction information can be extracted from the results to aid in understanding the effects of fuel pellet and clad interface bonding on SNF system integrity during transport.

CIRFT provides the following:

1. **Testing and characterization of the mechanical response of SNF rods in quasi-static loading conditions.** The dual linear motor (model LM2) test bench has a maximum load capacity of ±3,000 N and a maximum stroke of ±25.6 mm. Bending is imposed through a U-frame with dual driving points and a 101.60 mm loading arm. Rod specimen curvature deformation is measured through three linear variable displacement transducers (LVDTs). A segment of SNF rod is tested. The rod specimen is 152.40 mm long and 9.70–11.74 mm in diameter with a gage section of 50.80 mm. CIRFT can define a rod's failure moment.
2. **Testing and characterization of the dynamic cyclic fatigue response of SNF rods under reversible bending conditions.** CIRFT can deliver dynamic loading to a rod specimen in the load-control mode at 5 to 10 Hz. Online monitoring can capture mechanical property changes to reveal fatigue behavior during testing.
3. **Testing and measurement of the lifetime of SNF rods under simulated transportation conditions.** CIRFT's driving system uses a roller-bearing-based specimen-grip design and electromagnetic force-based Bose linear motors. Hot cell tests have shown that CIRFT is reliable and capable of fatigue testing at both high loads and high cycles (10^3–10^7 cycles). The curve relating stress (S) to cycles to failure (N) (i.e., the S-N curve) and the fatigue limits of SNF rods can be determined. The generated S-N curve (including the estimate material properties) will be the major input to allow evaluation of the SNF's vibration integrity during transportation.

B. Principal applications

CIRFT resolves issues associated with nuclear fuel assembly integrity as a result of transport-induced vibration and assists with transportation system structural design to maintain SNF integrity during transportation.

Spent nuclear fuel rod vibration integrity is particularly important for high-burnup fuel (i.e., fuel utilization > 45 gigawatt days per metric ton of uranium). As the fuel irradiation (burnup) in a reactor increases, changes to the clad and fuel structural characteristics can affect subsequent performance of the fuel and cladding during storage and transportation. These changes include formation of a high-burnup structure at the surface of the fuel pellets and increases in cladding corrosion layer thickness, cladding hydrogen content, cladding creep strains, and fission gas release. When the hydrogen concentration exceeds the solubility limit, zirconium hydrides form. Depending on size, distribution, and orientation, these hydrides can embrittle the cladding and

reduce ductility. Furthermore, the presence of hydrides can facilitate cracking if the hydrides are perpendicular to the tensile stress field. Hydride reorientation and diffusion can result in cracked cladding that must be evaluated to determine clad failure risk during normal handling or transportation.

The CIRFT test equipment fills a critical technical gap in testing systems by providing spent fuel owners and regulators with a significantly simplified technique to test the SNF rod directly, rather than test material substitutes and extrapolate results. CIRFT test results will provide the most direct and applicable data possible to enhance the knowledge base to support safe SNF transportation.

C. Market benefits

Because of its high heat load and radioactivity, SNF is initially stored in water-filled pools for several years for cooling and shielding. As these storage pools reach capacity, SNF assemblies are placed into long-term dry cask storage. The ability of structures, systems, and components to meet long-term safety criteria and applicable safety functions when SNF is transported to its final location must be determined. To facilitate disposition and maintain retrievability during expected back-end fuel disposal operations, researchers must understand the likelihood of SNF remaining undamaged after storage and transportation.

Transportation packages for spent fuel must meet federal safety requirements under normal and accident conditions. For normal conditions, including vibration loads incident to transport, the licensee must ensure that there will be no loss or dispersal of spent fuel, no significant increase in external surface radiation levels, and no substantial reduction in effectiveness of the spent fuel package. The completed structural evaluation of a spent fuel package requires data on spent fuel's vibration behavior.

Through 2012, it is estimated that the commercial nuclear industry will have generated approximately 70,000 MTU of spent fuel contained in about 245,000 assemblies (140,000 from boiling-water reactors and 105,000 from pressurized-water reactors) (Carter et al. 2012). According to data collected by Ux Consulting, as of September 2012 a total of 65,261 assemblies were being stored in 1,650 casks, with approximately 73% of the total fuel inventory discharged remaining in wet storage (UxC 2011). It is projected that by 2020, total SNF discharges will be approximately 88,000 MTU (Carter et al. 2012). Roughly 35,000 metric tons of heavy metal (MTHM) of that is expected to be in dry storage by that time with the remaining 53,000 MTHM in the reactor pools. By law, spent fuel transportation packages must pass structural testing and evaluation under normal and accident conditions to ensure that the cask and contents can travel safely. At the same time, spent fuels have potential damage from in-reactor processes and are susceptible to damage from transport loading. CIRFT can effectively test and characterize the dynamic response of fuel rods during NCT and will attract interest from national and international organizations in the field of SNF regulation, management, and disposal.

D. Other applications for which CIRFT can now be used

1. **Fatigue testing in reversible pure bending.** Conventional three- and four-point bending tests are not appropriate for pure bending applications that exclude shear stress (e.g., composites and ceramics). These tests are usually conducted with a simple (instead of free-fixed) support and unidirectional bending. CIRFT induces reversible pure bending to the specimen and provides robust protection for the test sample at the grip ends. The driving system, a Bose dual LM2, can deliver ±25.4 mm linear displacement. The flexible applied curvature can be designed on the basis of loading arm and gage length.
2. **Custom cyclic fatigue testing.** In conventional reversible bending tests, an AC motor is used with a complicated crank and transmission system with limited frequency and cycles. Testing using that type of design is severely constrained in a hot cell environment. CIRFT, however, can work from very low frequencies to potentially 100 Hz.
3. **Bending fatigue testing under special environments.** Although designed for the hot cell environment, the CIRFT can be used in an environmental chamber for temperature studies.

9. TECHNOLOGY DESCRIPTION

A. How CIRFT operates

CIRFT features a U-frame testing setup with two rigid arms, connecting plates, and universal testing machine links. The rod specimen is coupled to the rigid arms through two specially designed grips. The U-frame setup is oriented in a horizontal plane and is driven by electromagnetic-force-based Bose dual linear motors. With help from the coupling, linear motions applied at the loading points of the rigid arms are converted into bending moments exerted to the rod. Under a pair of forces or displacements that are facing off, the rigid arms are opened, and bending moments force the rod to deflect outward. Under a pair of forces facing each other, the rigid arms are closed, forcing the rod to deflect inward. Three LVDTs measure rod deflections at three neighboring points to estimate rod curvature, which is then correlated to the applied moment to characterize the mechanical property of the bending rod. In a hot cell test, installation of a rod specimen involves removing the end blocks, inserting the rod, and closing and tightening the end blocks. Specimen detachment involves the reverse process of loosening the end blocks and removing the tested rod.

B. Scientific theory behind CIRFT

Both rigid and hinged joints are available between the rigid arms and connecting plates. Rigid joint connecting plates serve as a flexure subjected to axial loading and bending. External bending is shared between the rod and the flexure, depending on the flexural rigidities. However, rigid joints are subjected to yielding, which converts the rigid joint into a plastic hinge joint.

Theoretical examination shows that usable rotation at the rod holding area is limited by θ_p, which is given by

$$\theta_p = \frac{\sigma_y}{E}\frac{L_V}{h}$$

where σ_y = yielding stress, E = Young's modulus, L_v = gage length, and h = thickness (diameter) of the rod. The bending moment M is defined by the product of point load P and loading arm L, or

$$M = PL\,.$$

Finite element analysis (FEA) was used to study the arrangement of a rod specimen within offset and coplanar U-frame designs. A 152.4 mm long rod specimen was considered. Two sizes of rigid arms were studied: 50.8 × 50.8 × 266.7 mm for the offset design and 50.8 × 50.8 × 203.2 mm for the coplanar design. Both have a 50.8 × 50.8 mm beam section with the required rigidity and secondary loading arms for converting external force couples into bending moments. Side plates are the same length as the rod. A gage length of 50.80 mm is obtained when the rod is inserted into the CIRFT in a test configuration. At a load of 178 N, the maximum stresses in pellet and cladding change from 20 and 11 MPa in the offset design to 210 and 117 MPa in a coplanar design, respectively. Enhancing the stresses shows that the coplanar design was more efficient than the offset design in converting external loads into rod stresses. Thus, the coplanar design was adopted.

Also studied with FEA were the effects of design aspects on U-frame setup performance. A vertical U-frame setup subjects the rod to deformation because of component weights (gravitational effects) and necessitates the use of counterweights. Conversely, a horizontal U-frame setup design eliminates the effect of test equipment weight on test rod deformation. The FEA study suggested that reducing the load arms from 152.40 mm to 101.6 mm could shift the resonant frequency from 2.56 Hz to 4.19 Hz, which drastically improved the setup response at high frequency. Therefore, a horizontal U-frame with 101.6 mm load arm length is used in CIRFT.

C. Building blocks of the technology

CIRFT features a U-frame testing setup with two rigid arms, connecting plates, and linkages to a universal testing machine. The rigid arm joints and connecting plates are designed as hinges with precision bearings. The rod specimen (diameter 9.7–11.74 mm and length 152.40 mm) is coupled to the rigid arms through two specially designed grips. Half of each grip body uses a modified V-shaped end face on the rigid arm; the other half uses a modified V-shaped surface on the movable end block. Four linear roller bearing sets are embedded in each grip to enable free

longitudinal movement of the specimen. The specimen is engaged with each grip through a 50.80 mm long octagonal rigid sleeve. Installation involves closing and bolting the two end blocks in place. Preloading to eliminate backlash during reversible bending is applied by tightening the bolts with a torque wrench to 10 lb-in. With help from the coupling, the linear motions applied at the loading points of the rigid arms are converted into bending moments exerted directly to the rod. The linear roller bearing sets embedded in the grips serve as load-transferring elements of the bending moments and enable free axial motion of the rod. The stainless steel U-frame setup is suitable for a hot cell environment.

Set in a horizontal plane, the U-frame setup is driven by electromagnetic force-based Bose dual linear motors that can load the setup symmetrically. The setup is integrated into the Bose test bench through two interfaces. A turnbuckle in the first interface on each side of the test bench connects the U-shaped beam of the setup to the load cell. The second interface involves the connection between the U-frame components to the test bench. Two stands equipped with roller bearing sets underneath the two U-shaped beams support two rigid arms. Another stand with a straight rail is set underneath the connecting plate perpendicular to the two stands.

The CIRFT system has both displacement control and load control modes for reversible bending fatigue testing; load control is preferred. A symmetrical loading is achieved when the dual motors are synchronized. The maximum dynamic displacement and load ranges are ±25.4 mm and ±3,000 N. Three LVDTs measure the deflections of the rod at three neighboring points on the test rod to calculate curvature. A sensor clamp with alternating openings holds the LVDTs parallel and mounted to one of the connecting plates to ensure measurements free of rigid motions. The deformation of a bending rod can be monitored or measured at specified points during bending fatigue testing. The acquisition of bending moments and curvatures provides a basis for characterizing the rod's mechanical properties.

10. PRODUCT COMPARISON

A. Competitors by manufacturer, brand name, and model number

1. Servo-hydraulic four-point bending tester, MTS Landmark 370.10 (force, 25 kN; stroke, 150 mm)
2. Electromechanical four-point bending tester, such as MTS and Instron testers.
3. Electromagnetic four-point bending tester, Bose ElectroForce 3520 (±7500 N, ±25.4 mm); Instron ElectroPuls E3000 (±3000 N, ±30.0 mm)
4. IPC four-point bending fatigue tester
5. Composite four-point bending fatigue tester (O'Brien, T. K., A. D. Chawan, R. Krueger, and I. L. Paris. 2002. Int. J. Fatigue 24 127–145.)
6. Self-aligning four-point bending fatigue tester (Zhai, T., Y. G. Xu, J. W. Martin, A. J. Wilkinson, and G. A. D. Briggs. 1999. Int. J. Fatigue 21 889–894.)

7. Roller joint-based plate four-point bending fixture (Bertele, L., A. Papack, and K.-H. Wichmann. 1993. “Testing Device for Performing Four Point Fatigue Strength Tests under Alternating Bending Stresses.” US Patent 5231882.)
8. Flexure-based four-point bending fatigue fixture (Bowman, W. D. 1989. “End Constraint and Alignment Effects in Three and Four Point Tension-Compression Bending Tests.” In Factors that Affect the Precision of Mechanical Tests, ed. R. Papirno and H. C. Weiss. ASTM STP 1025, ASTM, Philadelphia. 174–184.)
9. Rigid sleeve-based pure bending fixture (Zineb, T. B., A. Sedrakian, and J. L. Billoet. 2003. Compos. B: Eng. 34, 447–458.)
10. Forrest–Penfold bending fatigue tester (Forrest, P. G., and A. B. Penfold. 1961. Engineering (London) 192, 522–523.)

B. Comparison to existing products or technologies

Name	Boundary condition	Pure bending	Reversible bending	Working frequency	System size	Adaptable to hot cell
CIRFT	Free-fixed (i.e., free axial rod motion and fixed transverse rod motion	Yes	Yes, with full scale of tension to compression	High. 5–10 Hz range has been demonstrated. The driving system can deliver a constant response to 40 Hz, which provides room for improvement	Compact desktop test bench can be handled easily	Yes. Specimen installation is simple with the U-frame. Electromagnetic force-based motors are reliable and friendly for hot cell operation
Servo-hydraulic four-point bending tester	Simply supported; can be used only for unidirectional bending	No	No	The working frequency is inherently limited because of hydraulic driving	The system is generally bulky and cannot easily be installed into the hot cell	No. The hydraulic components are susceptible to radiation-induced degradation, especially in nuclear fuel testing. Oil leakage can be problematic in the hot cell. Specimen installation is difficult
Electromechanical four-point bending tester	Simply supported	No	No	Intensive wear occurs owing to mechanical contact between the screw and nut. Usable frequency is low	Large	No. Specimen installation is difficult; loading rate is slow, making dynamic fatigue testing difficult
Electromagnetic four-point bending tester	Simply supported	No	No	High	Generally too large to fit into the hot cell	No. Specimen installation is difficult
IPC four-point bending fatigue tester	Simply supported	No	No	High	Large	No. Specimen installation is not feasible

Name	Boundary condition	Pure bending	Reversible bending	Working frequency	System size	Adaptable to hot cell
Composite four-point bending fatigue tester	Simply supported	No	No	High	Large	No. Fixture is driven by a servo-hydraulic machine that is hard to maintain. Specimen installation is not feasible
Self-aligning four-point bending fatigue tester	Simply supported	No	No	High	Large	No. Fixture is driven by a servo-hydraulic machine that is hard to maintain. Specimen installation is not feasible
Roller joint-based plate four-point bending fixture	Free-fixed	No	Yes	High	Not available	No. Specimen installation is not feasible
Flexure-based four-point bending fatigue fixture	Free-fixed	No	Yes	High	Large	No. Specimen installation is not feasible
Rigid sleeve-based pure bending fixture	Simply supported	Yes	No	High	Large	No. Specimen installation is not feasible
Forrest–Penfold bending fatigue tester	Free-fixed	Yes	Yes	Complex crank and linkage are used. Usable frequency is low	Large	No. Specimen installation is not feasible

C. Benefits of CIRFT over the competitors

1. The overall system is quite small compared to conventional testers, so it is easy to install and maintain during hot cell testing.
2. A rod specimen can be installed simply by inserting it into the specimen grips and tightening the grips. A conventional point-bending tester involves complicated specimen installation and alignment operations that are not feasible or user-friendly for hot cell testing. Misalignment in the point bending testers makes replication of results difficult.
3. The CIRFT is designed for cyclic pure bending, the loading condition that dominates the response of SNF rods in the transportation environment. The majority of conventional testers adopt three-point and four-point bending that subjects a large part of a specimen to shearing forces, which may result in a failure not representative of the target failure mode. The robust CIRFT test mechanism ensures its test results reproducibility.
4. The embedded and preloaded linear roller bearing sets enable free axial movement and eliminate the backlash existing in conventional reversible bending. Both free axial movement and restraint in transverse rod movement at the grips are essential requirements of free-fixed boundary conditions in reversible pure bending for the target cyclic fatigue and are effectively implemented in the CIRFT. Most conventional testers either involve shear stress or lack the mechanism for free-fixed bending and so cannot achieve a reversible pure bending testing condition.
5. Linkages to a universal machine have been minimized. Only two linkages are needed (at the two loading points of the U-frame setup), whereas a conventional three- or four-point bending demands at least three linkages.
6. Electromagnetic force-based dual linear motors are used to drive the test setup. They are more reliable and more user friendly when conducting hot cell tests than a conventional servo-hydraulic or electromechanical tester. The dual motor configuration ensures symmetrical loading on the U-frame setup at medium and high frequencies, where the two synchronized motors drive the two arms of the U-frame under identical parameters but in opposite directions.
7. The curvature measurement is enabled and immune to the effects of compliant layers and rigid body motion in the machine. Curvature measurement is usually unavailable in conventional point bending testing. The LVDT technique is robust in a hot cell environment and is free from the restraints related to noncontact measurements.
8. A uniquely developed in-house finite element code, CIRFT-PCBE, can be used effectively to investigate the dynamic interaction of nuclear fuel pellet and clad at pellet-pellet interface regions and to estimate the associated effective lifetime of SNF under transport.

D. Limitations of CIRFT

The available displacement range depends on the linear motors adopted.

11. SUMMARY

Spent nuclear fuel (SNF) from reactors around the world must be transported as part of its eventual disposal, and the cyclic integrated reversible-bending fatigue tester (CIRFT) is the first machine to test and characterize in a hot cell the mechanical properties of the fuel/clad system for the expected normal conditions of transport (NCT). Nuclear industries and regulatory bodies can for the first time evaluate and understand SNF vibration integrity during transportation. The knowledge gained from SNF dynamic reliability evaluation can also be used to improve SNF transport system performance.

Although mechanical properties of high-burnup fuel cladding have been studied, no system has been developed to effectively investigate the mechanical properties of the cladding and the fuel as a single unit under the reversible bending conditions expected under NCT. A bending fatigue test is used to test and characterize various engineering materials and their components (e.g., concrete, composites, ceramics, and metal alloys). However, these conventional test methods cannot fulfill SNF testing requirements in addition to exerting the forces expected during NCT.

CIRFT addresses these concerns. The system features a U-frame setup integrated with a dual Bose linear motor test bench. The U-frame setup consists of two rigid arms, connecting members, and linkages to a universal testing machine. Reverse bending on the specimen is accomplished through push-and-pull motion at the loading points of the rigid arms. Compared with previous bending fatigue testers, the CIRFT system has the following unique features:

1. The test is conducted in pure bending, unlike three- or four-point bending, where shear stress complicates the bending and makes the specimen susceptible to unwanted shear failure. Furthermore, the constraint locations in three- or four-point bending testing are prone to causing localized failures in the specimens, thus reducing its data reproducibility.
2. The bending is fully reversible, whereas most four-point tests are only applicable to unidirectional loading. Reversible bending is the target loading case to be simulated for normal conditions of SNF transportation.
3. A wide frequency range is available to a reversible bending test. The capability for a high-frequency test is critical for simulating a transportation environment where loading is dominated by ground-vehicle interaction.
4. Integrating the test setup into the testing machine in a load train involves only two linkages, whereas four-point bending involves four linkages. This reduces required alignments and improves equipment lifetime and data reliability in the long term.
5. Specimen installation is achieved simply by insertion and tightening. This simple specimen-handling process is not available in conventional three-point or four-point bending. The simplification of specimen installation and the system’s self-alignment mechanism is extremely important for hot cell testing with limited manipulator operation. These features further improve the test data reliability and reproducibility.

6. Deformation of a rod specimen is measured by the curvature obtained using three LVDTs at three points to eliminate the effect of contact at specimen-holding areas.
7. The CIRFT, a compact tabletop system, is smaller than conventional testers and is much easier to install and maintain in a hot cell environment.
8. Based on CIRFT test results, CIRFT-PCBE code can be used effectively to investigate the dynamic interaction of nuclear fuel pellet and clad at pellet–pellet interface regions and to estimate the associated effective lifetime of the SNF system under transport.

12. AFFIRMATION

By submitting this entry to *R&D Magazine,* we affirm that all information submitted as a part of, or supplemental to, this entry is a fair and accurate representation of this product. We affirm that we have read the instructions and entry notes and agree to the rules specified in those sections.

APPENDIX A: DEVELOPMENT TEAM INFORMATION

Team Member: **Jy-An John Wang**
Title: **Distinguished R&D Staff**
Organization: **Oak Ridge National Laboratory**
Address: 1 Bethel Valley Road
City/State: Oak Ridge, TN
Zip/Postal: 37831-6069
Country: USA
Phone: 865-574-2274
Fax: 865-574-6098
Email: wangja@ornl.gov

Team Member: **Ed Moriarty**
Title: **General Manager**
Organization: **Bose Corporation, ElectroForce Systems Group**
Address: 10250 Valley View Road, Suite 113
City/State: Eden Prairie, MN
Zip/Postal: 55344
Country: USA
Phone: 952-278-3042
Fax: 952-278-3071
Email: ed_moriarty@bose.com

Team Member: **Hong Wang**
Title: **R&D Staff Member**
Organization: **Oak Ridge National Laboratory**
Address: P.O. Box 2008
City/State: Oak Ridge, TN
Zip/Postal: 37831-6069
Country: USA
Phone: 865-574-5601
Fax: 865-574-6098
Email: wangh@ornl.gov

2014 R&D 100 AWARDS ENTRY FORM
OAK RIDGE NATIONAL LABORATORY

Team Member:	**Hao Jiang**
Title:	**Post-Doctoral Research Associate**
Organization:	**Oak Ridge National Laboratory**
Address:	P.O. Box 2008
City/State:	Oak Ridge, TN
Zip/Postal:	37831-6069
Country:	USA
Phone:	865-574-5712
Fax:	865-574-6098
Email:	jiangh@ornl.gov

Team Member:	**Bruce B. Bevard**
Title:	**Program Manager**
Organization:	**Oak Ridge National Laboratory**
Address:	P.O. Box 2008
City/State:	Oak Ridge, TN
Zip/Postal:	37831-6069
Country:	USA
Phone:	865-574-0279
Fax:	865-574-0382
Email:	bevardbb@ornl.gov

Team Member:	**Rob L. Howard**
Title:	**Program Manager**
Organization:	**Oak Ridge National Laboratory**
Address:	P.O. Box 2008
City/State:	Oak Ridge, TN
Zip/Postal:	37831-6069
Country:	USA
Phone:	865-241-5750
Email:	howardrl1@ornl.gov

2014 R&D 100 AWARDS ENTRY FORM
OAK RIDGE NATIONAL LABORATORY

Team Member:	**Chuck Baldwin**
Title:	**Senior R&D Staff**
Organization:	**Oak Ridge National Laboratory**
Address:	P.O. Box 2008
City/State:	Oak Ridge, TN
Zip/Postal:	37831-6295
Country:	USA
Phone:	865-574-6552
Email:	baldwinca@ornl.gov

Team Member:	**Scot Thurman**
Title:	**Hot-cell Operator**
Organization:	**Oak Ridge National Laboratory**
Address:	P.O. Box 2008
City/State:	Oak Ridge, TN
Zip/Postal:	37831-6295
Country:	USA
Phone:	865-574-7111
Email:	thurmanjs@ornl.gov

Team Member:	**Bryan Woody**
Title**:**	**Hot-cell Operator**
Organization:	**Oak Ridge National Laboratory**
Address:	P.O. Box 2008
City/State:	Oak Ridge, TN
Zip/Postal:	37831-6295
Country:	USA
Phone:	865-574-7111
Email:	woodybl@ornl.gov

Team Member:	**Tin Tan**
Title:	**Assistant Professor**
Organization:	**The University of Vermont**
Address:	Votey 215, 33 Colchester Ave.
City/State:	Burlington, VT
Zip/Postal:	05405
Country:	USA
Phone:	802-656-0067
Email:	ting.tan@uvm.edu

2014 R&D 100 AWARDS ENTRY FORM
OAK RIDGE NATIONAL LABORATORY

Team Member:	**Thomas Cox**
Title:	**Technician**
Organization:	**Oak Ridge National Laboratory**
Address:	P.O. Box 2008
City/State:	Oak Ridge, TN
Zip/Postal:	37831-6069
Country:	USA
Phone:	865-824-8048
Email:	kbit01@gmail.com

Team Member:	**Matt Thompson**
Title:	**Senior Engineer**
Organization:	**Bose Corporation, ElectroForce Systems Group**
Address:	10250 Valley View Road, Suite 113
City/State:	Eden Prairie, MN
Zip/Postal:	55344
Country:	USA
Phone:	417-581-5900
Fax:	952-278-3071
Email:	matt_thompson@bose.com

APPENDIX B: MARKETING AND MEDIA INFORMATION

1. MARKETING

Contact: **Leigha Edwards**
Title: **Community Outreach Officer**
Organization: **Oak Ridge National Laboratory**
Address: P.O. Box 2008
City/State: Oak Ridge, TN
Zip/Postal: 37831-6255
Country: USA
Phone: 865-241-9309
Fax: 865-241-2967
Email: ledwards@ornl.gov

Contact: **Lynn Kszos**
Title: **Honors & Awards program manager**
Organization: **Oak Ridge National Laboratory**
Address: P.O. Box 2008
City/State: Oak Ridge, TN
Zip/Postal: 37831-6251
Country: USA
Phone: 865-574-4784
Fax: 865-576-6183
Email: kszosla@ornl.gov

2. MEDIA

Contact: **David Keim**
Title: **Director**
Organization: **ORNL Communications**
Address: P.O. Box 2008
City/State: Oak Ridge, TN
Zip/Postal: 37831-6266
Country: USA
Phone: 865-576-9122
Fax: 865-574-0595
Email: keimdm@ornl.gov

APPENDIX C: ATTACHMENTS

1. List of Publications/Patents/Presentations (2 pages)

2. Letter of receipt for patent application (3 pages)

3. Letter of support from Ed Moriarty, General Manager, BOSE ElectroForce Systems Group, Bose Corporation (1 page)

4. Letter of support from Paul Murray, Vice President, Reactor & Fuels, AREVA Federal Services LLC (1 page)

5. Letter of support from Dr. Poh-Sang Lam, Fellow ASME, Senior Fellow Engineer, Savannah River National Laboratory (2 pages)

6. Letter of support from Dr. Holger Völzke, Head of Division 3.4 Safety of Storage Containers, BAM Federal Institute for Materials Research and Testing, Germany (2 pages)

7. Letter of support from Ken B. Sorenson, Manager, Advanced Nuclear Fuel Cycle Technologies, Sandia National Laboratories (1 page)

8. Letter of support from Michelle Flanagan, Senior Reactor Systems Engineer, US Nuclear Regulatory Commission (1 page)

9. Letter of support from Dr. Brady D. Hanson, Used Fuel Project Manager, Pacific Northwest National Laboratory (2 pages)

10. Letter of support from Dr. Jwo Pan, Professor of Mechanical Engineering, University of Michigan (1 page)

11. Letter of support from Michael C. Billone, Manager, Irradiation Performance Section, Argonne National Laboratory (1 page)

12. Letter of support from Dr. Dryver R. Huston, Professor of Mechanical Engineering, University of Vermont (1 page)

13. Fact sheet on “Cyclic Integrated Reversible-Bending Fatigue Tester (CIRFT) for Investigating Vibration Reliability of Spent Nuclear Fuel during Transportation” (2 pages)

14. Publication: H. Wang, J.-A. J. Wang, T. Tan, H. Jiang, T. S. Cox, R. L. Howard, B. B. Bevard, and M. E. Flanagan, "Development of U-frame Bending System for Studying the Vibration Integrity of Spent Nuclear Fuel," *Journal of Nuclear Materials* **440**, 201–213 (2013). (13 pages)

15. Publication: J.-A. J. Wang, H. Wang, B. B. Bevard, R. L. Howard, and M. E. Flanagan, *Reversal Bending Fatigue Test System for Investigating Vibration Integrity of Spent Nuclear Fuel during Transportation*, PATRAM 2013, DOE/NRC/DOT, San Francisco, Calif., August 18–23, 2013. (17 pages)

16. Publication: H. Jiang, J.-A. Wang, and H. Wang, "Potential Impact of Interfacial Bonding Efficiency on High-Burnup Spent Nuclear Fuel Vibration Integrity during Normal Transportation." WM2014 International Waste Management Conference, Phoenix, Ariz., March 2–6, 2014; published in the proceedings. (15 pages)

17. Publication: H. Jiang, J.-A. Wang and Hong Wang, "Reversible Bending Fatigue Testing System Design Concepts for Spent Fuel Vibration Integrity Study." ASME 2014 Pressure Vessels & Piping Conference, Anaheim, Calif., July 20N24, 2014; to be published in the proceedings. (7 pages)

Attachment 1

List of Publications/Patents/Presentations

a. J.-A. J. Wang and H. Wang, *Progress Letter Report on Reversal Bending Fatigue Testing of Zry-4 Surrogate Rod (Out-of-Cell Fatigue Testing Development–Task 2.4)*, ORNL/TM-2013/297, Oak Ridge National Laboratory, Oak Ridge, Tenn., August 2013.

b. J.-A. J. Wang, H. Wang, B. B. Bevard, R. L. Howard, and M. E. Flanagan, *Reversal Bending Fatigue Test System for Investigating Vibration Integrity of Spent Nuclear Fuel during Transportation*, PATRAM 2013, DOE/NRC/DOT, San Francisco, Calif., August 18–23, 2013.

c. J.-A. J. Wang, H. Wang, T. Cox, and C. Baldwin, *Progress Letter Report on Bending Fatigue Test System Development for Spent Nuclear Fuel Vibration Integrity Study (Out-of-Cell Fatigue Testing Development–Task 2.4)*, ORNL/TM-2013/225, Oak Ridge National Laboratory, Oak Ridge, Tenn., July 2013.

d. H. Wang, J.-A. J. Wang, T. Tan, H. Jiang, T. S. Cox, R. L. Howard, B. B. Bevard, and M. E. Flanagan, "Development of U-frame Bending System for Studying the Vibration Integrity of Spent Nuclear Fuel," *Journal of Nuclear Materials* **440**, 201–213 (2013).

e. J.-A. J. Wang, H. Wang, B. B. Bevard, R. L. Howard, and M. E. Flanagan, *SNF Test System for Bending Stiffness and Vibration Integrity*, International High-Level Radioactive Waste Management Conference, Albuquerque, N.M., April 28–May 2, 2013.

f. J.-A. J. Wang, H. Wang, and Ting Tan, *An Innovative Dynamic Reversal Bending Fatigue Testing System for Evaluating Spent Nuclear Fuel Rod Vibration Integrity or Other Materials Fatigue Aging Performance*, ORNL Invention Disclosure 201102593, DOE S-124,149, April 8, 2011. Patent in review, 13/396,413, February 14, 2012.

g. J.-A. J. Wang, H. Wang, T. Cox, and Y. Yan, *Progress Letter Report on U-Frame Test Setup and Bending Fatigue Test for Vibration Integrity Study (Out-of-Cell Fatigue Testing Development–Task 2.3)*, ORNL/TM-2012/417, Oak Ridge National Laboratory, Oak Ridge, Tenn., August 2012.

h. J.-A. J. Wang, H. Wang, T. Tan, H. Jiang, T. Cox, and Y. Yan, *Progress Letter Report on U-Frame Test Setup and Bending Fatigue Test for Vibration Integrity Study (Out-of-Cell Fatigue Testing Development–Task 2.2)*, ORNL/TM-2011/531, Oak Ridge National Laboratory, Oak Ridge, Tenn., January 2012.

i. J.-A. J. Wang, H. Wang, Y. Yan, R. Howard, and B. Bevard, *High Burn-up Spent Fuel Vibration Integrity Study Progress Letter Report (Out-of-Cell Fatigue Testing Development–Task 2.1)*, ORNL/TM-2010/288, Oak Ridge National Laboratory, Oak Ridge, Tenn., January 2011.

j. J.-A. Wang, H. Wang, B. Bevard, and R. Howard, "Reversible Bending Fatigue Testing on Zry-4 Surrogate Rods." WM2014 International Waste Management Conference, Phoenix, Ariz., March 2–6, 2014; to be published in the proceedings.

k. H. Jiang, J.-A. Wang, and H. Wang, "Potential Impact of Interfacial Bonding Efficiency on High-Burnup Spent Nuclear Fuel Vibration Integrity during Normal Transportation." WM2014 International Waste Management Conference, Phoenix, Ariz., March 2–6, 2014; to be published in the proceedings.

l. J.-A. J. Wang, H. Wang, B. Bevard, and R. Howard, "The CIRFT Development and Its Application to UNF Vibration Integrity Study." Presentation at the Joint UFD-ST Experiments and Analysis Working Group Meeting, January 21–22, 2014, U.S. Department of Energy, Las Vegas.

m. J.-A. Wang, et al., "The Development of Cyclic Integrated Reversible-bending Fatigue Tester and Its Application to SNF Vibration Integrity Study." Presentation at the 2013 EPRI Used-Fuel Extended Storage Collaboration Program Meeting, December 3–5, 2013, Charlotte, N.C.

n. J.-A. Wang and H. Jiang, *The Impact of Interface Bonding Efficiency on High-Burnup Spent Nuclear Fuel Vibration Integrity during Normal Transportation*, ORNL/TM-2013/296, Oak Ridge National Laboratory, Oak Ridge, Tenn., August 2013.

o. J.-A. J. Wang and H. Wang, *Reversal Bending Fatigue Testing of Zry-4 Surrogate Rod (Out-of-cell Fatigue Testing Development—Task 2.4)*, ORNL/TM- 2013/297, Oak Ridge National Laboratory, Oak Ridge, Tenn., August 2013.

p. J.-A. Wang, "The Development of Reversal Bending Fatigue Tester for Spent Nuclear Fuel Vibration Integrity Study." Presentation at the DOE Used Fuel Disposition WG Meeting on UNF NCT Loading & Structural Performance, May 22, 2013, Las Vegas.

q. H. Jiang, J.-A. Wang and Hong Wang, "Reversible Bending Fatigue Testing System Design Concepts for Spent Fuel Vibration Integrity Study." ASME 2014 Pressure Vessels & Piping Conference, Anaheim, Calif., July 20–24, 2014; to be published in the proceedings.

UNITED STATES PATENT AND TRADEMARK OFFICE

UNITED STATES DEPARTMENT OF COMMERCE
United States Patent and Trademark Office
Address: COMMISSIONER FOR PATENTS
P.O. Box 1450
Alexandria, Virginia 22313-1450
www.uspto.gov

APPLICATION NUMBER	FILING or 371(c) DATE	GRP ART UNIT	FIL FEE REC'D	ATTY.DOCKET.NO	TOT CLAIMS	IND CLAIMS
13/396,413	02/14/2012	3745	590	8490-88203-01	22	3

CONFIRMATION NO. 3269

95832
Klarquist Sparkman, LLP
One World Trade Center
121 SW Salmon Street, Suite 1600
Portland, OR 97204

FILING RECEIPT

OC000000052908085

Date Mailed: 03/06/2012

Receipt is acknowledged of this non-provisional patent application. The application will be taken up for examination in due course. Applicant will be notified as to the results of the examination. Any correspondence concerning the application must include the following identification information: the U.S. APPLICATION NUMBER, FILING DATE, NAME OF APPLICANT, and TITLE OF INVENTION. Fees transmitted by check or draft are subject to collection. Please verify the accuracy of the data presented on this receipt. **If an error is noted on this Filing Receipt, please submit a written request for a Filing Receipt Correction. Please provide a copy of this Filing Receipt with the changes noted thereon. If you received a "Notice to File Missing Parts" for this application, please submit any corrections to this Filing Receipt with your reply to the Notice. When the USPTO processes the reply to the Notice, the USPTO will generate another Filing Receipt incorporating the requested corrections**

Applicant(s)

Jy-An John Wang, Oak Ridge, TN;
Hong Wang, Oak Ridge, TN;
Ting Tan, Oak Ridge, TN;

Assignment For Published Patent Application

UT-Battelle, LLC

Power of Attorney: The patent practitioners associated with Customer Number 95832

Domestic Priority data as claimed by applicant

Foreign Applications (You may be eligible to benefit from the **Patent Prosecution Highway** program at the USPTO. Please see http://www.uspto.gov for more information.)

Projected Publication Date: To Be Determined - pending completion of Security Review

Non-Publication Request: No

Early Publication Request: No
**** SMALL ENTITY ****

Title

REVERSAL BENDING FATIGUE TESTING

Preliminary Class

416

PROTECTING YOUR INVENTION OUTSIDE THE UNITED STATES

Since the rights granted by a U.S. patent extend only throughout the territory of the United States and have no effect in a foreign country, an inventor who wishes patent protection in another country must apply for a patent in a specific country or in regional patent offices. Applicants may wish to consider the filing of an international application under the Patent Cooperation Treaty (PCT). An international (PCT) application generally has the same effect as a regular national patent application in each PCT-member country. The PCT process **simplifies** the filing of patent applications on the same invention in member countries, but **does not result** in a grant of "an international patent" and does not eliminate the need of applicants to file additional documents and fees in countries where patent protection is desired.

Almost every country has its own patent law, and a person desiring a patent in a particular country must make an application for patent in that country in accordance with its particular laws. Since the laws of many countries differ in various respects from the patent law of the United States, applicants are advised to seek guidance from specific foreign countries to ensure that patent rights are not lost prematurely.

Applicants also are advised that in the case of inventions made in the United States, the Director of the USPTO must issue a license before applicants can apply for a patent in a foreign country. The filing of a U.S. patent application serves as a request for a foreign filing license. The application's filing receipt contains further information and guidance as to the status of applicant's license for foreign filing.

Applicants may wish to consult the USPTO booklet, "General Information Concerning Patents" (specifically, the section entitled "Treaties and Foreign Patents") for more information on timeframes and deadlines for filing foreign patent applications. The guide is available either by contacting the USPTO Contact Center at 800-786-9199, or it can be viewed on the USPTO website at http://www.uspto.gov/web/offices/pac/doc/general/index.html.

For information on preventing theft of your intellectual property (patents, trademarks and copyrights), you may wish to consult the U.S. Government website, http://www.stopfakes.gov. Part of a Department of Commerce initiative, this website includes self-help "toolkits" giving innovators guidance on how to protect intellectual property in specific countries such as China, Korea and Mexico. For questions regarding patent enforcement issues, applicants may call the U.S. Government hotline at 1-866-999-HALT (1-866-999-4158).

LICENSE FOR FOREIGN FILING UNDER

Title 35, United States Code, Section 184

Title 37, Code of Federal Regulations, 5.11 & 5.15

GRANTED

The applicant has been granted a license under 35 U.S.C. 184, if the phrase "IF REQUIRED, FOREIGN FILING LICENSE GRANTED" followed by a date appears on this form. Such licenses are issued in all applications where the conditions for issuance of a license have been met, regardless of whether or not a license may be required as

set forth in 37 CFR 5.15. The scope and limitations of this license are set forth in 37 CFR 5.15(a) unless an earlier license has been issued under 37 CFR 5.15(b). The license is subject to revocation upon written notification. The date indicated is the effective date of the license, unless an earlier license of similar scope has been granted under 37 CFR 5.13 or 5.14.

This license is to be retained by the licensee and may be used at any time on or after the effective date thereof unless it is revoked. This license is automatically transferred to any related applications(s) filed under 37 CFR 1.53(d). This license is not retroactive.

The grant of a license does not in any way lessen the responsibility of a licensee for the security of the subject matter as imposed by any Government contract or the provisions of existing laws relating to espionage and the national security or the export of technical data. Licensees should apprise themselves of current regulations especially with respect to certain countries, of other agencies, particularly the Office of Defense Trade Controls, Department of State (with respect to Arms, Munitions and Implements of War (22 CFR 121-128)); the Bureau of Industry and Security, Department of Commerce (15 CFR parts 730-774); the Office of Foreign AssetsControl, Department of Treasury (31 CFR Parts 500+) and the Department of Energy.

NOT GRANTED

No license under 35 U.S.C. 184 has been granted at this time, if the phrase "IF REQUIRED, FOREIGN FILING LICENSE GRANTED" DOES NOT appear on this form. Applicant may still petition for a license under 37 CFR 5.12, if a license is desired before the expiration of 6 months from the filing date of the application. If 6 months has lapsed from the filing date of this application and the licensee has not received any indication of a secrecy order under 35 U.S.C. 181, the licensee may foreign file the application pursuant to 37 CFR 5.15(b).

SelectUSA

The United States represents the largest, most dynamic marketplace in the world and is an unparalleled location for business investment, innovation and commercialization of new technologies. The USA offers tremendous resources and advantages for those who invest and manufacture goods here. Through SelectUSA, our nation works to encourage, facilitate, and accelerate business investment. To learn more about why the USA is the best country in the world to develop technology, manufacture products, and grow your business, visit SelectUSA.gov.

BOSE

Monday, February 03, 2014

Editors, R&D Magazine; and Judges, R&D 100 Awards

RE: R&D 100 Awards for CIRFT: Cyclic Integrated Reversible-bending Fatigue Tester - for Investigating Vibration Integrity of Spent Nuclear Fuel during Transportation

To Whom It May Concern:

The Bose Corporation is pleased to jointly submit the CIRFT System for R&D 100 Award with the Oak Ridge National Laboratory (ORNL) team headed by Dr. Jy-An John Wang. The Bose Corporation has extensive experience in the area of ElectroForce System development and such innovative electromagnetic drives were integrated into CIRFT system development.

The Bose Corporation recognizes that safe transportation of spent fuel rods from the point-of-use to storage facilities is of utmost concern, and recent events highlight the importance of research into safety in and around facilities using nuclear fuel. Bose also recognizes that the staff at Oak Ridge National Laboratory has extensively evaluated methods for testing the fatigue properties of spent nuclear fuel rods, which still exhibit highly-radioactive properties, and therefore must be tested in an irradiation hot cell environment. The ORNL staff has designed a unique method and instrument that allows for testing of actual nuclear fuel rods, as opposed to material substitutes, which will provide the most valuable data for development of safe transportation methods.

Bose is very excited about the achievement of the CIRFT system and the associated analytical tools; which has transformed the very complicated spent nuclear fuel mechanical aging behavior under dynamic loading into a simple prediction aging response formulation that is ready to be applied to the nuclear industry or regulatory body for spent nuclear fuel transportation operation and management efforts.

As the world increasingly relies on nuclear materials for production of usable energy sources, the safe transportation and storage of these materials is of critical importance. We feel that these new testing capabilities are a vital step in ensuring the safety of our communities, and are pleased to be included as a joint submitter for the R&D 100 award consideration.

Sincerely,

Ed Moriarty,

General Manager

BOSE ElectroForce Systems Group

BOSE CORPORATION • ELECTROFORCE SYSTEMS GROUP • 10250 VALLEY VIEW ROAD • SUITE 113 • EDEN PRAIRIE • MN 55344-3544 • USA
TEL: 952-278-3070 • FAX: 952-278-3071 • WWW.BOSE-ELECTROFORCE.COM

Attachment 4

February 10, 2014

Editors, *R&D Magazine*
Judges, R&D 100 Awards

Dear Judges, R&D 100 Awards

Letter of Support for the R&D 100 submittal entitled " CIRFT: Cyclic Integrated Reversible-Bending Fatigue Tester - for Investigating Vibration Integrity of Spent Nuclear Fuel (SNF) during Transportation"

AREVA is pleased to endorse and support the entry of Dr. Jy-An Wang and his colleagues from Oak Ridge National Laboratory (ORNL) for a 2014 R&D 100 Award for the CIRFT System.

Transportation packages for spent nuclear fuel (SNF) must meet stringent safety requirements under both normal and accident conditions as specified by federal regulations. During normal rail or truck transportation of SNF assemblies, SNF systems will undergo vibration induced inertia loading. Thus, the potential SNF system fatigue aging and the associated fatigue strength properties need to be well understood. The development of the CIRFT system and the associated analytical tools have significantly improved the understanding of the SNF dynamic behavior due to vibrational loading, especially for SNF that has been subject to extended irradiation in commercial nuclear reactors.

The CIRFT system is the first test equipment that can evaluate the SNF fuel/clad system reliability under reversible bending conditions. Furthermore, the underlining mechanisms of the fuel pellet-clad interactions and the effect of SNF interface-bonding efficiency on the SNF system integrity can be clearly evaluated from the CIRFT test results. The effect of SNF interface-bonding efficiency on the SNF system integrity is a new finding that will have a significant impact on the research being conducted in the nuclear fuel transport reliability field. Thus, the CIRFT technology is unique and innovative in that it is able to evaluate both the SNF vibration aging microstructure evolution as well as the SNF system dynamic performance.

We fully support the nomination of CIRFT for the 2014 R&D 100 Award. Please don't hesitate to contact me if you require more information.

Sincerely,

Paul Murray
VP, Reactor & Fuels
AREVA
7207 IBM Drive
Charlotte NC 28262
704-805-2751

SAVANNAH RIVER NATIONAL LABORATORY
OPERATED BY SAVANNAH RIVER NUCLEAR SOLUTIONS

February 10, 2014

R&D 100 Awards
100 Enterprise Drive
Suite 600, Box 912
Rockaway, NJ 07866-0912

To: Editors of R&D Magazine and Judges of 2014 R&D 100 Awards

Subject: Letter of Support for 2014 R&D 100 Award entitled "Cyclic Integrated Reversible- bending Fatigue Tester (CIRFT) System used for spent nuclear fuel (SNF) vibration integrity study"

Dear Editors and Judges,

It is my great pleasure to write this letter to support the nomination of Dr. Jy-An Wang and his colleagues at Oak Ridge National Laboratory for the 2014 R&D 100 Award on the subject entitled "Cyclic Integrated Reversible-bending Fatigue Tester (CIRFT) system used for spent nuclear fuel (SNF) vibration integrity study."

Dr. Jy-An Wang and I have been working together in the Materials and Fabrication Technical Committee within the American Society of Mechanical Engineers (ASME) for over ten years so I know very well about his technical competency. In addition, I am also involved in the U. S. Department of Energy Used Fuel Disposition Campaign programs and I know exactly what is needed to accomplish to close the nuclear fuel cycle before the spent nuclear fuel run out of temporary storage space, which will severely impact the future of nuclear energy as one of the options for clean and renewable energy sources. Dr. Wang and his team's invention directly affect the capability of evaluation of the safety and structural integrity of the used fuel (i.e., SNF) during transportation of the fuel assembly from the storage facility to the final geological repository or to the fuel reprocessing plants. Their device, CIRFT, allows accurate determination of the critical frequencies or spectra of the transportation-induced vibration experienced by the used fuel.

It is well known that a good and reliable device for evaluating or measuring a scientific or engineering system must be conducted under well-defined conditions and eliminated all spurious parameters. Their CIRFT system satisfies these criteria which are essential for its intended use for SNF vibration analysis: 1) The amplitude of the reversible loading must be exact in magnitude, which is achieved by using a dual motor driving system; 2) The motion of the specimen must be independent of the inertial effects, which were eliminated by a clever design of a horizontal oscillatory loading frame, rather than the traditional vertical system, in which the gravity

contributes an irrelevant inertial force to the test specimen; 3) The device must be small enough to be fit in a radioactive hot cell, which must be kept as small as possible for the environmental and personnel exposure concerns, and the device must be a stand-alone system because there is no room to bring in a commercially available universal test machine to drive it; 4) All measurements, which include force and displacement, must be integrated in-situ within the system; 5) the test specimen must be constrained in a similar manner as the SNF in the actual transportation system, that is, the ends of the test sample must not be fixed in space, rather, the specimen is allowed to slide freely during the oscillatory loading; and 6) The loading of the test specimen must be as simple as possible, for which the research team developed a "drop-in" sample holder to minimize the personnel exposure in the radioactive hazardous environment (hot cell) when the specimen is being installed and aligned in the device ready for testing.

It should be mentioned that this sophisticated CIRFT system is not an overnight success. Dr. Wang and his team went through numerous designs and test runs, beginning with a vertical test system previously used at Oak Ridge National Laboratory. They constantly identified areas of continuous improvements during this multiple-year iterative and novel design process, and validated its performance with existing data and numerical simulations. I also believe that this compact and self-sufficient device can be used in a more general fatigue testing for any rod-like structures not limited to the used fuel. This innovative device will serve its purpose not only in the accurate determination of the vibration and fatigue characteristics of the used fuel during fuel transportation, but also has wide commercial applications.

I strongly recommend that the CIRFT system be considered for the 2014 R&D 100 Award. Please do not hesitate to contact me should you have additional questions.

Sincerely yours,

Poh-Sang Lam, Ph.D., Fellow ASME
Senior Fellow Engineer

U. S. DOE Savannah River National Laboratory
Materials Science and Technology
Aiken, South Carolina

Phone: 803-725-2922
Fax: 803-725-4553
Email: ps.lam@srnl.doe.gov

BAM
Bundesanstalt für Materialforschung und -prüfung

Your reference

Your message of

BAM · Federal Institute for Materials Research and Testing · 12200 BERLIN · GERMANY

Our reference
3.4/Dr. Völzke
Our Phone (direct)
+49 30 8104-1340
Our Fax (direct)
+49 30 8104-1337
Our e-Mail
holger.voelzke
@bam.de

Date
3 February 2014

R&D 100 Awards

100 Enterprise Drive
Suite 600, Box 912
Rockaway, NJ 07866-0912

Dear Editors of R&D Magazine, and
Judges of R&D 100 Awards,

Letter of Support for R&D 100 Awards entitled "CIRFT: Cyclic Integrated Reversible- bending Fatigue Tester System - for Investigating Vibration Integrity of Spent Nuclear Fuel during Transportation"

I am pleased to endorse and support the R&D 100 Award nomination for Dr. John Jy-An Wang and his team for their developed CIRFT system.

The research work of Dr. Wang and his team at ORNL has provided a greater understanding of the limitations and the underline mechanism of high burn-up spent nuclear fuel (SNF) material under normal transportation induced vibration loading. The testing and analysis procedures employed in CIRFT system represents a major leap forward in characterizing SNF dynamic response to support the back-end nuclear fuel cycle initiative that involved both nuclear industry as well as nuclear regulatory body for safe operation of spent nuclear fuel transport. This also has made CIRFT system a powerful tool for SNF dynamic reliability research to further develop the counter-measure, such as new fuel assembly transport cask design, that can mitigate the SNF system aging during transport and to meet long term safety of SNF assembly storage or its final repository.

The CIRFT system developed by Dr. Wang and his colleagues for the SNF system will enable the reliable operation of SNF transport as well as to ensure sufficient remaining life of the SNF system after transport to support follow-on long term SNF storage purpose. In particular, to assess its durability and reliability at target vibration loading during normal transportation conditions to assure the safety of the general public, and provide guidelines for the safe operation of SNF transport. Being Chair of the EPRI Extended Storage Collaboration Program (ESCP) International Subcommittee, I recognize that the SNF vibration aging evolution revealed by CIRFT also provides vital info for developing updated

Headquarters Lichterfelde
Unter den Eichen 87
12205 BERLIN
GERMANY

Branch Fabeckstraße
Unter den Eichen 44 - 46
12203 BERLIN
GERMANY

Branch Adlershof
Richard-Willstätter-Straße 11
12489 BERLIN
GERMANY

Phone: +49 30 8104-0
Fax: +49 30 8112-029
E-Mail: info@bam.de
Internet: www.bam.de/en/

Bank account
Deutsche Bundesbank
Branch Kiel
Account No.: 210 010 30
Sort Code: 210 000 00

SWIFT Code:
MARKDEF1210

IBAN:
DE42210000000021001030

standards regarding the benchmarking and verification of SNF dynamic behavior and its long-term performance.

In conclusion, CIRFT technology is an important breakthrough in nuclear fuel transport technology for monitoring SNF dynamic performance as well as for its effective lifetime estimate. It provides a new opportunity for understanding the behavior of the fuel-clad system and for developing a new generation of nuclear fuel assembly and the associated transport cask system to meet fuel dynamic performance safety demand. Please don't hesitate to contact me if you need more information.

Yours sincerely

Dr Holger Völzke
Director and Professor
Head of Division 3.4 Safety of Storage Containers

Sandia National Laboratories

February 11, 2014

Judges, R&D 100 Awards, and
Editors, R&D Magazine

Reference: Letter of Support for R&D 100 Award entitled: "CIRFT: Cyclic Integrated Reversible-bending Fatigue Tester for Investigating Vibration Integrity of Spent Nuclear Fuel during Transportation"

Dear Judges and Editors,

I am pleased to endorse the 2014 R&D 100 Award nomination for Dr. Jy-An Wang and his colleagues at Oak Ridge National Laboratory for the development of the CIRFT system for testing mechanical response characteristics of used nuclear fuel.

As the lead for the DOE laboratory support of storage and transportation R&D for used nuclear fuel, a principal part of our program is focused on the response of high burnup fuel to shock and vibration loadings that this fuel will experience during transportation operations. It is important that response characteristics of the fuel are well understood in order to confirm expected performance during transportation. The design of the test apparatus and resultant data will bridge an important technical gap in this understanding.

Of particular interest is the pellet-clad interaction, or PCI. For irradiated fuel, the fuel swells and binds to the inner diameter of the fuel cladding. The extent of this interaction strongly affects the response characteristics of the used fuel during loading. Data of this type has been very hard to come by as the testing must be done on irradiated fuel in a hot cell. The design of the test apparatus as well as the data that will be obtained is unique and will have a large impact in terms of development of the technical basis for transportation of high burnup used fuel.

The development of this test apparatus is timely and will have a significant impact in confirming expected behavior of high burnup fuel during transportation operations. I strongly support this nomination for the 2014 F&D 100 Award.

Sincerely,

Ken B. Sorenson
Manager, Advanced Nuclear Fuel Cycle Technologies
Sandia National Laboratories

Attachment 8

UNITED STATES
NUCLEAR REGULATORY COMMISSION
WASHINGTON, D.C. 20555-0001

February 4, 2014

Editors, R&D Magazine; and Judges, R&D 100 Awards

To Judges, R&D 100 Awards,

RE: R&D 100 Awards for "CIRFT: Cyclic Integrated Reversible- bending Fatigue Tester - for Investigating Vibration Integrity of Spent Nuclear Fuel during Transportation"

I am pleased to endorse the R&D 100 Award nomination for Oak Ridge National Laboratory (ORNL), led by Dr. Jy-An Wang, for developing the CIRFT system and the associated analyses tools for investigating spent nuclear fuel (SNF) vibration integrity.

Transportation packages for SNF must meet safety requirements under normal and accident conditions, as specified by federal regulations. ORNL has developed the CIRFT system that can be used to generate the data needed to verify the SNF vibration reliability in normal transportation operation. This represents a significant contribution to the nuclear industry and U.S. NRC mission to ensure safety and security of spent nuclear fuel storage and transport operations.

The CIRFT device and test protocol is the first testing device and protocol that performs reversible-bending fatigue testing on the SNF system. The CIRFT test results can also be used to investigate the underlining mechanism of fuel pellet and clad interaction and its effect to the SNF system reliability during transportation.

I am very excited about the achievement of the CIRFT system; which will provide data to revolutionarily advance our knowledge on the SNF vibration integrity. The results of the CIRFT tests represent a vital contribution to the nuclear industry with respect to safe operation of the back-end nuclear fuel cycle as well as in developing regulatory guides. In summary, we recognize that CIRFT technology is the recent breakthrough in nuclear material testing and it provides important new opportunities for understanding the dynamic behavior of the SNF systems.

Sincerely,

Michelle Flanagan

Michelle Flanagan
Senior Reactor Systems Engineer
U.S. Nuclear Regulatory Commission
michelle.flanagan@nrc.gov

Attachment 9

Pacific Northwest
NATIONAL LABORATORY
Proudly Operated by Battelle *Since 1965*

Tel: (509) 375-5051
Fax: (509) 375-5052
MSIN: P7-27
Brady.hanson@pnnl.gov

January 31, 2014

Editors, R&D Magazine
Judges, R&D 100 Awards

Dear Judges, R&D 100 Awards,

Letter of Support for R&D 100 entitled "CIRFT: Cyclic Integrated Reversible-bending Fatigue Tester – for Investigating Vibration Integrity of Spent Nuclear Fuel during Transportation

I am pleased to endorse and support the 2014 R&D 100 Award nomination for Dr. John Jy-An Wang and his colleagues for their developed CIRFT system.

The basic concept and theory of bending fatigue mechanics have been well established. However, the development of rigorous experimental techniques to determine the intrinsic reversal bending fatigue strength of spent nuclear fuel rods during transportation has remained a challenge. The lack of an effective reversible bending tester to mimic the inertia force induced by random vibration loading conditions, as well as to test the complicated composite system of the spent nuclear fuel has, until now, hampered our progress in this field.

Many test methods that are currently used to evaluate the bending fatigue limit of materials are limited to unidirectional bending loading instead of reversal bending loading. In addition, tests are normally carried out with specimens that have a notch or reduced section at the gage section to ensure failure occurs at the gage section. Despite the international efforts on the development of testing techniques for spent fuel vibration integrity studies, no methods existed to accurately and effectively measure the spent fuel system fatigue strength.

The CIRFT system and the associated methodology developed by Dr. Wang et al., use a robust specimen design that bears no resemblance to conventional bend testing specimens that have been used in either the conventional bending testing or a conventional mode of loading.

Attachment 9

Therefore, the proposed method is unique and innovative in both specimen design as well as mode of loading.

The recognition of R&D 100 Awards for this novel device and the associated methodology is timely and will certainly speed up the application of this new technology.

Sincerely,

Brady D. Hanson, Ph.D.
Used Fuel Project Manager
Nuclear Chemistry & Engineering Group
Pacific Northwest National Laboratory

Attachment 10

UNIVERSITY OF MICHIGAN
COLLEGE OF ENGINEERING
MECHANICAL ENGINEERING

2250 GG BROWN
2350 HAYWARD STREET
ANN ARBOR, MICHIGAN 48109-2125
734 764-2694 FAX 734 647-3170
http://me.engin.umich.edu/

January 28, 2014

Judges, R&D 100 Awards, and
Editors, R&D Magazine

Reference: Letter of Support for R&D 100 Award Entitled "CIRFT: Cyclic Integrated Reversible-bending Fatigue Tester - for Investigating Vibration Integrity of Spent Nuclear Fuel during Transportation"

Dear Judges,

I am very pleased to endorse and support the 2014 R&D 100 Award nomination for Dr. Jy-An John Wang and his colleagues for their developed CIRFT system at Oak Ridge National Laboratory.

Many test methods that are currently used to evaluate the bending fatigue strength of materials are limited to unidirectional bending loading instead of reversal bending loading; and tested specimen are normally required to have either a pre-notch or a reduced section in the test specimen to ensure failure initiated at the target gage section. However, due to composite nature of spent nuclear fuel (SNF), which consists of nuclear fuel pellets and clad tubing with inherited hydride and flaws due to irradiation history, SNF rod sample with a pre-notch or reduced section can significant reduce the test specimen strength, thus, to generate non-conservative or misleading test results. Secondly in order to be fully compatible with the fracture mechanics test practices for the target material as well as for specific specimen design configuration, especially for a high burn-up SNF cladding rod under transportation vibration loading, CIRFT system uses reversal pure bend loading as the primary driver and equips with uniquely designed grips to implement such loading. Despite the international efforts on the development of testing techniques for SNF vibration integrity study, no methods currently exist for such initiative to accurately and effectively measure the SNF system fatigue strength.

The reversal pure bending device and the associated methodology, developed by Dr. Wang and his colleagues, uses a robust specimen design that bears no resemblance to conventional bend testing specimens used in the conventional bending testing nor a conventional mode of loading. Therefore, the developed CIRFT system is unique and innovative in both specimen design as well as mode of loading, in addition to its compact desktop design. This new invention also enables the technical community to investigate pellet-clad interaction and the associated interface bonding efficiency, and their effects on SNF system reliability during transport mode. The method is economical and direct without any data inferred required. Simplicity of the method is another virtue that can be used to determine the bending fatigue strength of structural materials in general.

The recognition of R&D 100 Awards for this novel device and the associated methodology is timely and will certainly speed up the application of this new technology. I strong support this nomination for the 2014 R&D 100 Award without reservation.

Sincerely,

Jwo Pan

Jwo Pan
Professor of Mechanical Engineering

Attachment 11

Michael C. Billone
Manager, Irradiation Performance Section

Nuclear Engineering Division
Argonne National Laboratory
9700 South Cass Avenue, Bldg. 212
Argonne, IL 60439

1-630-252-7146 phone
1-630-252-2785 fax
billone@anl.gov

January 31, 2014

Editors, R&D Magazines and Judges, R&D 100 Awards

To Whom it may Concern:

Subject: Letter of support for the 2014 R&D 100 Award

I am pleased to write this letter in support of the 2014 R&D 100 Award nomination of Dr. Jy-An Wang, and his colleagues of Oak Ridge National Laboratory for their development of a Cyclic Integrated Reversible-bending Fatigue Tester (CIRFT) system used for spent nuclear fuel (SNF) vibration integrity study.

I learned about this development from a joint project sponsored by DOE Used Fuel Disposition Campaign program. I am extremely impressed by the clever and useful ideas that went into the development of this test system and the associated analyses procedures. I feel that the CIRFT test opens up new doors for conducting valid bending fatigue strength tests on very complicated composite samples of spent nuclear fuel (SNF) materials. In addition to providing a needed stress state for a valid bending fatigue test, it allows testing of SNF material samples under reversible loading, as well as doing so to ensure failure occurred at the gage section instead of at grips because of the use of pure bending loading and uniquely designed specimen grips. One of the most attractive features is the simple nature of the test equipment and the associated in-situ curvature measurement instrumentation needed for this test. It can be easily performed in almost any laboratory, including in an irradiation hot-cell environment, and requires only a universal test machine and conventional instrumentations.

In summary, CIRFT test is a substantial contribution to the technical community, is both innovative and practical, and has many useful applications to materials testing, especially in applying to SNF vibration reliability study. I strongly support the **CIRFT** for the 2014 R&D 100 Award.

Sincerely,

Michael C. Billone

Michael C. Billone

Attachment 12

The University of Vermont
Department of Mechanical Engineering
201 Votey Bldg., 33 Colchester Ave.
Burlington, VT 05405-0156
Phone: 802-656-3320
Fax: 802-656-1929
E-mail: mecheng@emba.uvm.edu

January 30, 2014

Editors, *R&D Magazine*
Judges, R&D 100 Awards

Letter of Support for the R&D 100 submittal entitled "CIRFT: Cyclic Integrated Reversible-bending Fatigue Tester - for Investigating Vibration Integrity of Spent Nuclear Fuel (SNF) during Transportation"

Dear R&D 100 Awards Judges,

I am writing in support of nomination of Dr. Jy-An Wang, Dr. Ting Tan and their colleagues for their developed CIRFT systems at Oak Ridge National Laboratory (ORNL) for a 2014 R&D 100 Award.

By providing a credible resource to meet the growing national demand for dependable electric energy while emitting no greenhouse gases, nuclear power continues to be instrumental in our nation's energy mix. As the nation evaluates methods to store and eventually dispose of the spent nuclear fuel (SNF) resulting from nuclear energy generation, it is critical that fundamental issues such as SNF degradation over time and during transport be understood.

During transportation, SNF systems are experienced unique challenges to fuel cladding integrity due to inertia induced dynamic loading during road or rail shipment. In order to understand and quantify these potential challenges, ORNL has developed the unique testing capabilities and the associated analytical tools that can be used to evaluate the potential impacts on SNF system vibration integrity due to dynamic loading, especially for SNF that has been subject to extended irradiation in commercial nuclear reactors.

The CIRFT system developed at ORNL tests SNF for measuring effective fatigue strength and determining the remaining clad effective lifetime of the SNF fuel/clad system during transportation. This is the first test system that can evaluate the SNF fuel/clad system reliability with an integrated experimental and analytical approach. Therefore, the CIRFT method is unique and innovative in that it is able to evaluate both the SNF vibration aging microstructure evolution as well as the SNF system dynamic performance.

Therefore, I fully support the nomination of CIRFT for the 2014 R&D 100 Award.

Sincerely,

Dryver R. Huston, Ph.D.
Professor of Mechanical Engineering

OAK RIDGE NATIONAL LABORATORY
MANAGED BY UT-BATTELLE FOR THE DEPARTMENT OF ENERGY
FACT SHEET

Cyclic Integrated Reversible-Bending Fatigue Tester (CIRFT) for Investigating Vibration Reliability of Spent Nuclear Fuel during Transportation

Our Mission

Transportation packages for spent nuclear fuel (SNF) must meet safety requirements under normal and accident conditions, as specified by federal regulations. Oak Ridge National Laboratory has been developing test facilities that can be used to verify the SNF vibration reliability, especially for high burn-up SNF due to decreased fuel cladding ductility , both in normal transportation operation and impact loading conditions to meet the nuclear industry and U.S. Nuclear Regulatory Commission (NRC) needs in

- **Safety and security of spent nuclear fuel storage and transport operations**
- **Ensure regulatory effectiveness in a dynamic environment**
- **Nuclear waste confidence and evolving national policy for SNF disposal**

ORNL also develops the methodology to investigate the underline failure mechanism of SNF behaviors under dynamic service environments in support of national long-term spent fuel transportation and management initiatives.

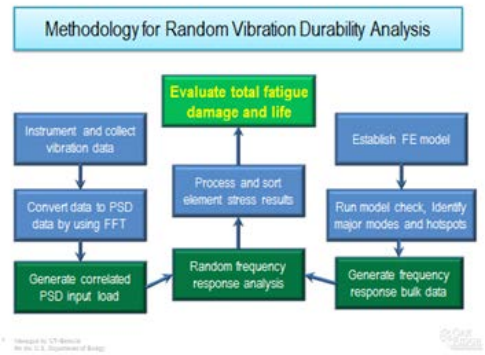

Technical Approach

ORNL developed an innovative test system that can perform reversible-bending fatigue test to evaluate the static and dynamic-mechanical response of SNF rods under simulated loads in hot cell. The system contains a U-frame set-up that has unique features. 1) Effective specimen design with protective test rig to ensure valid test results, especially fit for testing high burn-up SNF rod samples. 2) Reversible-cyclic bending test is achieved by push and pull at the loading point of setup. 3) The in-situ curvature of specimen measurement is obtained through in-house developed three LVTDs setup (shown in the picture).

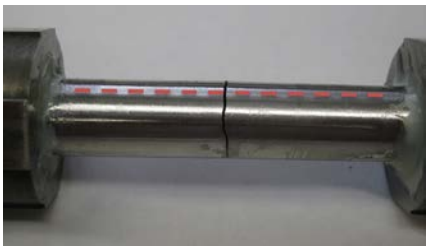

Fractured surrogate rod made of stainless steel tube under cycling: ±4mm, 2Hz; $N_f = 2.95\times10^4$ cycles

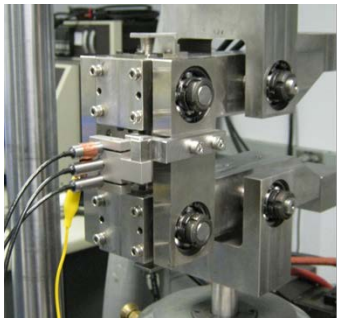

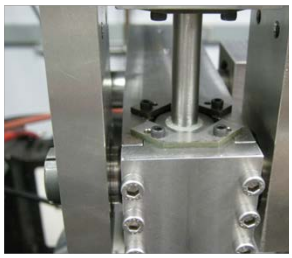

ORNL U-frame setup equipped with linear roller bearings that are preloaded by bolt-tightening the end blocks. The enlarged view on the right side shows the rod inserted with LVDT bracket removed.

UT-BATTELLE

Technical Development

Surrogate rods have been used extensively in calibrating the developed test system setup as well as in performing systematic cyclic fatigue tests. The surrogate rod tests assist both in developing testing protocols and understanding the potential failure modes of SNF rods under vibration. The failure behaviors observed in testing the surrogate rods also provides fundamental understanding on the underline failure mechanism of the SNF surrogated rod performance under vibration that has not been achieved in the past. Wide varieties of surrogate rods have been tested, including stainless (SS) cladding, SS cladding with epoxy cast inside it, and SS cladding with alumina pellets inserts. It has been shown that the interface bonding between the SS cladding and alumina pellets has a significant impact on the bending response of rods. S-N curve revealed a defined trend over the total strain levels from 0.1 to 0.3%.

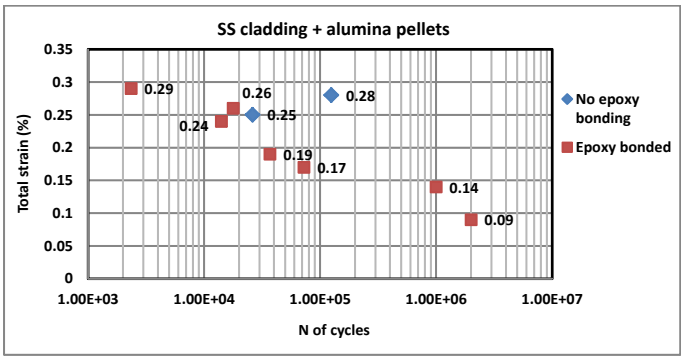

Summary of cyclic tests using stainless steel cladding + alumina pellets inserts; data were generated in MTS 810 servo-hydraulic tester.

ORNL has finished a prototype reversible pure bending fatigue tester for SNF vibration integrity study. The tester uses the state-of-the-art linear motor technology from BOSE that is based on electromagnetic force. The U-frame test rig is set horizontally for an optimized dynamic performance, to ensure effective operation of the test rig at higher frequencies. The system is being made ready for hot cell testing.

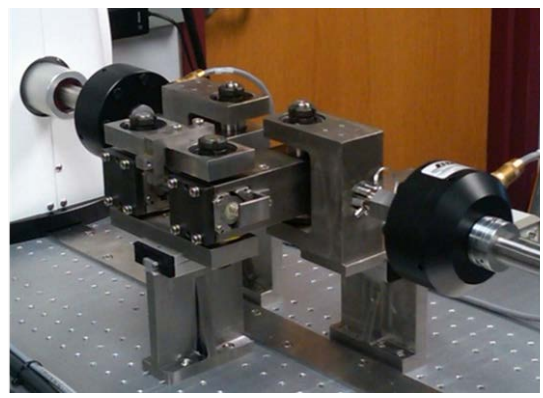

ORNL U-frame integrated into Bose dual linear motor TestBench. A horizontal arrangement is used to eliminate the weight effect on rod in bending.

Core Competencies

- Spent fuel transportation integrity study
  - Vibration loading
  - Dynamic impact loading
  - Failure mechanism analysis
- Reversible bending fatigue of solid structures
  - Vehicle suspending system
  - Turbine blade
  - etc.
- Materials science
  - Mechanical performance in large deformation and high cycles.

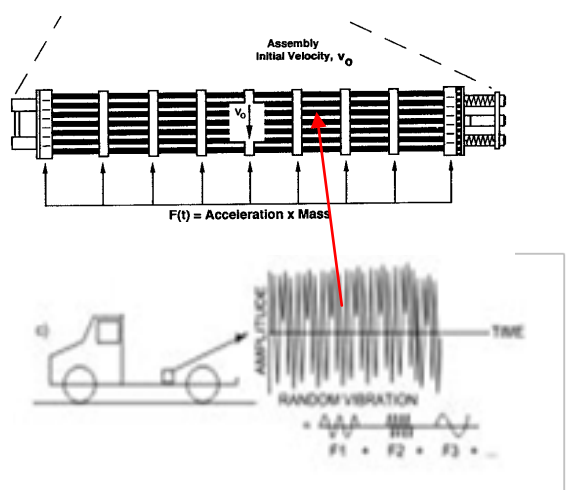

Point of Contact:
Jy-An John Wang, PhD, PE
Distinguished R&D Staff
Materials Science and Technology Division
Oak Ridge National Laboratory
P.O. Box 2008
Oak Ridge, TN 37831-6069
Phone: 865-574-2274
Fax: 865-574-6098
E-mail: wangja@ornl.gov

Journal of Nuclear Materials 440 (2013) 201–213

Contents lists available at SciVerse ScienceDirect

Journal of Nuclear Materials

journal homepage: www.elsevier.com/locate/jnucmat

Development of U-frame bending system for studying the vibration integrity of spent nuclear fuel

Hong Wang [a], Jy-An John Wang [a,*], Ting Tan [a], Hao Jiang [a], Thomas S. Cox [a], Rob L. Howard [b], Bruce B. Bevard [b], Michelle Flanagan [c]

[a] Materials Science and Technology Division, Oak Ridge National Laboratory, One Bethel Valley Road, Oak Ridge, TN 37831, United States
[b] Reactor and Nuclear Systems Division, Oak Ridge National Laboratory, One Bethel Valley Road, Oak Ridge, TN 37831, United States
[c] Office of Nuclear Regulatory Research, U.S. Nuclear Regulatory Commission, Washington, DC 20555, United States

ARTICLE INFO

Article history:
Received 7 November 2012
Accepted 3 May 2013
Available online 16 May 2013

ABSTRACT

A bending fatigue system developed to evaluate the response of spent nuclear fuel rods to vibration loads is presented. A U-frame testing setup is used for imposing bending loads on the fuel rod specimen. The U-frame setup consists of two rigid arms, side connecting plates to the rigid arms, and linkages to a universal testing machine. The test specimen's curvature is obtained through a three-point deflection measurement method. The tests using surrogate specimens with stainless steel cladding revealed increased flexural rigidity under unidirectional cyclic bending, significant effect of cladding-pellets bonding on the response of surrogate rods, and substantial cyclic softening in reverse bending mode. These phenomena may cast light on the expected response of a spent nuclear fuel rod. The developed U-frame system is thus verified and demonstrated to be ready for further pursuit in hot-cell tests.

© 2013 Elsevier B.V. All rights reserved.

1. Background

When fuel is no longer capable of efficiently contributing to a chain reaction, it is removed from the reactor and is termed spent nuclear fuel (SNF). Because of its high heat load and radioactivity, SNF is initially stored in water-filled pools to provide both cooling and shielding. As the pools reach capacity, it is necessary to remove assemblies and place them into dry cask storage. Until a disposition pathway, either recycling or geologic disposal, is chosen and implemented, the storage periods for SNF will likely be longer than originally intended. Therefore, the ability of the important-to-safety structures, systems, and components (SSCs) to continue to meet safety functions over extended times must be determined. In addition, whether SSCs can meet applicable safety functions when the spent nuclear fuel is transported to its final location must be determined. To facilitate all options for disposition and to maintain retrievability and normal back-end fuel cycle operations, the structural integrity of the spent nuclear fuel after storage and subsequent transportation needs to be evaluated.

The fuel assemblies are loaded in a transportation cask or in a dual-purpose canister with a transportation overpack. The transportation cask is then loaded onto a truck or railcar and is usually transported in a horizontal position. The interaction between the vehicle and the ground creates vibration, which in turn is transmitted into the transportation cask internal structure (baskets) and fuel assembly spacer grids. A cross section of a typical pressurized water reactor fuel assembly is given in Fig. 1. Transportation packages for spent fuel must meet safety requirements under normal and accident conditions, as specified by federal regulations. For normal conditions of transport, it is required that the licensee assure that there will be no loss or dispersal of spent fuel, no significant increase in external surface radiation levels, and no substantial reduction in the effectiveness of the spent fuel package. This includes vibration loads incident to transport [1]. The loads contain frequency components around or less than 100 Hz, depending on the vehicles used [2].

Spent fuel rod vibration during normal transport is important because of the sustained loads and this is particularly important for high-burnup fuel (>45 GWd/MTU). As the burnup of the fuel increases, a number of changes occur that may affect the performance of the fuel and cladding in storage and transportation. These changes include increased cladding corrosion layer thickness, increased cladding hydrogen content, increased fission gas release, and formation of a high burnup structure (HBS) at the surface of the fuel pellets. With respect to cladding hydrogen content, the solubility of hydrogen in zirconium increases with higher temperatures. When the concentration of hydrogen exceeds the solubility limit, zirconium hydrides form. Depending on the size, distribution, and orientation, these hydrides can embrittle the cladding and reduce ductility. Furthermore, the presence of hydrides can facilitate cracking if the hydrides are aligned radially, perpendicular to the tensile stress field. Although cladding hydrides are typically observed to be oriented in the circumferential

* Corresponding author. Tel.: +1 865 574 2274; fax: +1 865 574 6098.
E-mail address: wangja@ornl.gov (J.-A.J. Wang).

0022-3115/$ - see front matter © 2013 Elsevier B.V. All rights reserved.
http://dx.doi.org/10.1016/j.jnucmat.2013.05.009

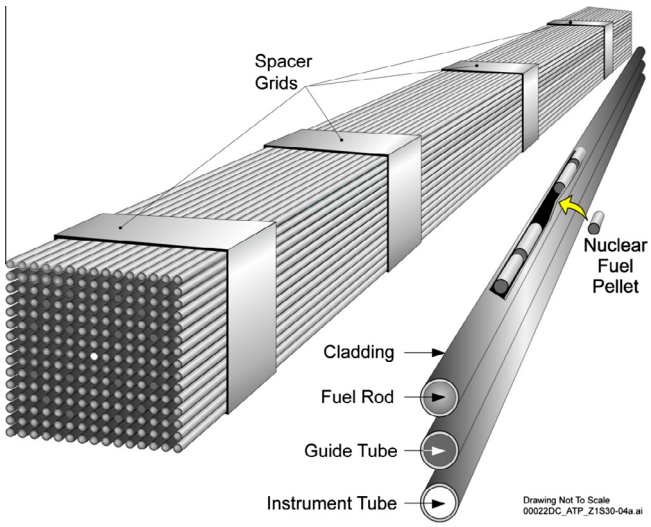

Fig. 1. Cross-sectional illustration of typical pressurized water reactor fuel assembly. The spacer grids can impart vibration loads to spent fuel rods during transportation.

direction, they can be reoriented to the radial direction, depending on the stress level of the cladding when it is cooled. Such cooling will occur following the drying process during the transfer of the fuel from the pool to a transportation cask or dual-purpose canister. Hydrides have also been shown to diffuse to colder regions of the cladding under a relatively small temperature gradient. The reorientation and diffusion of hydrides can result in cladding cracking. Even if a through-wall crack is not formed, the extent of cracking needs to be evaluated to determine if clad will fail due to stresses caused by normal handling or transportation [3]. Therefore, the evaluation of spent fuel rod integrity under vibration loading is an important part of the safety assessments needed for the extended storage and transportation of high-burnup spent fuel.

Although the mechanical properties of high-burnup cladding have been studied by subjecting the materials to longitudinal (axial) tensile tests, ring-stretch tests, ring-compression tests, and biaxial tube burst tests, no method or testing system has been developed to investigate the mechanical properties and behavior of both the cladding and the fuel in it under unidirectional bending and reverse bending (vibration/cyclic) loads until now.

2. Introduction

Testing a SNF rod is not trivial. First, SNF rods are highly radioactive. SNF testing has to be conducted in a hot-cell environment, and the rods can be accessed only by manipulators. Thus, the test setup, specimen loading, and test operations must be as simple as possible. Second, a fuel rod has a composite structure originally composed of fuel pellets and cladding, which has been modified significantly by high burnup process. Various failure modes could be triggered in transportation, including fracture, splitting, etc. The bending-induced failure can be captured only by an effective testing approach. Last, rod vibration in transportation is not well characterized. Moreover, the transportation environmental assessment indicated that the frequencies are much higher than what can be achieved by a convention bending fatigue system (within the category of non-rotational bending fatigue).

Bending fatigue testing has been around for some time [4–7]. On the basis of the beam's boundary condition, the testing can be classified as cantilever beam flexure [8], three-point bending and four-point bending [9–12], and pure bending [13–19]. Bending fatigue tests also include variants that have been developed in response to environmental factors, particularly temperature [20].

The main observations on the current status of bending fatigue testing and related issues can be summarized as follows: (1) Four-point bending fatigue has been proven to be a mature experimental technique in testing materials and components that have limited deformation before failure. The technique is mostly used in fatigue tests without bending reversal. (2) Four-point/three-point bending and cantilever bending all suffer from the inherent drawback related to transverse shear. This has a significant impact on materials that are sensitive to shear. (3) Various supports have been developed in bending fatigue testing, including flexures [11], rotary joints [12], slide connections [13], and motorized clamps [21]. They are neither demonstrated nor enabled in reverse mode. (4) Pure bending fatigue has been used for high strain and low cycle fatigue in testing metallic alloys and composites. The implementation of the pure bending concept is usually application-based with partial success. (5) Environmental chambers and/or high temperature furnaces are currently incorporated into some critical bending fatigue tests. The setup of specimens and tests is all accomplished manually.

It becomes clear that these developed methods cannot be directly used in testing and characterizing the SNF rods, and a new test system is required. Among the test methods examined, pure bending has been identified as a leading candidate for bending fatigue testing of SNF rods. Pure bending eliminates the shearing-induced failure to which the SNF would be subjected if three- or four-point bending were used. Several important aspects of the new system with emphasis on pure bending have been identified as the initial condition for subsequent development. First, a universal materials testing machine or equivalent system is used as a driving mechanism in the targeted frequency range 1–100 Hz. Second, rigid sleeves serve as a device to convert external force couples into bending moments. Third, the specimen supporting or holding mechanism allows the rod to deform freely with axial motion but no transverse rigid-body motion so that reverse bending can be applied. Such boundary condition is apparently different from the pivot or simply supported and is called frixed [11].

Testing setup plans were investigated, including horizontal and vertical test setups [22]. In the horizontal setup, loading is introduced vertically with the loading points offset from the supporting points for an effective loading arm. In the vertical setup, bending is performed through vertical loading with the assistance of a reoriented U-frame whose opening faces aside. The U-frame is constructed with two rigid arms and a linking member. The rod specimen is coupled into the co-linear holes in the two rigid arms (Fig. 2). In this case, the rod is offset to the linking member or flexure in the longitudinal direction of the rigid arms. The rod and the linking member can be overlaid or both in the same plane normal to the rigid arms. These two cases are named as offset and co-planar rod arrangement in the following, respectively. In addition, the corners or joints of the U-frame can be rigid or pivoting. The bending moment applied to the rod depends on the arrangement of the rod and the mechanism used in the corners.

A comparison between the two testing setup plans highlighted many advantages of the vertical setup. Particularly, the vertical setup uses only two linkages at the ends of the rigid arms to the driving system. The installation of a rod specimen can be accomplished by simply dropping the rod into the holes once the U-frame is set up. The drop-in feature is shown to be extremely important for SNF testing because it simplifies the operation of manipulators in a hot-cell environment. The U-frame setup was thus selected in this project to test and investigate the bending fatigue and vibrational integrity of the SNF rods. A preliminary introduction to the U-frame setup was given in a separate report [23]. This work summarizes the development of the U-frame bending system and recent

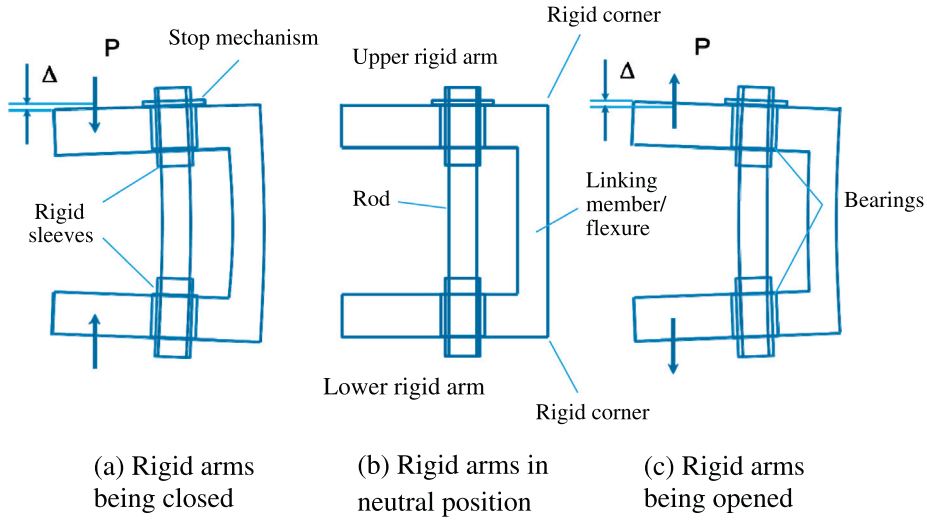

Fig. 2. U-frame-assisted bending fatigue testing setup for reversal bending when rigid arms are (a) closing, (b) neutral, and (c) opening. The rod is offset from the vertical linking member.

progress on our effort in out-of-cell development. The design, engineering, and application are presented in the following sections, including out-of-cell test results using surrogate rods.

3. Design and analysis of U-frame test setup

The variations in the joint mechanism used in the U-frame corners and the arrangement of the rod specimen relative to the linking member provide many options for the design. The investigation indicated that pivoting corners fit into both the offset and co-planar designs, while rigid corners are feasible only in the offset design. In the case of rigid corners, the linking member acts as a flexure to enable the rotation of the two rigid arms while being axially loaded. Controlled by the displacement, the moment applied to the rod depends on the flexural rigidity of the rod and on the flexure as well. Thus, the rigidity of the flexure needs to be calibrated first in order to define the moment. The reliability of the rigid corners and the durability of the flexure are major concerns in cycles of long duration.

In the case of pivoting corners, the moment applied is defined by the external force and the loading arm with respect to the pivot. The linking member serves as an axial loading rod without flexing, and the system has none of the reliability issues found with rigid corners. One minor concern with pivoting corners relates to U-frame set up process because the U-frame itself functions as a structure only if a rod is inserted, and the two rigid arms need to be set to a predetermined position beforehand. Overall, pivoting corners are shown to be much better than rigid corners. The selection of pivoting corners means that both offset and co-planar designs of specimen holes can be accommodated. Design screening depends on whichever is more effective and efficient in converting force couples into bending moments or flexural stresses.

3.1. Design of U-frame setup

The size of the U-frame design depends on the rod specimen to be tested. For the SNF rods that are the focus of this study, the cladding is made of Zircaloy-4 (Zry-4) and inside and outside diameters (ID and OD) of the cladding are 9.46 and 10.70 mm, respectively. The fuel pellets are made of UO_2 and each sized $\varnothing 9.30 \times 15.2$ mm. Because a regular fuel rod is quite long and it is not feasible to test an entire SNF rod in hot cell, a section of 152.40 mm length was used for this study.

Two sizes of rigid arms were studied: $50.80 \times 50.80 \times 266.70$ mm for the offset design and $50.80 \times 50.80 \times 203.20$ mm for the co-planar design. Both sizes of rigid arms have a beam section of 50.80×50.80 mm, which offers the rigidity and secondary loading arms required for converting the external force couples into bending moments. A gage length of 50.80 mm is available when the rod is installed. In both the offset and co-planar designs, the rod is located 152.40 mm away from the loading point. The linking member is designed as an H-shaped structure and is located 236.22 mm from the rod specimen in the offset design. In the co-planer design, the linking member is actually composed of two side connecting plates. Compliant layers 1.143 mm thick were used in two holding areas of the rod to protect it from contact damage.

The durability of the bending system suggests that the U-frame components should be capable of surviving radiation and fatigue. For this reason, stainless steel (SS) 304 was considered as a primary material for these components. An investigation was also conducted to identify engineering plastics for the compliant layers, and polycarbonate was screened out on the basis of several sources [24–26]. A solid model of the U-frame in a co-planar configuration is shown in Fig. 3 with the major components included: two rigid arms, side connecting plates, and rod specimen/compliant layer.

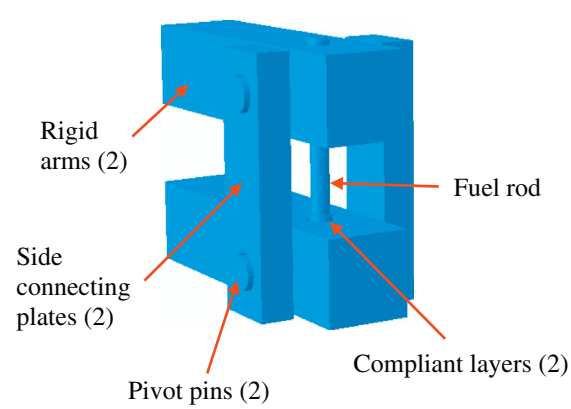

Fig. 3. Three-dimensional solid modeling of U-frame test setup; the rod is co-planar with the vertical linking members.

3.2. Finite element analysis

The mechanical properties of the cladding and pellets (Zry-4 and UO_2) were based on a PNNL report [27] and BARC research [28]. The main mechanical properties of these materials are summarized in Table 1 along with SS and alumina (will be discussed later) [29,30]. Two stress-level solutions were pursued in the finite element analysis (FEA) [23]. The first was elastic solution in which the fuel pellet, cladding and compliant layers are all within the elastic range; the second was yielding solution in which all these components become yield. The elastic solution was achieved when the loading of the rigid arm was 178 N. The stress distribution within the fuel rod and compliant layer shows that the Mises stress contours are typical of pure bending. Additionally, no stress concentration exists in the cladding. The compliant layers thus worked as a buffer as designed and suppressed the effect of the contact. A detail examination showed that the maximum stresses were actually developed on the surface of the fuel pellet, obviously due to the higher Young's modulus of the pellet.

The FEA results are summarized in Table 2 for the two rod arrangements. Under the given load of 178 N, a significant increase in the fuel rod stress was observed when the design was switched from the offset to the co-planar configuration. Therefore, placing the fuel rod in the same plane as the linking members of the U-frame is more efficient in converting the external forces into the bending moment than offsetting the rod, and the co-planar arrangement of the rod will be the focus of the following discussion. It is our interest to investigate the yield case. Such a situation defines the maximum load level to which the U-frame will be subjected and, further, the required capacity of the testing machine. The load-bearing capacity of the U-frame with the co-planar configuration of the rod has been determined to be around 1780 N. The maximum displacement at the loading point also increased from 1.83 mm to 17.86 mm when the load increased from 178 N to 1780 N. As a result, the relative movement at the loading ends can be as high as 35.56 mm. This is also the minimum stroke of the actuator required in a universal testing machine.

The dynamic FEA was performed by including additional material properties [23]. While the density depended on the materials used in individual components, the damping ratio was set to 0.05 for the system. A steady-state solution was investigated, in which input had load amplitudes of 178, 267, and 356 N and a frequency range of 10–100 Hz. The results obtained indicated that the maximum stress again occurred near the surface of the fuel rod and all the components stayed within the elastic condition. For instance, the maximum Mises stresses for 356 N at 10 Hz were 123.421, 66.192, and 11.722 MPa for pellet, cladding, and compliant layers. These values are relatively low, only 22–28% of those in the static case (Table 2). Such levels of stresses occurred in the fuel rod as a substantial amount of input energy was spent in driving the components of the U-frame instead of the rod specimen.

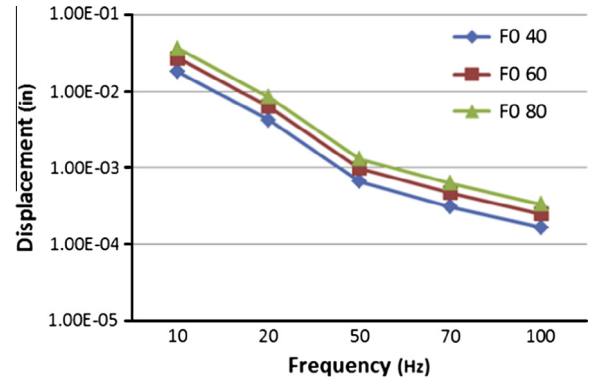

Fig. 4. Dynamic response of U-frame setup obtained by steady-state analysis; F_0 is load amplitude 40, 60, 80 lb or 178, 267, and 356 N. The displacement is measured at the loading point of the U-frame setup in inches.

The displacement response of the U-frame obtained by the steady-state solution is presented in Fig. 4. As expected, the displacement decreased significantly with increasing frequency under defined load amplitude. With the input of 178 N, switching from static to 10 Hz of dynamic loading resulted in a pronounced displacement drop from 1.829 mm to 0.455 mm at the loading ends of the rigid arms. The dynamic responses of the U-frame at two typical frequencies (10 and 20 Hz) are summarized in Table 3 along with the static results.

3.3. Implication

The pure bending demonstrated by the FEA study suggested that the free movement of the fuel rod in the axial direction (as required by the frixed condition) could be enabled largely by the use

Table 1
Mechanical properties of U-frame component materials used in FEA.

Materials	Density (kg/m^3)	Young's modulus (GPa)	Poisson's ratio	Yield strength (MPa)
Stainless steel[a]	8030	193	0.30	290
Polycarbonate[b]	1210	7	0.35	69
UO_2[c]	10,970	201	0.32	2146
Zry-4[d]	6560	91	0.33	906
Al_2O_3[e]	3920	372	0.22	2500

[a] Ref. [29].
[b] Refs. [24,26].
[c] Ref. [28].
[d] Ref. [27].
[e] Ref. [30].

Table 2
Maximum stress in fuel rod specimen and compliant layer (MPa) obtained by FEA.

Rod arrangement	Solution	Pellet	Cladding	Compliant
Offset	Static, 178 N	20.437	10.963	12.763
Co-planar	Static, 178 N	219.606	117.215	26.091
	Static, 356 N[a]	439.212	234.430	52.181
	Dynamic, 10 Hz, 356 N	123.421	66.192	11.722

[a] Based on the elastic result at 178 N.

Table 3
Summary of FEA results for U-frame setup in static and dynamic loading conditions.

Test condition	Frequency (Hz)	Force amplitude (N)	Relative displacement amplitude[a] (mm)
Static		178	3.66
Static[b]		1780	35.56
Dynamic	10	178	0.91
	10	356	1.82
Dynamic[c]	10	1780	9.10
	20	356	0.42
Dynamic[c]	20	1780	2.12

[a] Relative displacement of the U-frame is twice that of the single arm.
[b] Load at which fuel rod and compliant layer yield.
[c] Based on the elastic result at 356 N.

of compliant layers. By using such a design, free axial movement of the fuel rod hinges on the performance of the compliant layers. Particularly, the frictional coefficient between the compliant layers and the surfaces of specimen hole must be sufficiently low. With this regard, Teflon can be a better selection for the compliant layers, considering the frictional coefficient of Teflon against steel is as low as 0.04 and the mechanical properties of Teflon are equivalent to those of polycarbonate [31–33].

UO_2 is characterized with unsymmetrical strength in the plane of principal stresses (σ_1 versus σ_3). The yield stress of the pellets in Table 1, in fact, corresponds to compressive loading because it was derived from the measured indentation hardness [28]. Similar to other structural ceramics, UO_2 features a low fracture stress. At room temperature, the rupture strength (from a bending test) was reported to be around 216 MPa [34]. The low rupture strength indicates that the pellets could be fractured well earlier than the predicted yield point. Once the fuel pellet is broken, a stress concentration will occur in the cladding near the fracture point. The strength of the fuel rod will be ultimately scaled down to a much lower level.

The FEA model assumed a perfectly plastic model for all fuel rod components. The use of a perfectly plastic model could lead to an underestimated ultimate load of the U-frame because extensive strain hardening is observed with the fuel cladding materials such as Zry-4. The strain–stress curve of the spent fuel cladding and the main controlling factors were also studied [27], but the effect of strain hardening on the bending performance of a spent fuel rod is unknown.

4. Engineering of U-frame setup

4.1. Performance target

The FEA study discussed in Section 3.2 showed that the yield load of the U-frame was 1780 N with a displacement range of ±35.56 mm at the loading ends of the rigid arms. This characteristic load can serve as the performance target of the U-frame under design. As mentioned, the conclusion was based upon assumptions including perfect plasticity and symmetry of the strength envelop in both directions of the stress axis. However, it is reasonable to use such a result as the starting point for the engineering process because determining the input data for high-burnup spent fuel indeed involves a substantial amount of uncertainty.

Testing and calibration of the setup dedicated to spent nuclear fuel largely relies on use of surrogate rods. High density alumina and stainless steel (SS 304) have been selected as the pellet and cladding materials, respectively, because their mechanical properties are in the same ranges of UO_2 and Zry-4 (Table 1). The alumina was also used by Papaioannou et al. to model fuel pellets in the fuel release tests related to impact-induced damage to the cladding [35]. The geometric size of the surrogate rods was taken as that of a spent fuel rod to meet the similarity requirements between model and prototype. A rod specimen was prepared in the initial stage of the project with the cladding ID 9.449 mm, OD 11.074 mm, and length 152.400 mm, and with a single pellet $\varnothing 9.449 \times 152.4$ mm. The Teflon tubes as compliant layers were prepared with a size of ID 11.07 mm, OD 16 mm, and length 55.88 mm. The Teflon tubes were slightly longer than the thickness of the rigid arms to prevent the fuel rod from contacting the edge of the hole.

4.2. Main components of U-frame setup

Engineering of the U-frame setup involves implementation of the designs of main components including rigid arms, side connecting plates, and linkage to the universal testing machine. The rigid arms function as loading arms and simultaneously as rod coupling devices. Each rigid arm features a vertical specimen hole to accommodate the rod. It can be seen that the coupling of rod to the rigid arms through Teflon layers, in fact, does not enable the drop-into be realized for the specimen installation. A press-fit process is generally required to have the compliant layer properly contacted with the specimen hole, which is not feasible in hot cell. Linear bearings have been investigated subsequently. Use of linear bearing allows the axial motion of the rod under bending, but also needs two rigid sleeves pre-mounted to the two holding areas of the rod. Between the rod and the rigid sleeve, a compliance layer is still used to transfer loading from the rigid arms to the rod and to protect the rod from the contact damage. Testing showed that direct integration of a linear ball bearing (LBB) into the rigid arm could create substantial backlash in reverse bending. In a more advanced design, the rigid arms were split along the LBB axis. Such splitting resulted in a large arm body and a small end-block for a given rigid arm. Linear roller bearings (LRBs, THK FT2515-45L) were embedded in the two V-shaped surfaces modified from the mating halves of cylindrical grooves. Thus, the rod specimen is installed into the test fixture by opening and closing the end-blocks in the upper and lower rigid arms. LRBs are preloaded through bolting and are secured with compression springs and associated retainers as demonstrated in Fig. 5. It is worthwhile noticing that the used LRBs have a higher dynamic loading capacity than LBBs and can provide a much more reliable performance in service. Although Teflon can be a plausible approach for compliance layer, cast epoxy has been adopted because the in situ casting of epoxy is considered to be more feasible in hot cell than the press-fit or shrink-fit required in assembling a Teflon tube to the rod.

Counterweights ($62 \times 38 \times 54$ mm) were introduced to eliminate the effect of self-weight on rod deformation. The original arms were, therefore, extended on the side opposite to the rod accordingly to accommodate such a need. A slope of 30° was created to prevent the upper and lower arms from interfering themselves in the extremely close position. Additional engineering of rigid arm involved shortening loading arm into 101.6 mm to optimize the dynamic behavior of the U-frame. This alternative loading arm for the bearing shafts of the straddle legs was made available simply by drilling an additional hole to the rigid arms. The maximum stress of rod was shown to be decreased due to the reduced loading arms. Nevertheless, shortening the loading arms apparently drives up the resonant frequency of the U-frame, as validated by the FEA study [23].

Although pins were used in our simulation, precision ball bearings have been shown to be a better solution for pivoting corners. The bearings are durable and do not require special maintenance such as oiling for pins, which is very important for testing in a hot-cell environment. Bearing 6302 was selected on the basis of the anticipated loading requirement (890 N). The bearing had a

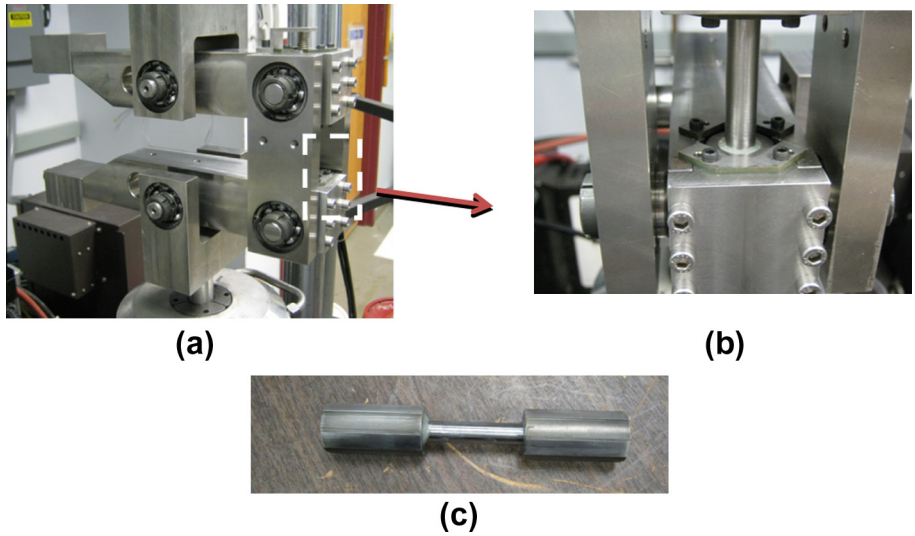

Fig. 5. (a) U-frame setup equipped with linear roller bearings (LRBs) that are preloaded by bolting the end blocks. The enlarged view in (b) shows the rod inserted. The rigid sleeves have an octagonal shape and are mounted to the rod with cast epoxy as shown in (c).

static and dynamic load rating of 5338 N and 8585 N, respectively. The lifetime (millions of revolutions) [24] of the bearing for the application is estimated as 8.98×10^8 cycles. A pair of ∅15 mm shafts was made symmetrically on both sides of the rigid arm for mounting the bearings. The shear stress of the shaft under the required loading capacity is critical and was found to be much lower than the shear yield stress of SS 304 (based on Mises criterion).

The purpose of side connecting plates is twofold. First, they connect the upper and lower rigid arms and, therefore, house the ball bearings used in pivoting corners. The cross section of the side plates was thus designed to measure 50.8×13 mm, with a thickness (13 mm) same as that of ball bearings. Second, they are subjected to push–pull motions transferred from the rigid arms. Thus, the tensile stress at the maximum cut of the section near the bearing shaft holes needs to be examined. The calculation under the designed load (890 N) indicated that the stress on the plates (8 MPa) was again far less than the yield stress of SS 304 (290 MPa).

The linkage of the rigid arm to the loading rod is achieved by use of a straddle structure. The cross member of the straddle was a thick T-shaped beam equipped with two legs at the side. A hinge connection was implemented between the rigid arm and the straddle by using the same bearings as those in the pivoting corners. However, the bearing shaft is not built in but coupled with the rigid arm through a set screw in the end face of the rigid arm. The link of the U-frame setup to the testing machine depends on the platen of the testing machine. For the MTS hydraulic testing machine with loading frame 810, collets are available for coupling the loading rod of the testing setup to the testing machine. The overall size of the completed U-frame setup including mounts and linkages is $319.74 \times 409.4 \times 116.8$ mm.

5. Instrumentation and measurement

5.1. Instrumentation for testing and measurement of fuel rod

Under an input load, instrumentation must accurately measure the deflection of the rod being bent. Non-contact measurement methods such as laser vibrometry and digital image correlation (DIC) were examined but were not found to be feasible because of some restrictions that these methods impose. First, the effect of the hot-cell window on the laser beam is unknown. Second, speckles of paint are needed in DIC on the surface of the fuel rod to track displacement, and uncertainty is involved with the reliability of paint speckles as the surface of a spent fuel rod itself is damaged. Among the contact methods, strain gages require dedicated mounting procedures, and the rough surface of spent fuel prevents an effective mounting. Finally, the instrument must survive a reasonable duration in the hot cell.

Both LVCs (linear variable capacitors) and LVDTs (linear variable differential transducers) were evaluated and compared. LVCs were used in an earlier stage of the project for calibrating the setup. LVDTs of the spring return version were finally chosen because they have been demonstrated to work in extreme environments like the hot cell. With the built-in spring, the probe or armature can maintain contact with the surface to be measured. A probe with a flat head can be used in cases where the surface is not flat, such as the rod. This can avoid wobbling of the head around the cylindrical rod if a spherical one is used.

5.2. Measurement of fuel rod in bending fatigue

Given the presence of the compliant material, how will the curvature of the rod be measured? Theoretically, the bending radius R and maximum strain ε_{max} of a rod can be readily estimated on the basis of the displacement at the loading end of the rigid arm. The displacement measured, however, is believed to contain the contribution of the compliant layers. To address this issue, Bjorkman proposed a three-point measurement method to evaluate the curvature of a bending rod [36]. The three-point measurement was performed in this study through the following approach. (1) Three LVDTs were used to capture the deflection of the rod. (2) A clamping mechanism integrated three C clamps with alternating openings to accommodate three sensors. (3) The sensor clamp was mounted on the side connecting plates of the U-frame to eliminate any unwanted rigid-body motion. The three-point measurement on the MTS 810 is illustrated in Fig. 6. Given the deflections from three LVDTs, d_1, d_2, and d_3, the radius of the bending rod can be evaluated (as shown in Fig. 7):

$$R = \sqrt{(x_0 - d_2)^2 + y_0^2}, \tag{1}$$

$$x_0 = \frac{-2m_a m_b h - m_a(d_2 + d_3) + m_b(d_1 + d_2)}{2(m_b - m_a)},$$

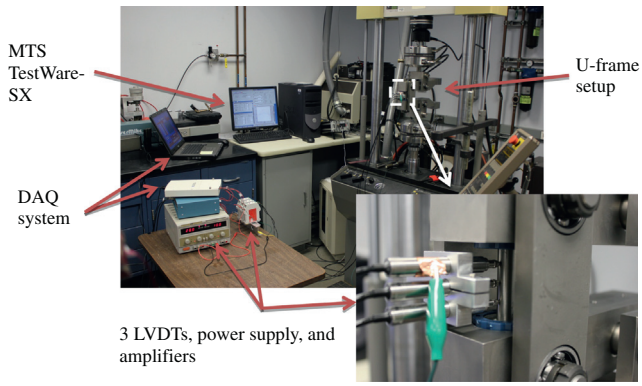

Fig. 6. Demonstration of the three-point measurement method using three LVDTs. The U-frame setup is equipped with LBBs and integrated on a MTS 810 servo-hydraulic testing machine.

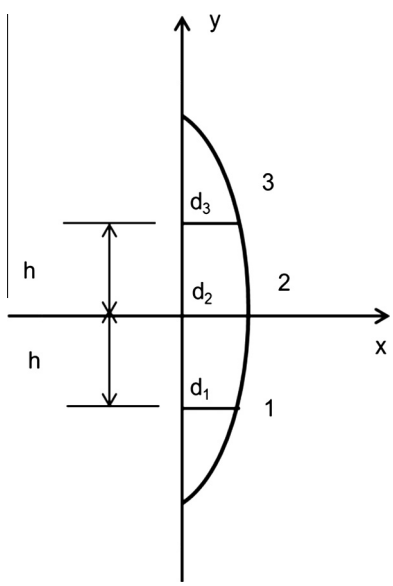

Fig. 7. Determination of the curvature of the bending rod by use of deflections measured at three points.

$$y_0 = -\frac{1}{m_a}\left(x_0 - \frac{d_1 + d_2}{2}\right) - \frac{h}{2},$$

where

$$m_a = \frac{h}{d_2 - d_1},$$

$$m_b = \frac{h}{d_3 - d_2},$$

and h is the sensor distance, 12 mm. The curvature κ can thus be determined as follows:

$$\kappa = 1/R. \quad (2)$$

Furthermore, the flexural rigidity EI (the product of Young's modulus E and moment of inertia I) of a rod can be estimated by using the applied moment M and the induced curvature,

$$EI = M/\kappa. \quad (3)$$

Young's modulus of a rod can be further written as

$$E = M/\kappa I.$$

At the same time, the fracture stress of the bending rod can be determined by

$$\sigma = Ma/I \quad (4)$$

in which a is the radius of the rod and M is the maximum moment applied.

6. Case study

Various surrogate rods were prepared to test the U-frame setup on the MTS 810 servo-hydraulic testing machine and to identify application issues. The conditions of the rods are listed in Table 4. All of the rods had SS 304 cladding except case 1 in which only a high density alumina rod was used. These rods were assembled with rigid sleeves using epoxy and, therefore, had epoxy as compliant layers. The surrogate rods in cases 1–3 featured the circular rigid sleeve used for the U-frame setup equipped with LBBs, whereas those in cases 4 and 5 had the octagonal one for the setup with LRBs.

6.1. Unidirectional bending test of alumina rod

Two as-received alumina rods (∅9.525 × 152.4 mm) were used to verify the response of the rod in the U-frame setup. The main mechanical properties of the rod material are given in Table 5 [37]. These rods were integrated to two rigid sleeves with cast epoxy. The compliant layers formed of the cast epoxy had ID 9.525 mm, OD 15.0 mm, and length 50.8 mm. Testing was conducted by use of the U-frame with LBBs on the MTS testing machine with force control; triangular waves in compressive mode were used. The periods of the waveforms were defined according to the peak load and loading/unloading rate. Specimen 1 was tested with peak loads of −100, −150, −200, −250, and −300 N. Specimen 2 was tested with two cycles whose peak loads were −200 and −300 N, respectively. The rate in all tests was maintained at ±10 N/s, which was considered quasi-static loading.

Both rods fractured when tested in the cycle to −300 N. The moment–deflection curves of the three LVDTs were linear before the rod fractures. The curvature was calculated from measurements of the three LVDTs as discussed in Section 5.2. The estimates of flexural rigidity, Young's modulus, and fracture stress were further made and are given in Table 6. A deviation of about 6–10% in Young's modulus was observed between the measurements and the data provided by the manufacturer. The discrepancy observed was mainly due to the variation in composition and fabrication of the alumina. The measurement method also has a certain effect on the mechanical results of brittle materials because a stress gradient is involved in bending but not in uniaxial loading. At the same time, the fracture stress actually fell in the data range provided by the manufacturer.

6.2. Displacement analysis in unidirectional bending

A surrogate rod composed of a SS tube and cast epoxy was used to develop an approach to analyzing the displacement measured at the loading end of the rigid arms. The SS tube had ID 9.45 mm, OD 11.07 mm, and length 152.4 mm. The cast epoxy was also used as a compliant layer with ID 11.07 mm, OD 15.00 mm, and length 50.80 mm. The test was conducted using the U-frame equipped with LBBs on the MTS testing machine in compressive mode. Five cycles were used with the peak levels −100, −150, −200, −250, and −300 N.

Fig. 8 illustrates the moment–curvature curve based on three LVDT measurements. Obviously, the loading/unloading cycles with increasing amplitude resulted in an increased irreversible or plastic

Table 4
Surrogate rod and test conditions used in application of the U-frame setup.

Case	Stainless steel (SS) tube (mm)	Content (mm)	Compliant layer, epoxy (mm)	Test condition
1	N/A	Alumina rod: ∅9.525 × 152.400	ID 9.525, OD 15.000, length 50.800	Unidirectional triangular wave in compressive mode
2	ID 9.450, OD 11.070, length 152.400	Epoxy: ∅9.450 × 152.400	ID 11.070, OD 15.000, length 50.800	Unidirectional triangular wave in compressive mode
3	ID 9.450, OD 11.070, length 152.400	Alumina rod: ∅9.450 × 152.400	ID 11.070, OD 15.000, length 50.800	Measurement: Unidirectional triangular wave in compressive mode. Cycling: Unidirectional sine wave in compressive mode
4	ID 9.525, OD 11.070, length 152.400 ID 9.600, OD 11.070, length 152.400 ID 9.525, OD 11.070, length 152.400	Empty Alumina pellets: 10 × ∅9.525 × 15.200 Epoxy: ∅9.525 × 152.400	ID 11.070, OD 15.000, length 50.800	Measurement: reverse triangular wave
5	ID 9.600, OD 11.070, length 152.400	Alumina pellets: 10 × ∅9.525 × 15.200	ID 11.070, OD 15.000, length 50.800	Measurement: reverse triangular wave. Cycling: reverse sine wave

Table 5
Main properties of alumina rod.

Diameter (mm)	Moment of inertia, I (mm^4)	Young's modulus[a] E (GPa)	Flexural strength[a] (MPa)
9.525	404.045	372.000	275.0–379.000

[a] Ref. [37].

Table 6
Young's modulus and fracture stress of alumina rods obtained by use of U-frame test setup.

Rod 1			
Load (N)	−200	−250	−294
Flexural rigidity, EI (N m^2)	160.020	151.384	
Young's modulus, E (GPa)	396.045	374.671	
Failure stress (MPa)			352.000
Rod 2			
Load (N)	−200	−286	
Flexural rigidity, EI (N m^2)	149.352	165.134	
Young's modulus, E (GPa)	369.641	408.702	
Failure stress (MPa)		342.000	

curvature; a cyclic strain–stress curve followed the monotonic curve once the reloading exceeded the unloading point in the previous cycle. The moment and flexural rigidity as a function of accumulated irreversible curvature can be seen from Fig. 9. The flexural rigidity is the ratio of moment change to curvature change over the unloading or loading path. The unloading flexural rigidity was defined over the initial unloading segment as shown in Fig. 8, which should reduce the uncertainty relevant to the kink in the unloading [23]. As a result, the value of the obtained unloading rigidity was higher than that of the loading. The unloading rigidity also changes more significantly than the loading one. The loading rigidity is thus used in the following discussion. Overall, the loading rigidity stayed between 65 and 70 N m^2. The loading rigidity at zero irreversible curvature is, in fact, quite close to the rigidity estimated (EI = 68 N m^2) based on geometries and Young's moduli of SS tube and epoxy [37,38]. The marginal difference can be attributed to the composition and stress history of SS or the bonding between the cast epoxy and SS tube.

The response of the compliant layers is important because the setup relies on these layers to transfer the bending moments to the rod. Within the assembled rod, the pressure created in the compliant layers by the loading is unevenly distributed over the length of the rigid sleeves, which causes the rigid sleeves to rotate relative to the rod. The rotation actually measures the response of the compliant layers because the deformation of the rigid sleeves is

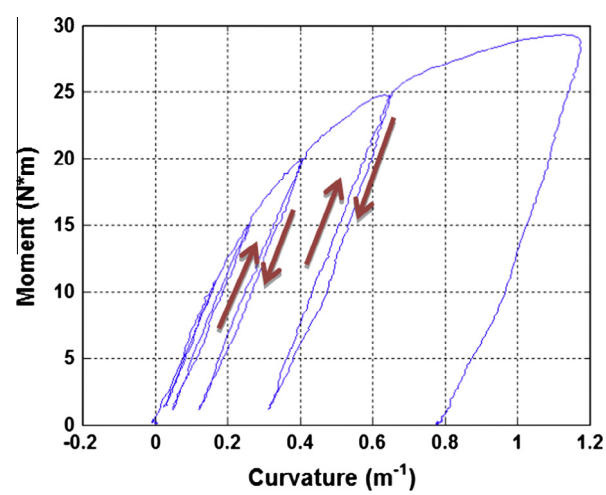

Fig. 8. The moment–curvature relationship of surrogate rod (SS plus epoxy) obtained with the LBB U-frame on the MTS testing machine in force control mode and with a 101.6 mm loading arm.

negligible. Nevertheless, the rotation could generate a sizable displacement at the loading point. With the aid of decomposition of displacement, the compliant-layer-induced displacement can be written as

$$\Delta Z_{comp} = \Delta Z_{total} - \Delta Z_{initial} - \Delta Z_{rod} \quad (5)$$

in which ΔZ_{total} is the total displacement at the loading point, $\Delta Z_{initial}$ is initial displacement due to the initial contact, and ΔZ_{rod} is displacement due to the bending rod. The latter can be estimated as

$$\Delta Z_{rod} = \kappa L d \quad (6)$$

where κ, L, and d are the curvature, gage length, and loading arm, respectively. Therefore, the compliant-layer-induced rotation can be quantified as follows:

$$\theta_{comp} = \tan^{-1}(0.5\Delta Z_{comp}/d). \quad (7)$$

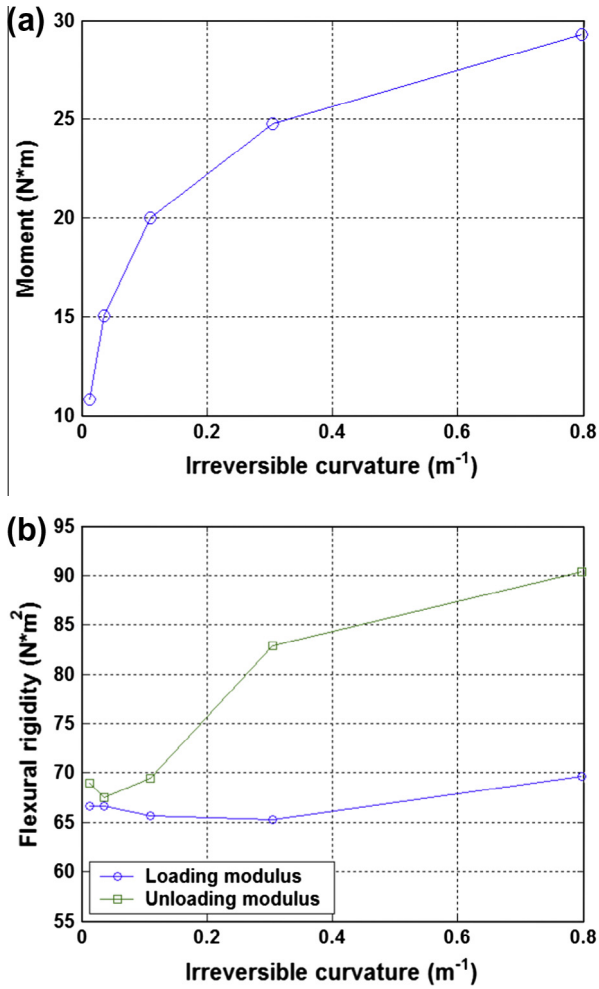

Fig. 9. Moment (a) and flexural rigidity (b) of the surrogate rod as a function of irreversible or plastic curvature.

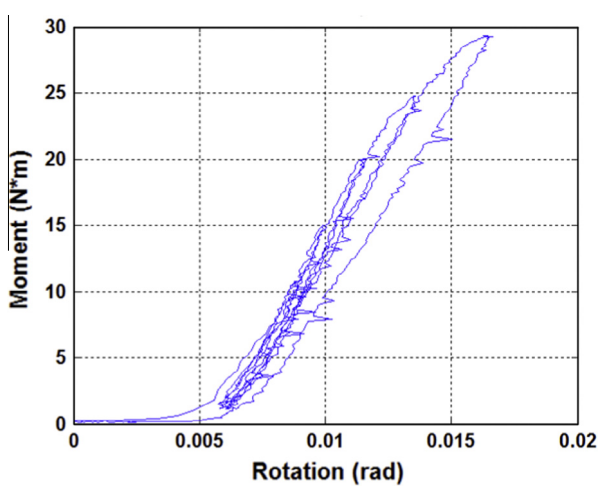

Fig. 10. The moment–rotation curve of the compliant layer (epoxy) used in mounting the rigid sleeves on the surrogate rod.

The moment–rotation relationship of the compliant layer is given in Fig. 10. The moment obviously increased with accumulated irreversible rotation. The rotational stiffness (moment per unit of rotation) of the compliant layer as a function of accumulated irreversible rotation is shown in Fig. 11. It can be seen that loading

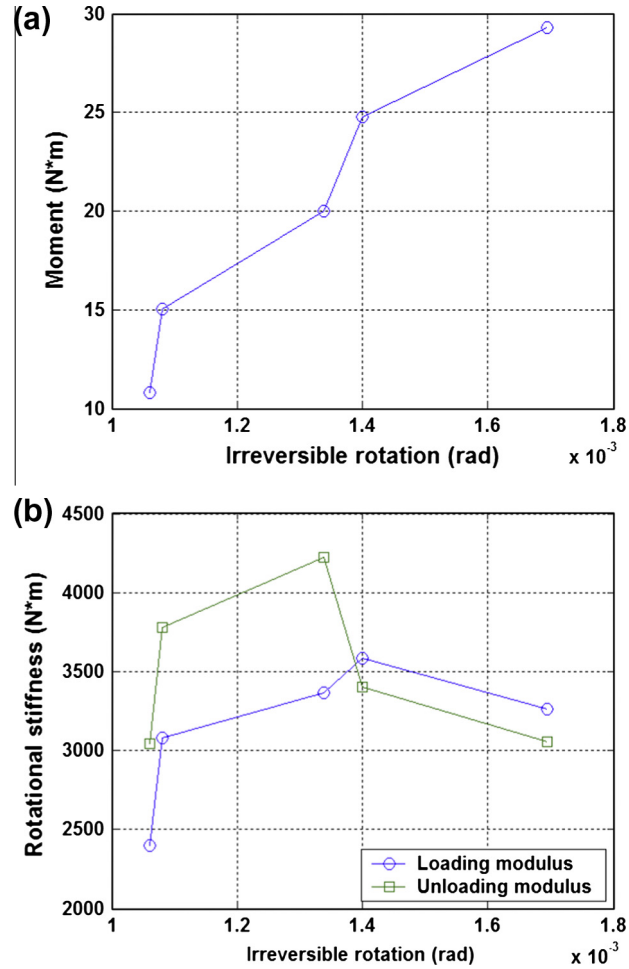

Fig. 11. (a) Moment and (b) rotational stiffness as a function of irreversible rotation for the compliant layer of the surrogate rod.

stiffness fluctuated a little after an initial rise. However, the variation was generally limited between 2400 and 3600 N m. Thus, the compliant layer retained its load-bearing capacity throughout the loading process.

6.3. Test protocol development using unidirectional cyclic bending

A rod composed of a SS tube with an alumina rod insert was used to develop a test protocol for a cyclic test. The SS tube was of the same size as that in Section 6.2. The alumina rod was essentially of the same material as that in Section 6.1, but the diameter was reduced to 9.45 mm by grinding to match the ID of the SS tube. The compliant layer, also of the same size as that in Section 6.2, was made of cast epoxy.

The cyclic bending test consisted of two parts. The first part was the measurement that served as the input to experimental design and as the evaluation of rod properties. The cycling was interrupted for measurement at the following cycles: 10^0, 10^2, 10^3, 10^4, 10^5, 3×10^5, 8×10^5, and 10^6. The measurement was conducted in compressive mode; two triangular waveforms were used in the measurement with peak loads of −200 N and −250 N, and a loading rate of 10 N/s. The second part was the cycling, which involved a unidirectional sine wave in compressive mode driving the specimen into the designed number of cycles. The input wave had a peak load of −250 N with frequencies varying from 1 to 5 Hz. Both measurement and cycling were carried out using the U-frame with LBBs on the MTS testing machine.

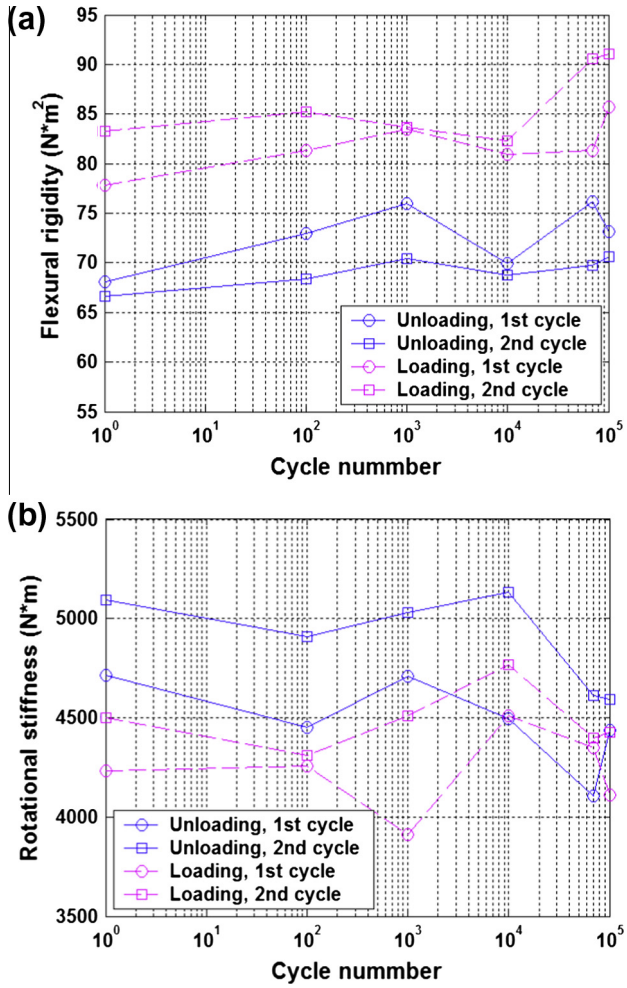

Fig. 12. (a) Flexural rigidity of surrogate rod and (b) rotational stiffness of compliant layer as a function of cycle number for composite rod (SS tube plus alumina rod). Results are based on measurements with two loading cycles: 1st cycle with 200 N, and 2nd with 250 N. Unidirectional cyclic bending was conducted using LBB U-frame setup.

A relatively large displacement was observed from the MTS readout in the first run. It was believed that the alumina rod had been damaged by the grinding performed in the specimen preparation, which resulted in a reduced flexural stiffness of rod and further an increased rotation of rigid arms. Nevertheless, the SS tube fractured when the cycling approached 3×10^5 cycles. Variations obtained for the flexural rigidity of the rod and the rotational stiffness of the compliant layers with the number of cycles are illustrated in Fig. 12. The unloading path of the measured moment–curvature curve was not a straight line, and the evaluation of unloading rigidity was subsequently based on a linear segment in later unloading [23]. The value of unloading rigidity was thus lower than that of loading rigidity. Meanwhile, the measured rigidity seemed to depend on the peak loads used; however, the variation due to the peak measurement loads was not as significant as that in the rigidity definition based on loading or unloading.

It can be seen that the flexural rigidity of loading tended to increase with the number of cycles to a certain degree. The increase in rigidity is believed mainly due to the cyclic hardening of SS, because the SS tube was the major load-bearing element after the alumina rod fractured. On the other hand, the rotational stiffness of the compliant layers experienced some fluctuations before 10^4 cycles but stabilized afterward. In other words, the epoxy layers have the durability required for the bending fatigue test. Overall, the rod delivered a loading flexural rigidity varying from 78 to

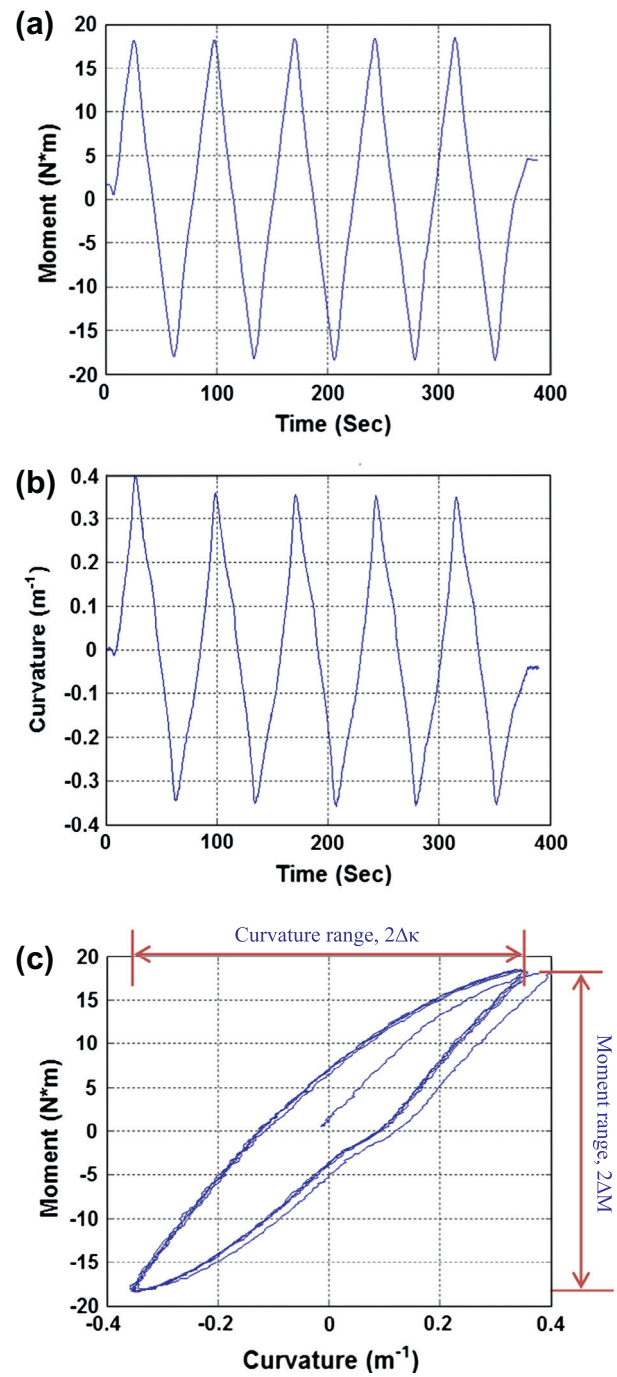

Fig. 13. (a) Moment curve, (b) curvature curve, and (c) moment–curvature loops obtained by use of the U-frame with preloaded LRBs. The results are based on testing of the surrogate rod made of SS tube only under ±180 N, 10 N/s.

90 N m^2, with a lower value but less fluctuation at the −200 N measurement. The pre-fatigue flexural rigidity of the measurement suggests that, if the SS tube retained its full rigidity, the residual rigidity of the fractured alumina rod was around 7.5% of its original rigidity.

6.4. Backlash evaluation and pellet effect in reverse bending

A surrogate rod composed of SS tube only was used in this case to demonstrate the effectiveness of the U-frame with LRBs in eliminating backlash. Octagonal rigid sleeves were integrated to the SS tube (ID 9.525 mm, OD 11.07 mm, and length 152.4 mm) by use of

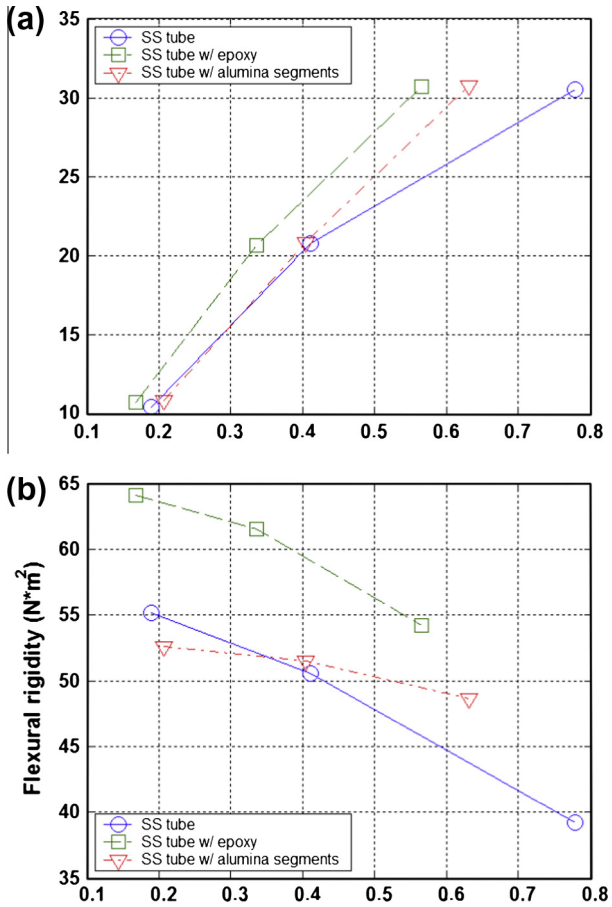

Fig. 14. (a) Moment and (b) rigidity range as a function of curvature obtained for SS tube only, SS plus alumina pellets, and SS plus epoxy. The data were obtained by use of the LRB U-frame setup.

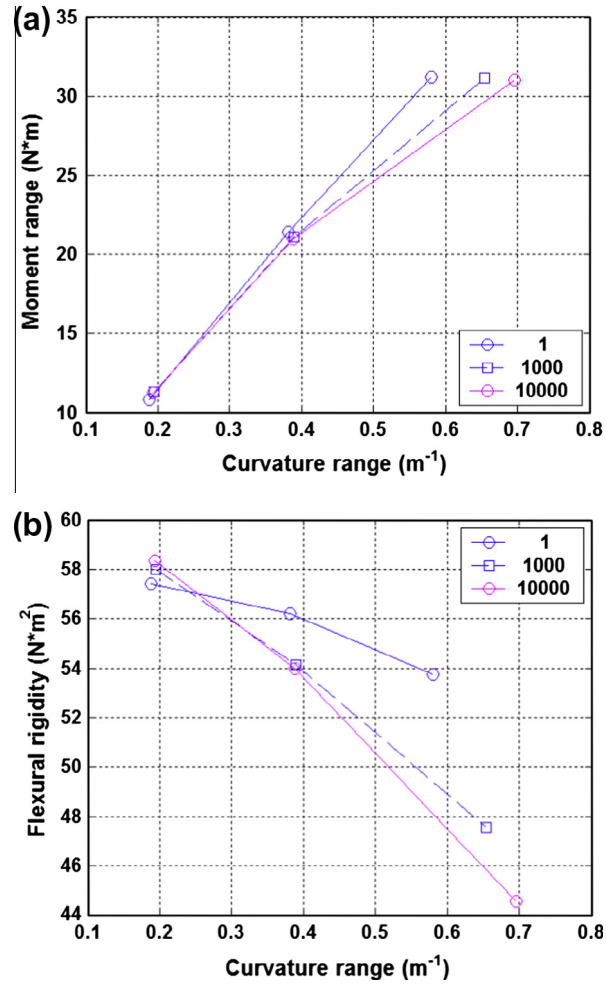

Fig. 15. (a) Moment and (b) rigidity range as a function of curvature obtained for surrogate rod (SS cladding plus 10 alumina pellets). The data were based on measurements. The reverse cyclic bending test was conducted using the LRB U-frame setup.

epoxy. The epoxy also served as compliant layers of the same size as that in Section 6.2. The tests were conducted on the MTS testing machine. Reverse triangular waves were used in testing with peaks of ±50, ±100, ±150, and ±180 N at a rate of ±10 N/s; the results for ±180 N are shown in Fig. 13. The loading curves indicate that the backlash related to the LBB U-frame setup was removed effectively by the U-frame with preloaded LRBs. The moment–curvature loops revealed a substantial hysteresis due to the plastic deformation involved. To characterize the rod properties in reverse bending, flexural rigidity was defined as the ratio of moment range to curvature range, or the slope of the secant line passing through the loop tips. This is different from the loading/unloading rigidity used in unidirectional bending.

Fig. 14 illustrates the variations of moment and flexural rigidity as a function of curvature for three types of surrogate rods. The rigidity increases in the following order: SS tube only, SS tube plus alumina pellets, and SS plus epoxy. It is worthwhile noting that the SS tube in the second group was made with a larger ID (9.6 mm) to allow the alumina pellets to fit inside. In total, 10 pellets (∅9.525 × 15.24 mm) were contained in the SS tube. These pellets were made contacted without any bonding. The different ID may explain the lower value for the SS tube plus alumina pellets in the lower curvature level, a value even lower than for the SS tube only. However, it can be seen that the rod picked up load quickly once the pellets became engaged with the SS tube, resulting in quite a large rigidity in the higher curvature levels. This is because the initial clearance between the pellets and inside surface of cladding prevents a full contact. The effect of epoxy on the surrogate rod response can be seen clearly from the parallel rigidity curves of the SS tube only and SS tube plus epoxy. The parallel curves illustrate that surrogate rod rigidity was enhanced over the whole range of curvature. This is reasonable because the epoxy bonded with the SS tube and was fully coupled during the entire process. This is markedly different from the case of SS tube plus alumina pellets.

The results of flexural rigidity are also observed to be lower than what was expected. For the surrogate rod of SS tube only, a flexural rigidity of 55 N m^2 near 0.2 m^{-1} curvature range suggests an approximately 15% decrease based on manufacturer's data sheet [37]. Besides the difference in material compositions, the machining required to modify an as-received tube into the target size may play a certain role. It is believed that the machining either modified mechanical properties of the SS tube or introduced the substantial variance in cladding thickness. Uniaxial tensile tests on the modified SS tube were designed and conducted as a part of verification, and it has been found that Young's modulus of the machined tube varied from 176 to 195 GPa. Such variation shall account for the discrepancy observed above for the flexural rigidity.

6.5. Reverse cyclic bending test and on-line monitoring

A surrogate rod made of SS cladding and 10 alumina pellets was used in this case to illustrate both the measurement and on-line

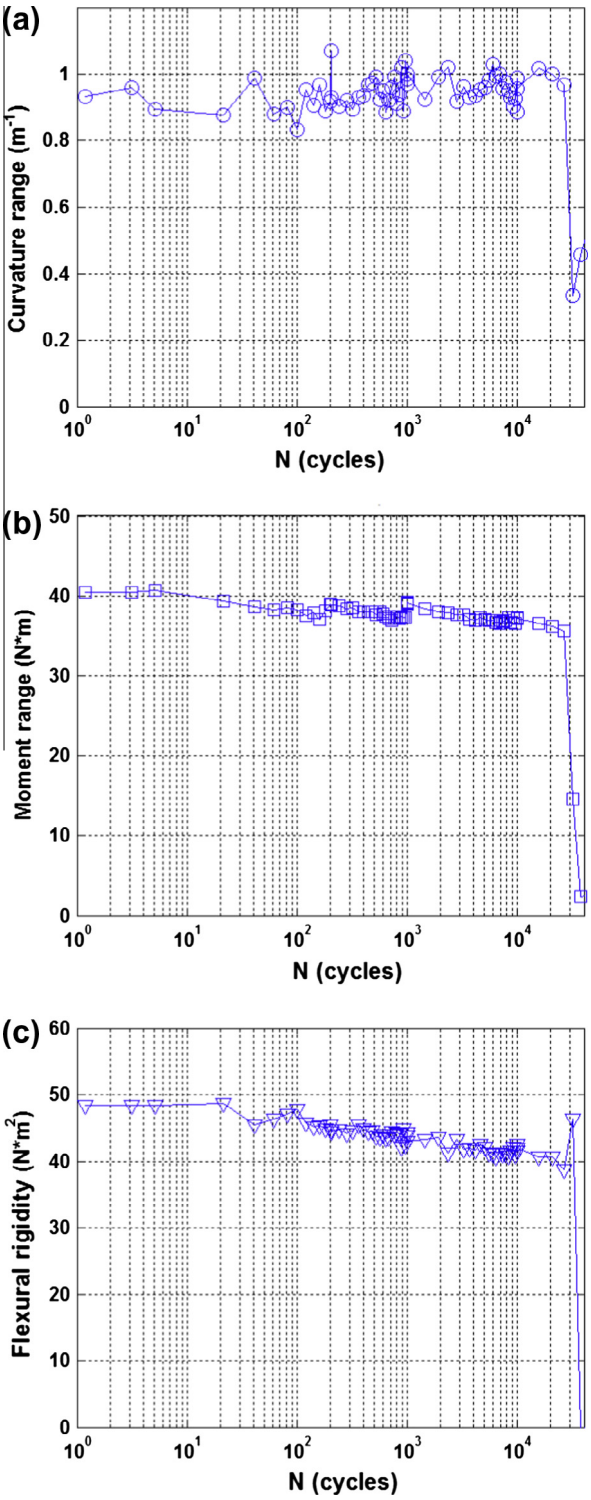

Fig. 16. (a) Curvature, (b) moment, and (c) rigidity as a function of number of cycles based on the on-line monitoring.

monitoring of the U-frame test system. The surrogate rod had the same configuration and materials as that used in Section 6.4. The octagonal rigid sleeves were mounted into the surrogate rod with cast epoxy as discussed above. Eight Teflon strips ($50.8 \times 8.0 \times 0.38$ mm) were attached to the rolling surfaces of the rigid sleeves to protect them from contact damage. The reverse cyclic bending testing consisted of measurements and cycling, and was carried out on the MTS machine with the U-frame equipped with LRBs. The measurements were conducted when the cycling was interrupted at the specified number of cycles and included three cycles of triangular waves with peaks of ±50, ±100, and ±150 N at a rate of ±10 N/s. The cycling involved sine waves with amplitude of ±4 mm at 2 Hz. On-line monitoring was enabled with data acquired during the cycling for force and displacement at loading point, and three-point deflections.

Fig. 15 illustrates the moment–curvature relationship and the variation in rigidity as a function of curvature based on the measurements before the fracture of the rod. In spite of variation with curvature, the initial level of rod rigidity in this test is close to that of the similar SS tube plus alumina pellets in Section 6.4. For example, the flexural rigidity was shown to be 54 N m^2 at load range 30 N m, which is near 49 N m^2 at the same load range in Section 6.4. Therefore, the measurement of flexural rigidity was reasonably consistent, considering the variation introduced by the machining. The decrease in rigidity induced by cyclic softening amounted to 19% at 10,000 cycles. On-line monitoring (Fig. 16) captured the fracture point near 2.62×10^4 cycles. It is shown that the curvature range was fairly stable around 0.95 m^{-1} because of displacement control, even though a certain fluctuation was observed. The rod rigidity was initially approximately 48 N m^2 and dropped to 39 N m^2 before failure. The extent of degradation in rigidity is equivalent to that captured by the measurement and can therefore serve as input to the lifetime prediction model of the rod.

7. Conclusion

A U-frame-assisted bending fatigue system was developed in this study, and the present paper has described design and analysis, engineering processes, and instrumentation and measurement. The U-frame bending system is mainly composed of a U-frame testing setup and a curvature measurement method. (1) The U-frame setup consists of two rigid arms, side connecting plates, and linkages to a universal testing machine. The rod specimen is arranged co-planar with the connecting plates and coupled with the rigid arms through a dedicated mechanism. In the advanced design, linear roller bearings are embedded into the split rigid arms to accommodate the rod through opening and closing. (2) The curvature of the bending rod is obtained through a three-point deflection measurement method. Three LVDTs are utilized and clamped into the side connecting plates of the U-frame to capture the deformation of the rod. The curvature measurement is immune to the effects arising from compliant layers and rigid-body motion of the machine.

The U-frame system has several unique features: (1) The setup enables installation of the rod by simple insertion and closing. (2) The reverse cyclic bending test can be conducted effectively and efficiently by push–pull at the loading point of the setup. Therefore, any test machine with a linear motion function can be used to drive the setup. (3) A minimal number of linkages (only two) to the universal machine are used. These features are crucial aspects of testing that facilitate the operation of manipulators in hot cell while reverse cyclic bending is being accomplished.

A test protocol for the reverse cyclic bending test was developed. The protocol consists of two important parts, measurements and cycling. The measurements are conducted at a specified number of cycles when the cyclic test is interrupted. The measurements offer an important approach to characterizing the rod properties. On the other hand, the cycling is implemented with the target cyclic condition; on-line monitoring provides continuous data acquisition during the cycling on the force and displacement at the loading points, and three point deflections in the gage section of the rod.

Several interesting phenomena have been revealed using surrogate rod testing that may cast light on the response of a spent fuel rod. (1) Unidirectional cyclic bending produced increased flexural rigidity of surrogate rods prior to fracture. The strain and cyclic hardening of SS cladding is believed to be responsible for the increased rigidity of the rods. (2) Meanwhile, the performance of cast epoxy layers was quite stable in cyclic bending as validated by the evaluation of rotational stiffness. (3) Pellets imposed a certain amount of effect on the response of surrogate rods. The pellet-cladding interaction during the loading seemingly depends on the epoxy bonding. (4) Dynamic cyclic load in reverse mode exhibited a substantial cyclic softening prior to the fracture of the surrogate rod. The degree of decrease in flexural rigidity is consistent in both measurements and on-line monitoring. The developed monitoring technique can thus serve as an important tool to predict the life of rod under test.

Acknowledgments

The authors gratefully acknowledge Dr. James Hemrick for reviewing this manuscript. Authors also want to thank Brian Sparks, and Randy J. Parten of ORNL for their help in machining the components of the U-frame setup. The research was sponsored by NRC RES under DOE contract DE-AC05-00OR22725 with UT-Battelle, LLC.

References

[1] NRC, General Standards for all packages, §43(f) in Title 10, Code of Federal Regulations, Part 71, Packaging and transportation for radioactive material, US Nuclear Regulatory Commission, Washington, DC, Dec. 6, 2010.
[2] F.E. Ostrem, W.D. Godshall, An Assessment of the Common Carrier Shipping Environment, General Technical Report FPL 22, Forest Products Laboratory Forest Service, US Department of Agriculture, Madison Wis., 1979.
[3] B. Hanson, H. Alsaed, C. Stockman, D. Enos, R. Meyer, K. Sorenson, Gap Analysis to Support Extended Storage of Used Nuclear Fuel, US DOE Used Fuel Disposition Campaign, FCRD-2011-000136 Rev. 0, January 2012.
[4] W. Weibull, Fatigue and Analysis of Results, Pergamon Press, New York, 1961. pp. 31–65.
[5] A.E. Carden, Fatigue at elevated temperatures: a review of test methods, in: A.E. Carden, A.J. McEvily, C.H. Wells (Eds.), Fatigue at Elevated Temperatures, ASTM STP 520, ASTM, Philadelphia, 1973, pp. 195–223.
[6] ASTM, Manual on Low Cycle Fatigue Testing, ASTM STP 465, ASTM, Philadelphia, 1969.
[7] ASTM E-9 Committee on Fatigue, in: S.R. Swanson (Ed.), Handbook of Fatigue Testing, ASTM STP 566, ASTM, Philadelphia, 1974, pp. 19–84.
[8] ASTM B 593-96, Standard Test Method for Bending Fatigue Testing for Copper-Alloy Spring Materials, ASTM International, West Conshohocken, PA, August 2009.
[9] M.A. Abojaradeh, M.W. Witczak, M.S. Mamlouk, K.E. Kaloush, J. Test. Eval. 35 (2007) 1–8.
[10] T.K. O'Brien, A.D. Chawan, R. Krueger, I.L. Paris, Int. J. Fatigue 24 (2002) 127–145.
[11] W.D. Bowman, End constraint and alignment effects in three and four point tension-compression bending tests, in: R. Papirno, H.C. Weiss (Eds.), Factors That Affect the Precision of Mechanical Tests, ASTM STP 1025, ASTM, Philadelphia, 1989, pp. 174–184.
[12] L. Bertele, A. Papack, K.-H. Wichmann, Testing Device for Performing Four Point Fatigue Strength Tests under Alternating Bending Stresses, US Patent 5231882, 1993.
[13] T.B. Zineb, A. Sedrakian, J.L. Billoet, Compos. B: Eng. 34 (2003) 447–458.
[14] H.R. Jhansale, T.H. Topper, Equipment for cyclic deformation and fatigue studies in pure bending, paper 1726, in: SESA Fall Meeting, Society for Experimental Stress Analysis, Boston, MA, Oct. 18–22, 1970.
[15] R. Lagneborg, R. Attermo, Metall. Trans. 2 (1971) 1821–1827.
[16] N. Gao, M.W. Brown, K.J. Miller, P.A.S. Reed, Int. J. Fatigue 29 (2007) 565–574.
[17] P.G. Forrest, A.B. Penfold, Engineering (London) 192 (1961) 522–523.
[18] D.J. White, Proc. Inst. Mech. Eng. 184 (1969) 223–240.
[19] A.D. Batte, R.A.T. Dawson, E.B. Evans, G. Thomas, Reverse-bend testing to obtain long-term endurance data, in: G. Sumner, V.B. Livesey (Eds.), Techniques for High Temperature Fatigue Testing, Elsevier Appl. Sci. Pub., London, 1985, pp. 97–115.
[20] T. Zhai, Y.G. Xu, J.W. Martin, A.J. Wilkinson, G.A.D. Briggs, Int. J. Fatigue 21 (1999) 889–894.
[21] A.A. Tayebali, J.A. Deacon, C.L. Monismith, National Research Council, Transportation Research Board, Transportation Research Record 1545 (1996) 89–97.
[22] J.-A.J. Wang, H. Wang, Y. Yan, R. Howard, B. Bevard, High Burn-up Spent Fuel Vibration Integrity Study Progress Letter Report (Out-of-Cell Fatigue Testing Development – Task 2.1), ORNL/TM-2010/288, Oak Ridge National Laboratory, Oak Ridge, TN, 2011.
[23] J.-A.J. Wang, H. Wang, T. Tan, H. Jiang, T. Cox, Y. Yan, Progress Letter Report on U-frame Test Setup and Bending Fatigue Test for Vibration Integrity Study (Out-of-Cell Fatigue Testing Development – Task 2.2), ORNL/TM-2011/531, Oak Ridge National Laboratory, Oak Ridge, TN, 2012.
[24] R.L. Norton, Machine Design, Prentice-Hall, London, 1996.
[25] http://www.engineersedge.com/plastic/materials_common_plastic.htm.
[26] http://www.eplastics.com/Plastic/Lexan_Polycarbonate_Sheet.
[27] K.J. Geelhood et al., PNNL Stress/Strain Correlation for Zircaloy, PNNL-17700, Pacific Northwest National Laboratory, Richland, WA, July 2008.
[28] BARC Highlights, Nuclear Fuel Cycle, Chapter 4, Bhabha Atomic Research Center, Trombay, Mumbai, India, 2007, pp. 35–39. <http://www.barc.ernet.in/publications/eb/golden/nfc/toc/Chapter%204/4.6.pdf>.
[29] Product Data Bulletin, 304/304L stainless steel, AK Steel Corporation. <http://www.aksteel.com>.
[30] Ceramic Properties Standard, CoorsTek, Inc. <http://www.coorstek.com>.
[31] http://www.engineeringtoolbox.com/friction-coefficients-d_778.html.
[32] http://www.bearingworks.com/content_files/pdf/retainers/PTFE%20datasheet.pdf.
[33] http://www.rpms.mace.manchester.ac.uk/cgi-bin/materials.pl/00039/.
[34] B.M. Ma, Nuclear Reactor Materials and Application, Van Nostrand Reinhold Co., New York, 1983. p. 175.
[35] D. Papaioannou, R. Nasyrow and V.V. Rondinella, W. Goll, H.-P. Winkler, R. Liedtke, D. Hoffmann, Fuel release experiments on irradiated fuel rodlets under transient impact conditions, in: European Commission, Joint Research Centre, Annual Meeting on Nuclear Technology, 12–14 May 2009, Dresden, Germany.
[36] G. Bjorkman, High burnup spent fuel testing program objectives, in: NRC Program Review Meeting, ORNL, Aug. 8, 2011.
[37] More About Glass, Ceramics, Carbon; More About Stainless Steel Alloys, Mechanical and Physical Properties. <http://www.mcmaster.com>.
[38] http://www.engineeringtoolbox.com/engineering-materials-properties-d_1225.html.

Proceedings of the 17th International Symposium on the Packaging and Transportation of Radioactive Materials
PATRAM 2013
August 18-23, 2013, San Francisco, CA, USA

Reversal Bending Fatigue Test System for Investigating Vibration Integrity of Spent Nuclear Fuel during Transportation*

J-A. Wang, H. Wang, B. B. Bevard, R. L. Howard
Oak Ridge National Laboratory

M. E. Flanagan
U.S. Nuclear Regulatory Commission

ABSTRACT

Transportation packages for spent nuclear fuel (SNF) must meet safety requirements under normal and accident conditions as specified by federal regulations. During transportation, SNF experiences unique conditions and challenges to cladding integrity due to the vibrational and impact loading during road or rail shipment. Oak Ridge National Laboratory (ORNL) has been developing testing capabilities that can be used to improve the understanding of the impacts on SNF integrity due to vibration loading, especially for high burn-up SNF in normal transportation operation conditions. This information can be used to meet the nuclear industry and U.S. Nuclear Regulatory Commission needs in the area of safety and security of spent nuclear fuel storage and transportation operations.

The ORNL developed test system can perform reversal-bending fatigue testing to evaluate both the static and dynamic mechanical response of SNF rods under simulated loads. The testing apparatus is also designed to meet the challenges of hot-cell operation, including remote installation and detachment of the SNF test specimen, in-situ test specimen deformation measurement, and implementation of a driving system suitable for use in a hot cell. The system contains a U-frame set-up equipped with uniquely designed grip rigs to protect the SNF rod sample and to ensure valid test results, and uses 3 specially designed LVDTs to obtain the in-situ curvature measurement.

A variety of surrogate test rods have been used to develop and calibrate the test system as well as in performing a series of systematic cyclic fatigue tests. The surrogate rods include stainless steel (SS) cladding, SS cladding with cast epoxy, and SS cladding with alumina pellet inserts simulating fuel pellets. Testing to date has shown that the interface bonding between the SS cladding and the alumina pellets has a significant impact on the bending response of the test rods as well as their fatigue strength. The failure behaviors observed from tested surrogate rods provides a fundamental understanding of the underlying failure mechanisms of the SNF surrogate rod under vibration which has not been achieved previously. The newly developed device is scheduled to be installed in the hot-cell in summer 2013 to test high burnup SNF.

*Notice: This manuscript has been authored by UT-Battelle, LLC, under contract DE-AC05-00OR22725 with the U.S. Department of Energy. The United States Government retains and the publisher, by accepting the article for publication, acknowledges that the United States Government retains a non-exclusive, paid-up, irrevocable, world-wide license to publish or reproduce the published form of this manuscript, or allow others to do so, for United States Government purposes.

I. INTRODUCTION

Spent fuel transportation has long been established as an important part of the industrial activities in the backend of the nuclear fuel cycle. An important factor to be taken into account is the current trend toward higher burnup, driven mainly by economic incentives in the competitive power market. Transportation packages for spent nuclear fuel (SNF) must meet safety requirements specified by federal regulations. For normal conditions of transport, vibration loads incident to transport must be considered. This is particularly relevant for high-burnup fuel (>45 GWd/MTU). As the burnup of the fuel increases, a number of changes occur that may affect the performance of the fuel and cladding in storage and during transportation. Spent fuel cladding has traditionally provided defense-in-depth as the primary fission product barrier in the nuclear fuel cycle, and has been relied upon to provide geometry control for criticality safety during transportation. The mechanical properties of high-burnup de-fueled cladding have been previously studied by subjecting defueled cladding tubes to longitudinal (axial) tensile tests, ring-stretch tests, ring-compression tests, and biaxial tube burst tests. The objective of this study is to investigate the mechanical properties and behavior of both the cladding and the fuel in the cladding (including inertia induced fuel pellet and clad interaction) under vibration/cyclic loads similar to the sustained vibration loads experienced during normal transport.

The vibration loads experienced by SNF rods during transportation can be characterized by dynamic, cyclic, bending loads. The transient vibration signals in a specified transport environment can be analyzed, and frequency, amplitude and phase components of the vibration can be identified. The methodology being developed at Oak Ridge National Laboratory (ORNL) is a novel approach to support the study of the vibration integrity of actual SNF rod segments through the testing and evaluation of the fatigue performance of SNF rods at defined frequencies and loads. ORNL has developed a reversal pure bending fatigue system to evaluate the response of the SNF rods to vibration loads as noted in Refs 1, 2 and 3. A three-point deflection measurement technique using linear variable differential transformers (LVDTs) is used to characterize the rod curvature of samples under test conditions, and electromagnetic force linear motors are used as the driving system to provide the mechanical load. ORNL plans to use the test system in a hot cell to perform SNF vibration testing on high burnup fuel to evaluate the effect of pellet-clad interaction and effects of material bonding on the effective lifetime of the fuel-clad structure bending fatigue performance. A brief introduction of this test system will be provided in this paper along with some preliminary test results.

II. TEST SYSTEM CONCEPT

The reversal pure bending is conducted using a U-frame testing setup. A vertical U-frame setup is shown in Fig. 1. The U-frame is constructed with two rigid arms and the associated linking members. The rod specimen is coupled with the U-frame by inserting it into the co-linear holes within the two rigid arms. As a result, reversal bending will be applied to the rod specimen when a controlled push-pull force is applied to the two loading points of the rigid arms. To control any contact-induced damage to the rod specimen, compliant layers are used between the test rod and the rigid arm. This proposed test system is able to capture the pure reversal bending as desired and at the same time, is easy to use and compliant with all requirements of the hot cell test facility. The system has a minimal number of moving parts, and test sample installation can be achieved using a simple drop-in action. The

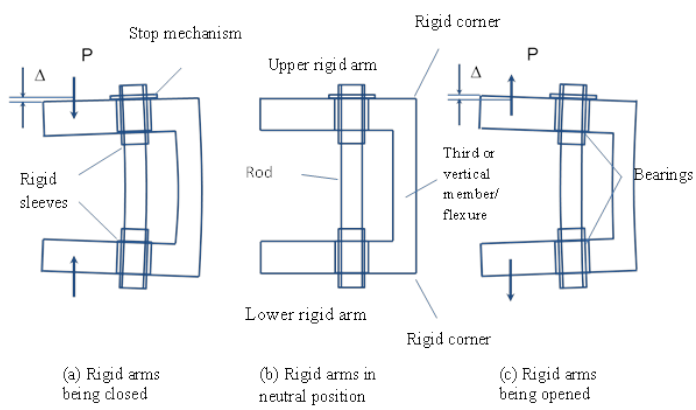

Fig. 1. U-frame-assisted bending fatigue testing setup for reversal bending when rigid arms are (a) closing, (b) neutral, and (c) opening.

test system is designed to use a 6-inch rod segment with 2-inch gage section. Initial test specimens will come from high burnup SNF rods with Zircaloy-4 cladding. The majority of the test system components are made of stainless steel (SS) 304. Prior to initial equipment design, 3-D finite element analysis (FEA) showed that the position of the rod specimen relative to the linking member of the U-frame has a significant impact on the amount of stress applied to the specimen. Using appropriate compliant layers allows a pure bending moment to be achieved in the gage section as shown in Fig. 2. The maximum von Mises stress level occurs at the pellet-clad interface.

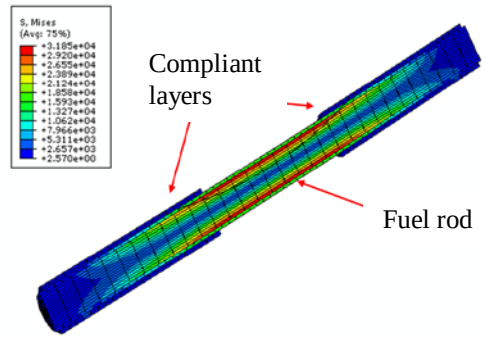

Fig. 2 Stress distribution in a fuel rod with compliant layer when the applied force was 178 N; the unit of stress is psi. The maximum von Mises stress is 220 MPa (3.185×104 psi).

III. DEVELOPMENT OF TEST SYSTEM

The first generation (1G) of the test setup was fabricated and assembled on an MTS servo-hydraulic test machine, shown in Fig. 3. It was discovered that the use of a PTFE (Teflon) compliant layer required a press-fit process for installation on the rod specimen, and the press-fit installation apparently offsets the advantage of the U-frame setup of easy installation of the test sample.

A fundamental change was made to the test setup to introduce linear ball bearings (LBB) into the rigid arms. Using LBB, the test specimen can be "dropped-in" the U-frame; that significantly reduces the effort to install the test specimen. Also, it was found that the specimen needed to be prepared for installation into the U-Frame with pre-machined rigid sleeves already assembled onto the rod specimen using a dedicated procedure. A more advanced modification developed for the 3G setup involved the use of pre-loaded linear roller bearing (LRB) sets embedded in the rigid arms along with the hexagonal rigid sleeves for the test specimen. The introduction of LRB removed the backlash experienced during reverse bending in previous designs, while at the same time, maintained the feature of using the test specimen dropping-in design. A 3G U-frame setup is shown in Fig. 4.

An additional difference between the 1G and 3G setup (Fig. 3 and Fig. 4) is the addition of counterweights on the side of the rigid arms opposite the rod specimen in the 3G design. The

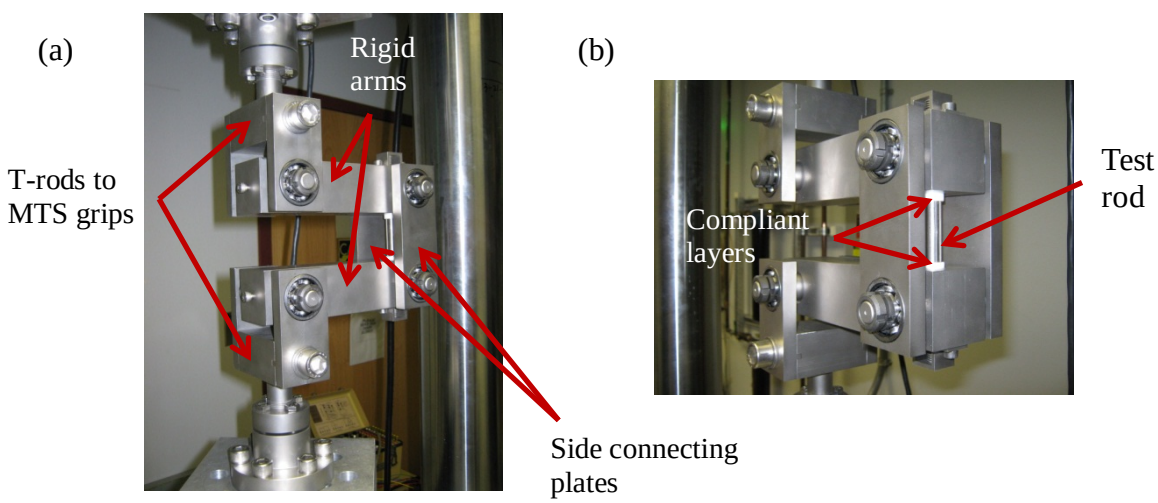

Fig. 3. (a) Assembled U-frame setup on MTS testing machine (809), and (b) end view illustrating the rod under test. Loading arm is 152.4 mm. Teflon is used as compliant layers, and the rod is press-fit into the specimen holes of the two rigid arms.

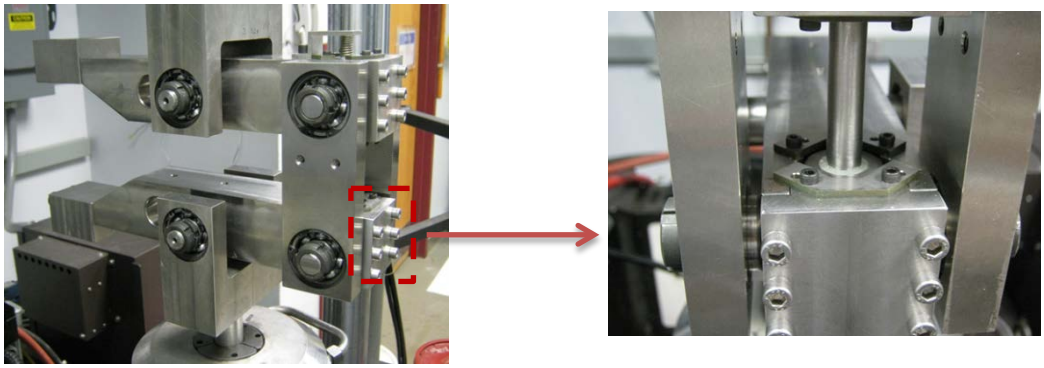

(a) (b)

Fig. 4. (a) 3G U-frame setup equipped with linear roller bearings (LRBs) that are preloaded by bolt-tightening the end blocks. The enlarged view in (b) shows the rod inserted.

counterweights mitigate the effect of the self-weight of the U-frame components due to gravity, and ensure that the stress state of the rod specimen is pure bending as designed. Upon further testing, it was noted that the use of counterweights could potentially limit the usable frequency range of the system or limit the dynamic displacement because the system would have to consume a substantial amount of input energy to overcome the inertia and damping effect.

A new generation of U-frame has been developed that has the U-frame set horizontally, and uses a dual Bose linear motor TestBench (Fig. 5). This alignment eliminates the effect of the U-frame self-weight entirely; also the push-pull force is applied symmetrically at both loading points by use of the dual motors. This design allows the use of a wide frequency range when applying pure bending to the test specimen during dynamic cycling. Moreover, the Bose linear motors use electromagnetic forces to generate the driving forces and thus there are no oil issues as would occur when using a servo-hydraulic test machine.

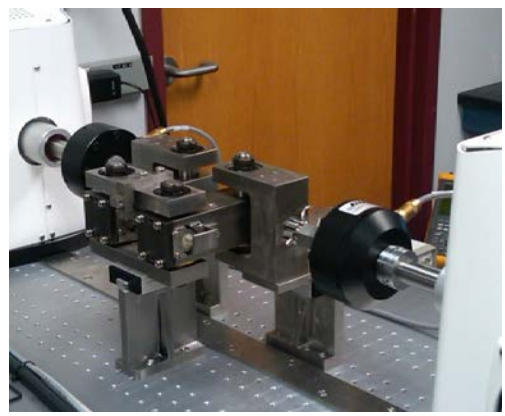

Fig. 5. Integrated ORNLU-frame Bose dual linear motor TestBench. A horizontal arrangement is used to eliminate the effect of the U-frame mass on the specimen.

IV. DEVELOPMENT OF MEASUREMENT METHODS

In a hot cell or out-of-cell environment, LVDTs are one of the most reliable methods available for measuring the deformation of a rod specimen during bend testing. Even when using this measurement method, there is still a significant challenge to collecting accurate bending data because both the deformation of the compliant layers and the rigid body motion of the test frame contribute to the measured results. A three-point measurement system has been implemented to accurately capture the deformation of the rod specimen during testing. The three-point measurement system involves using three LVDTs spaced along the test specimen to accurately measure the deflection over a wide area of the specimen. The three LVDTs are assembled into a single sensor clamp and are mounted to the side connecting plates. The total curvature of specimen can be deduced from the LVDT measurements and this information can be used to characterize the true deformation of the specimen. The deformation information collected using this measurement system is relatively independent of the compliant layers and rigid body motion of the U-frame system. The three-point measurement method is shown in Fig. 6.

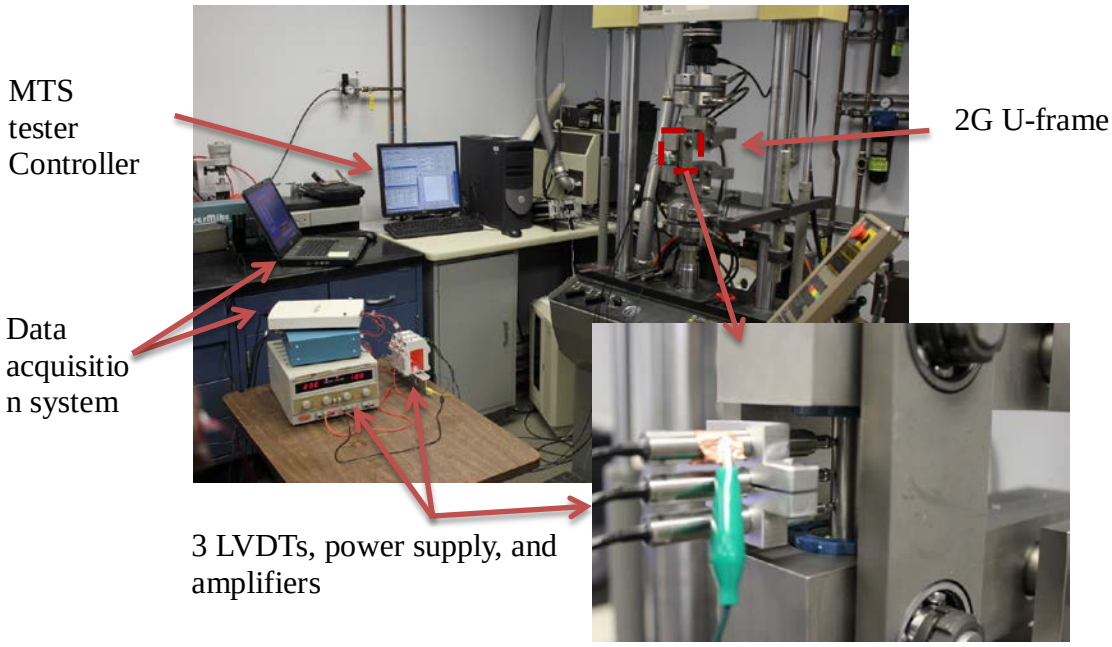

Fig. 6. Three-point measurement method for the curvature of specimen through three LVDTs. The demonstration is on the U-frame setup equipped with linear ball bearings and integrated onto a MTS 810 servo-hydraulic test machine.

The use of curvature along with the bending moment enables the rod specimen to be tested and characterized more appropriately than using a single point deflection measurement, substantially reducing the uncertainty. The curvature obtained using a surrogate rod made of SS tube is given in Fig. 7. It can be clearly seen that in a force control mode, the waveform of curvature followed that of the moment.

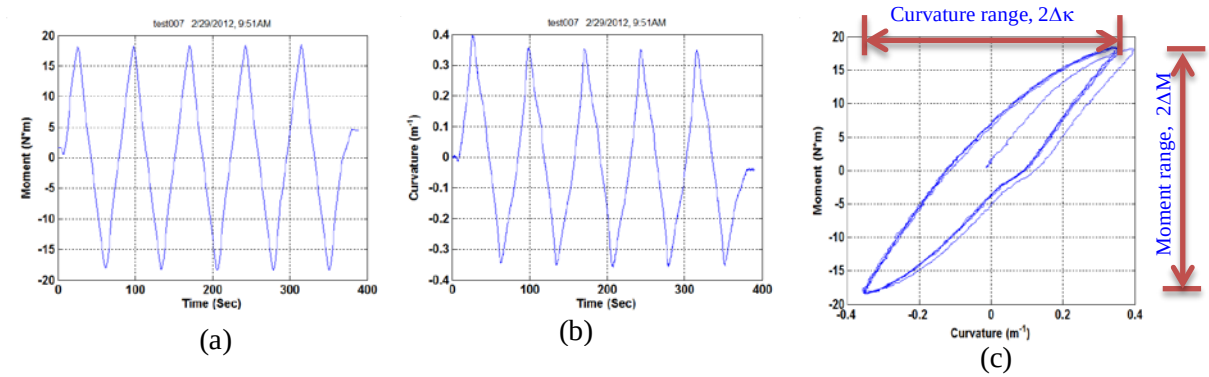

Fig. 7. (a) Moment curve, (b) curvature curve, and (c) moment–curvature loops obtained by use of 3G U-frame with preloaded LRBs. The results are based on the rod made of SS tube only using the LRB U-frame on MTS 810 test machine under ±180 N, 10 N/s.

The moment-curvature relationship revealed a significant amount of hysteresis because of plastic deformation. However, the amplitude response will be focused as follows: the flexural rigidity is defined as a ratio of moment range, ΔM to curvature range; Δκ will be used to characterize the property of the rod specimen,

Flexural Rigidity, $EI = \Delta M/\Delta\kappa$. (1)

It is seen that in an elastic system, the flexural rigidity is determined by $E*I$ in which E is Young's modulus and I is the moment of inertia. The flexural rigidity should characterize the bending stiffness in some sense, while the latter also depends on the gage length. It is noted here that for a SNF rod, if one assumed perfect bonding between fuel and clad the system flexural rigidity (EI) can be written as,

$$EI_{System} = E_{Fuel}\, I_{Fuel} + E_{Clad}\, I_{Clad}$$

However, if the cohesion bonding at the pellet-clad interface was not good or compromised due to vibration loading, the SNF system EI can be written as

$$EI_{System} = E_{Fuel}\, I_{Fuel} + E_{Clad}\, I_{Clad} - f\,(loading,\ frequency,\ temperature,,)$$

Where, function f is the correction factor to take into account the interface cohesion bond evolution, and is function of vibration loading, frequencies, and temperature as well as clad-pellet interaction mechanism. As shown in Fig. 7 (c), the hysteresis (loop area) is another important physical quantity revealed from the reversal bending vibration testing, which will be studied in the future.

The flexural rigidity of testing rod depends on both rod structure and curvature (load) level as shown in Fig. 8. This characteristic was illustrated from a series of testing on the surrogated rods, made of SS tube, SS tube with alumina pellet (no epoxy bond, which resemble fresh fuel pellet inserts), and SS tube filled with epoxy. The moment-curvature relation is strongly related to rod structure as shown in Fig. 8 (a), while as system flexural rigidity of tested rods, shown in Fig. 8 (b), is dependent on both rod structure and curvature level. The epoxy has significant lower stiffness compared to alumina, however, it provides continuous support and has strong bonding to the SS tube, this in turn provides a higher system stiffness (EI) compared to that of the SS tube with alumina insert only; while as for SS tube with pellet inserts, the pellet insert will start to carry more load when the clad reaches certain curvature levels. SS tube w/o internal support from alumina insert or filled epoxy has the lowest flexural rigidity.

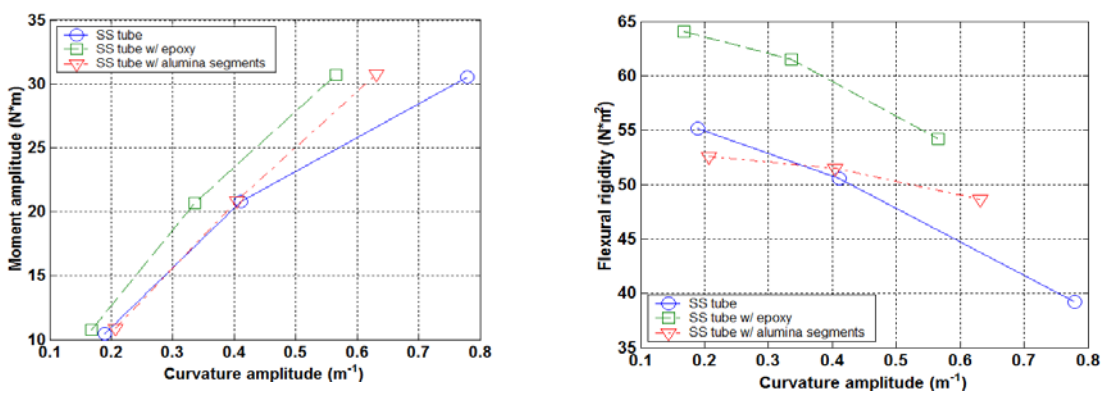

(a) (b)

Fig. 8 Moment-curvature response and the associated system rigidity evaluation.

V. TEST PROTOCOL AND EXPERIMENTAL DEMONSTRATION

A test protocol has been proposed as shown in Fig. 9 for the reversal pure bending fatigue test. The protocol mainly consists of the measurement under quasi-static cyclic loading at the specified number of cycles and the cycling itself. The latter is the dynamic cyclic test at a defined frequency and amplitude.

Surrogate rods have been used extensively in the out-of-cell U-bent integrated fatigue bending tester development. Two series of surrogate rods were made using SS cladding and alumina pellets. One series had the alumina pellets press-fit into the SS cladding and the second series had the alumina pellets bonded both to themselves and to the SS cladding using cast epoxy, expressed with prefixed SSAP.

Initial tests were conducted on a MTS 810 servo-hydraulic machine in displacement control mode using the 3G U-frame test setup. Results for one of the tests, SSAP05, with bonded pellets are shown in Fig. 10. The curvature of this test was fairly flat. The measurement process obviously captured the fracture of the rod specimen indicated by the sudden drop in monitored moment. The flexural rigidity dropped due to cyclic fatigue, with a 16% decrease in rigidity prior to failure. This shows that the flexural rigidity can serve as an index of the structural integrity of rod specimens. Fig. 11 shows curvature and hysteresis loop responses under cyclic bending for the SSAP06 sample under different loading amplitudes applied at U-bent rigid arms. SSAP06 test result shows that the increased curvature and the decreased flexural rigidity are due to cyclic loading.

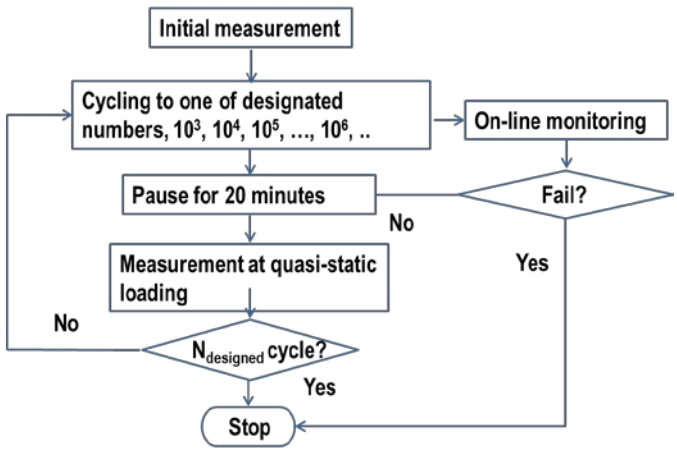

Fig. 9 Test protocol for reversal bending test.

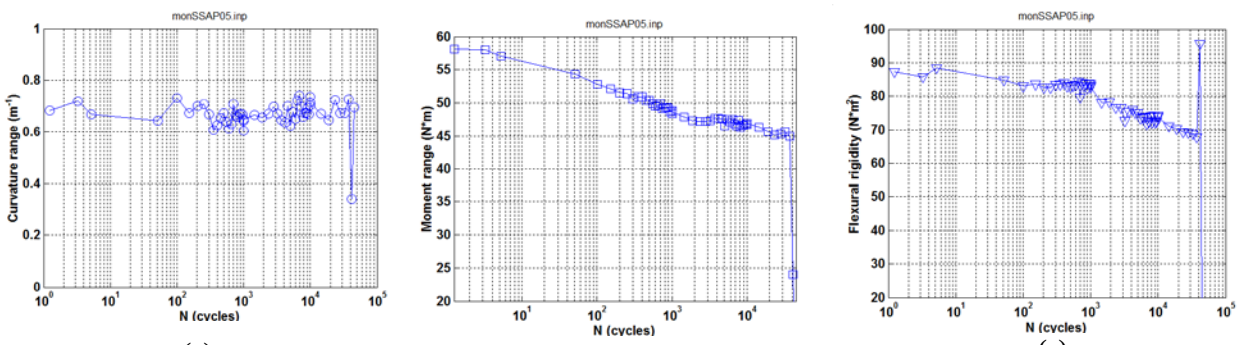

(a) (b) (c)

Fig. 10. Variation of (a) curvature, (b) moment, and (c) rigidity based on on-line monitoring of SSAP05: ±3 mm, 2 Hz. Specimen with octagonal rigid sleeve without Teflon sheets attached; $N_f = 3.7\times10^4$ cycles.

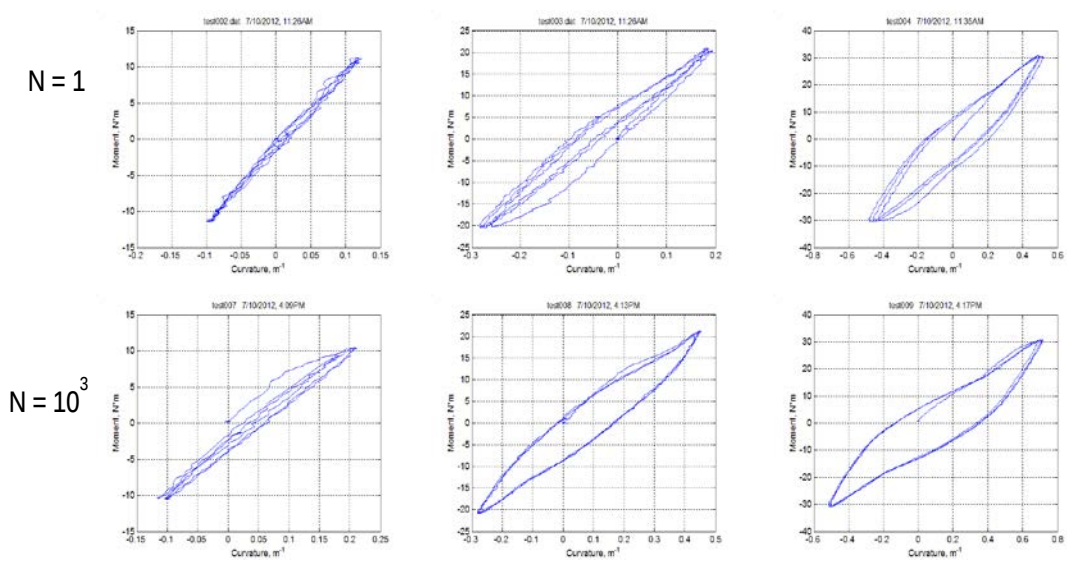

Load amplitude: 100N 200N 300N

Fig. 11 Cycling loading results in increases in curvature and hysteresis; measurements were conducted under load control mode on SSAP06 sample.

Other examples of property changes during the cyclic bending loading from flexural rigidity curves is illustrted in Fig. 12. Fig. 12(a) shows decreased flexural rigidity under increased load and under increased loading cycles from SSAP02 sample, at interval of 1, 1000 and 10000 cycles. It's noted here that SSAP02 has alumna pellet inserts but w/o epoxy bond. The decreased flexural rigidity with increase load level can be referred to test rod nolinear response (or yield) under increased loading. Significant decrease in flexural rigidity of SSAP02 could be the reault of direct pining effect of alumina pellet to the clad and resulting in localized yielding at the clad tube. Fig. 12(b) shows opposite trends under increased curvature, and reveal similar trends of flexural rigidity decrease under increased loading cycles. Due to the linear response of moment-curvature responses, no crack growth in SSAP system will be expected, the decreased flexural rigidity related to cycle frequency of SSAP04 is likely associated with the progressive degradation of the interface bonding between pellet-pellet and pellet-SS tube.

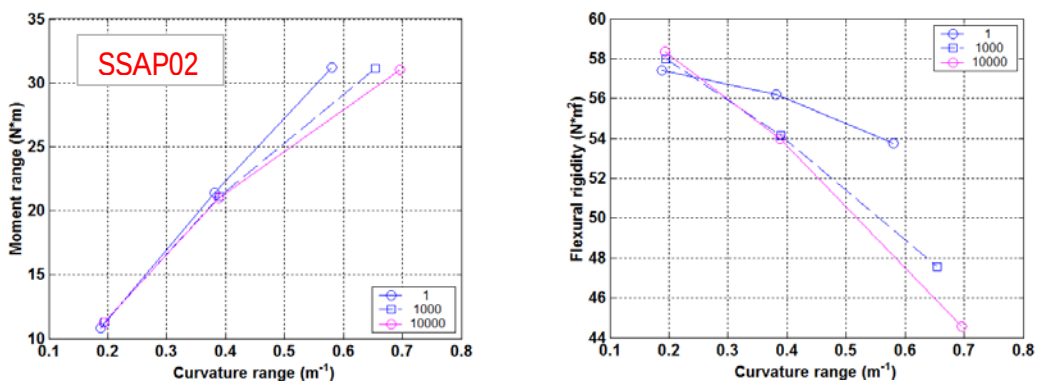

Fig. 12(a) Flexural rigidity property change results from cyclic loading. The measurements were conducted under static cyclic loading at specified points of cycle test.

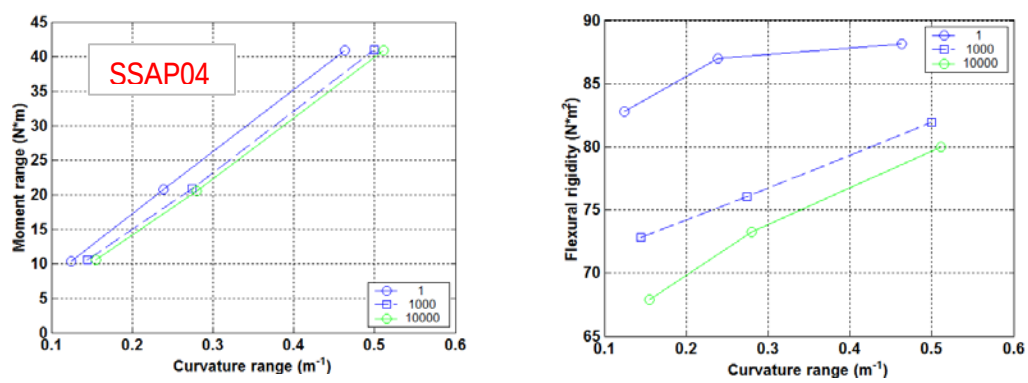

Fig. 12(b) Moment-curvature curves appeared to be quite linear in the tested range for SSAP04. Higher flexural rigidity was observed compared to SSAP02 due to epoxy bond of SSAP04. More significant decrease was observed in rigidity at higher cycles.

VI. OUT-OFF-CELL PROOF OF METHODOLOGY TEST PLAN

The proof of principle demonstrations were performed on the integrated Bose U-bent tester under the load control mode. The main purpose of the proof-of-the principle testing is to demonstrate the repeatability and reliability of the developed reversal U-bent tester in applying to SNF vibration integrity investigation. The surrogate rods made of SS tube embedded with epoxied alumina pellets (SSAP samples) were used for demonstration testing. The tensile test results of the SS tube, based on ASTM E8 tubular testing, is shown in Fig. 13, and the estimated mechanical properties are: E = 176 GPa, YS at 0.2% offset = 325 MPa, UTS = 664 MPa.

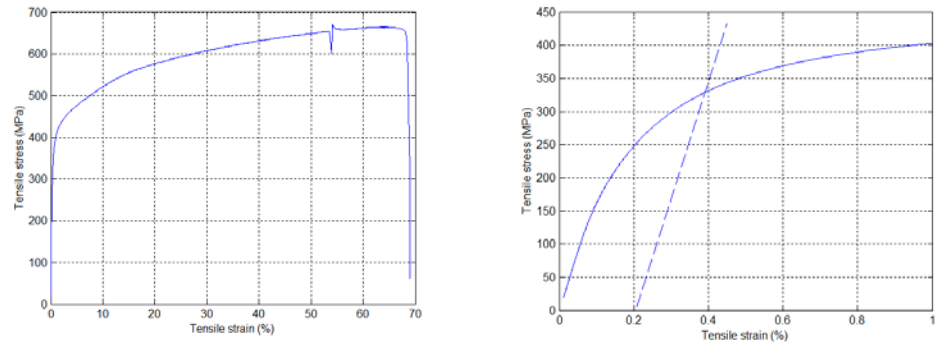

Fig. 13 Axial tensile test results for stainless steel tubing used as surrogate rod for bending testing.

The reversal U-bent apparatus was integrated into a dual motor Bose system and served as the driver to conduct both the static and dynamic fatigue bending tests. The integrated testing device is shown in Fig. 14, where the Bose linear motors are shown to the left, the curvature measurement device of 3-LVDTs is shown to the right of Fig. 14.

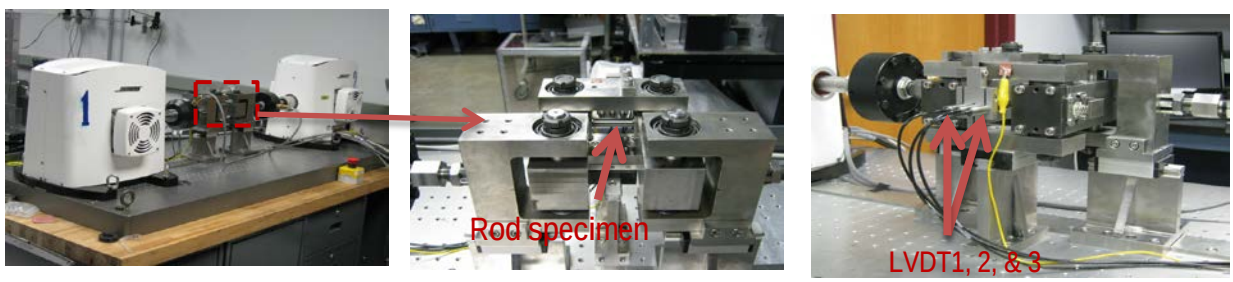

Fig. 14 Integrated Bose reversal U-bent tester used for static and dynamic fatigue bending testing.

Three static bending tests were conducted with a maximum displacement amplitude of 20-mm at the loading point, and the static bending test results are shown in Fig. 15. Based on these test data, the three targeted dynamic bending loading levels were selected, namely, 20 N-m, 25 N-m, and 30 N-m ranges. Based on these moment loading ranges, a series of reversal bending fatigue tests were conducted. The summary of fatigue test results are shown in Fig. 16, and showed that the general trend of fatigue strength is consistent with that of typical S-N trend curve. In order to validate the reliability of epoxy compliance materials, two of the SSAP samples were exposed to spent fuels; the test results show that the compliance material was intact and the fatigue data are consistent with these of non-irradiated SSAP samples.

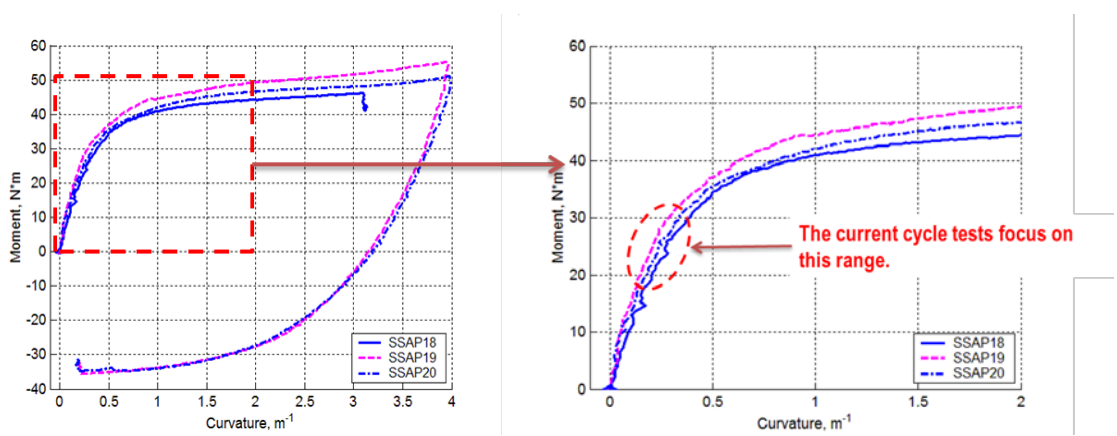

Fig. 15 Static bending test result reveals good repeatability of developed testing protocol.

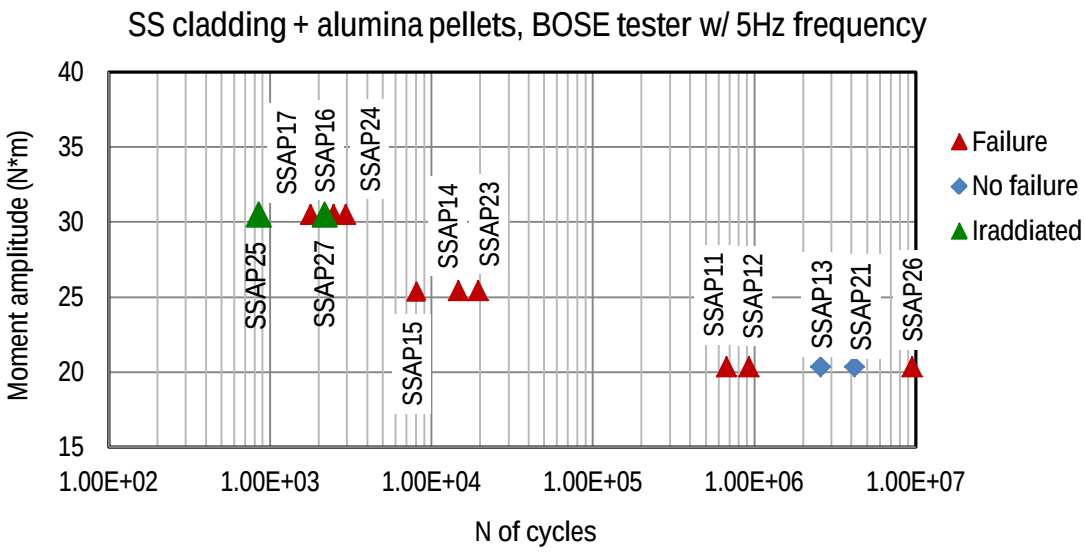

Fig. 16 Reversal bending fatigue tests of SSAP samples show typical S-N trend; cycles of SSAP26 include 5.4M at 10Hz testing; SSAP25 was irradiated 2 weeks between 6- and 7-fuel rod layers and SSAP27 was irradiated in the same fuel pile for 4 weeks.

The above mentioned proof-of-principle testing successfully demonstrated the following:

(1) Repeatability of static testing results for a SSAP material,
(2) Static testing data can be used to set meaningful test conditions for dynamic testing,
(3) Repeatability of dynamic testing results for SSAP material,
(4) The trend for dynamic testing at three different levels produced the expected S-N curve behavior,
(5) Exposing the epoxy in the compliant layer to an irradiation environment revealed no deleterious effects of irradiation on the epoxy.

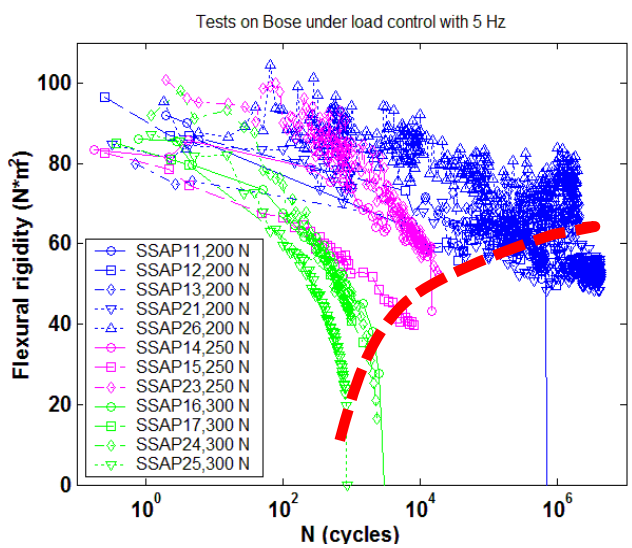

Fig. 17 The evolution of SSAP flexural rigidities under different reversal bending fatigue loadings.

A summary plot of real-time flexural rigidity evolution for tested SSAP samples fracture on the Bose machine is shown in Fig. 17. There are five repetitions at 200 N, three repetitions at 250 N and four repetitions at 300 N loading levels; and there is more variability for the tests at 200N loading level. A red dash line indicated in Fig. 17 is used to connect the residual flexural rigidity strength upon final fracture of SSAP samples. Such a trend curve can be useful in developing governing equations to predict the lifetime of SNF rods under vibration induced accumulated fatigue damage.

All the fractured SSAP samples failed at the gage section as designed, some of the fractured samples and the associated flexural rigidity evolution are shown in Fig. 18 and Fig. 19 for SSAP 11 and SSAP 12 samples, respectively.

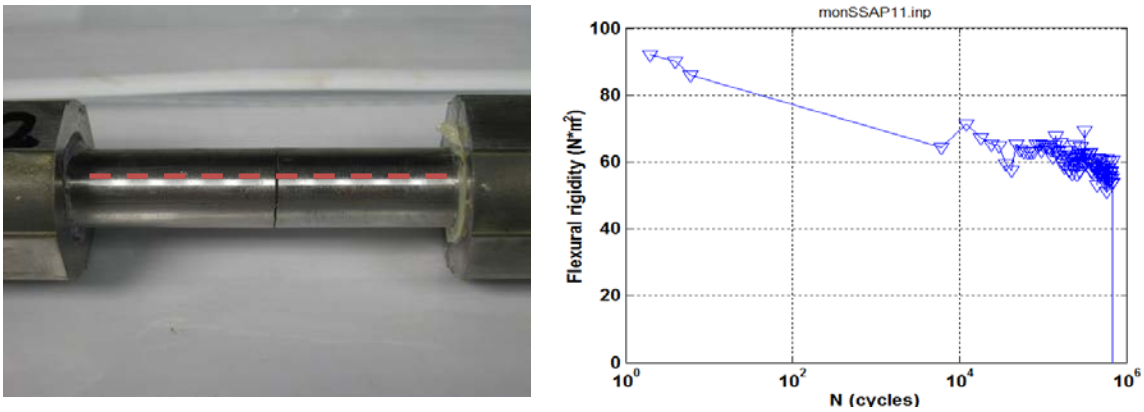

Fig. 18 Test for SSAP11 was conducted on Bose with original setup: load ±200 N, moment ±20.38 N*m, 5 Hz. Initial displacement ±2.5 mm, initial curvature ±0.27 /m, initial strain ±0.14%. Specimen fractured near 678K cycles. About 40% drop in flexural rigidity occurred.

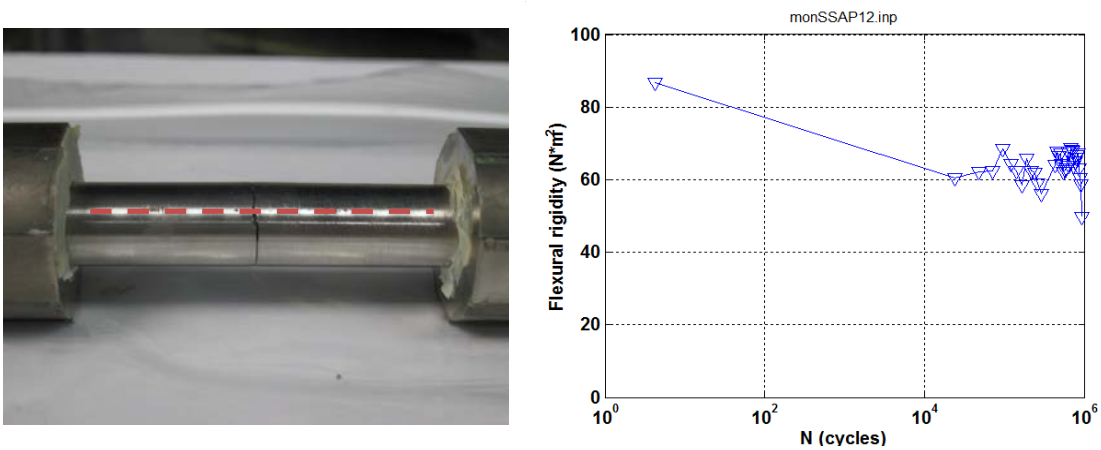

Fig. 19 Test for SSAP12 was conducted on Bose with modified setup under condition: load ±200 N, moment ±20.38 N*m, 5 Hz. Initial displacement ±2 mm, initial curvature ±0.23/m, initial strain ±0.13%. Specimen fractured near 936K cycles. About 42% drop in flexural rigidity.

VII. LOAD CONTROL VS DISPLACEMENT CONTROL BENDING DATA

The reversal bending fatigue tests under displacement control were conducted on the MTS machine with a maximum of 2 Hz cyclic loading frequency. The real-time moment and curvature data comparison between the Bose (load control test) and MTS (displacement control test) tester are shown in Fig. 20. The load control protocol is immune to the impact of the system compliance to the moment value, and appears to be more robust for hot-cell application and further fatigue data analysis.

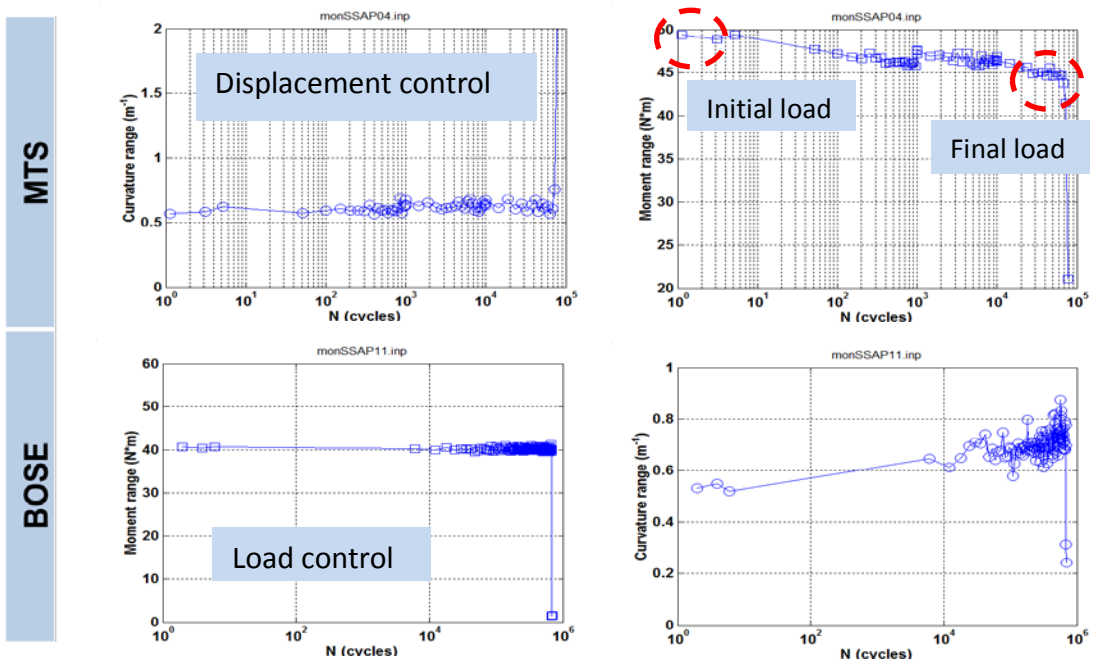

Fig. 20 The degraded surrogate rod due to cyclic loading reveals itself with a decrease in bending moment resistance from MTS displacement control mode data; while as in Bose load control mode data an increase in curvature was observed.

Fig. 21 shows the summary of the Bose and MTS bending fatigue data, where the load control Bose data is within the bonds between the initial load and final fracture load observed from the displacement control MTS data. The load specified in the vertical axis is referred to the force applied at the end of the rigid arms (4-in. long) of the U-bent tester to induce pure moment on the surrogate rods.

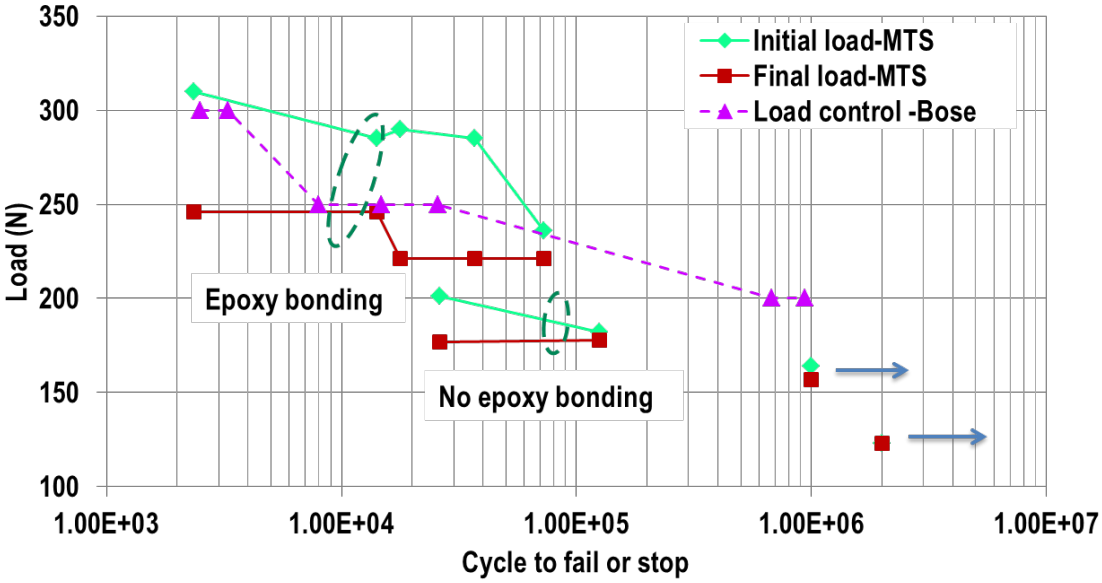

Fig. 21 Similar S-N curve trend was shown from displacement control data and load control data. The fatigue strength also appears to be dependent on interface bonding, SSAP samples w/o epoxy bond appears to have much lower fatigue endurance limit.

A SS tube with a single alumina rod insert (w/o epoxy bond) was also tested with reversal pure bending on a MTS machine with increased applied displacement at the rigid arms of the U-bent tester. The test results are shown in Fig. 22. In the low deflection region, the composite rod behaves like linear elastic material, and most of the load was carried by the alumina rod due to higher rigidity. While upon fracture of the inserted alumina rod, Fig. 22 shows a sudden load drop at 9-mm displacement cycle and an initiation of nonlinear (or yield) response with hysteresis loop formed accordingly. This indicates that composite rod load carrying capacity was suddenly transferred to the SS clad and results in localized yield of SS clad due to pellet-clad pinning, at region near the alumina rod fractured site. This observed composite rod load transferred mechanism may deserve our special attention; since it may imply to that the fuel integrity can have adverse impact to the fuel clad performance/integrity. Thus, a failed fuel pellet, such as crack or fracture, can certainly increase the inertia load carrying capacity to clad as well as to increase the probability of pellet-clad pinning interaction during transportation.

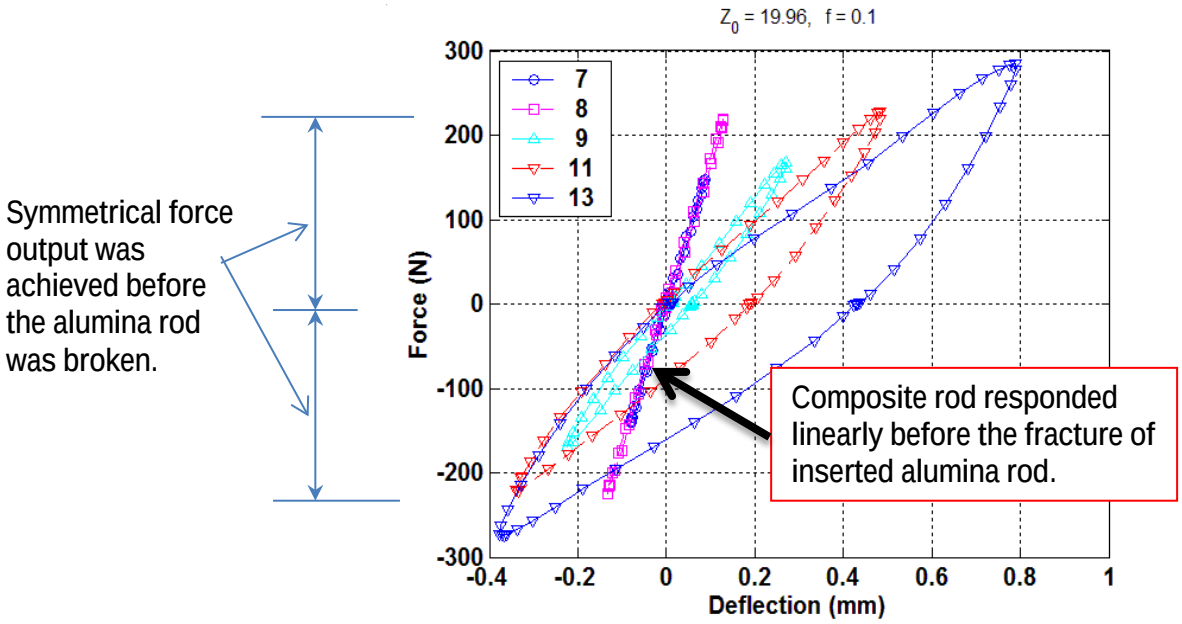

Fig. 22 Displacement control was used on MTS with amplitude 3-13-mm (as indicated in the legend) and the deflection was measured at mid-point of the rod. The composite rod bending test results indicate that before inserted alumina rod fracture, most of the bending load carrying capacity was resided on alumina rod. Upon alumina insert fractured, sudden load transfer will occur and SS tube starts to carry majority of bending moment; which results in plastic deformation of SS clad.

VIII. PRE-HYDRIDE ZR-4 SURROGATED ROD BENDING FATIGUE TESTING

The pre-hydride Zr-4 clad material was prepared with 500 ppm hydrogen content. The composite rod made of pre-hydride Zr-4 tube was filled with cast epoxy and used as a surrogate rod for the bending fatigue integrity study. The cast epoxy filled surrogate rod performs better than the SSAP sample due to a lack of pellet-clad pinning interaction. Some comparison results for the SS tube only and SSAP 02 (no epoxy bond), and composite rod of SS or pre-hydride Zr-4 tube filled with cast epoxy, are shown in Fig. 23 and Fig. 24, respectively. The SEM examination was also performed on the fractured ZrE01 pre-hydride sample, as shown in Fig. 25. The second pre-hydride surrogated rod ZrE02 was also under cyclic bending fatigue test, starting with lower displacement amplitudes of 4-mm and 6-mm. However, after 2.5M cycles no apparent degradation was observed so the test specimen was subjected to additional cycling with displacement amplitude of 8-mm. The ZrE02 finally failed at 1.9E+4 cycles with 5% reduction in flexural rigidity. The associated flexural rigidity and fracture images are shown in Fig. 26 and Fig. 27, respectively.

SS02, SS tube only	SSAP02, SS tube + 10 alumina segments
Cycling: ±4mm, 2Hz; Nf = 2.95E+04	Cycling: ±4mm, 2Hz; Nf = 2.62E+04

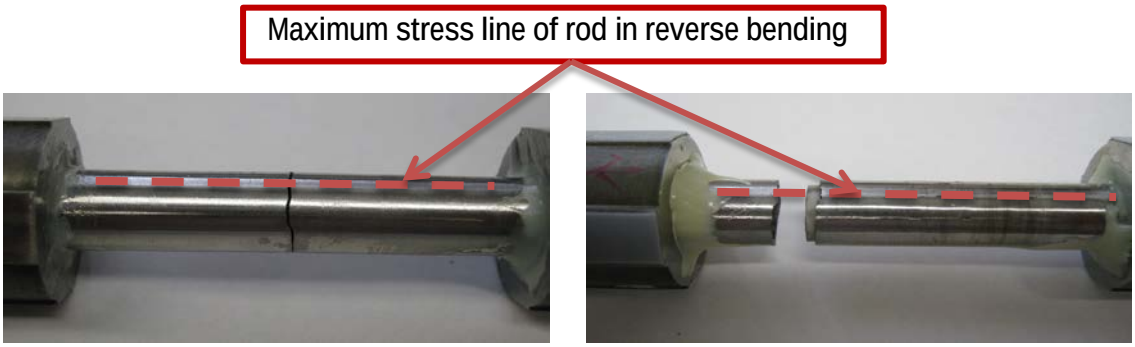

Fig. 23 Both tests are failed at gage section, done on a MTS machine. SSAP02 (w/o epoxy bond) failed earlier than tested sample of SS tube only.

SSE01, SS tube + cast epoxy	Hydrided Zry-4 tube + cast epoxy
Cycling: ±4mm, 2Hz; Nf = 5.45E+05	Cycling: ±8mm, 2Hz; Nf = 1.45E+04

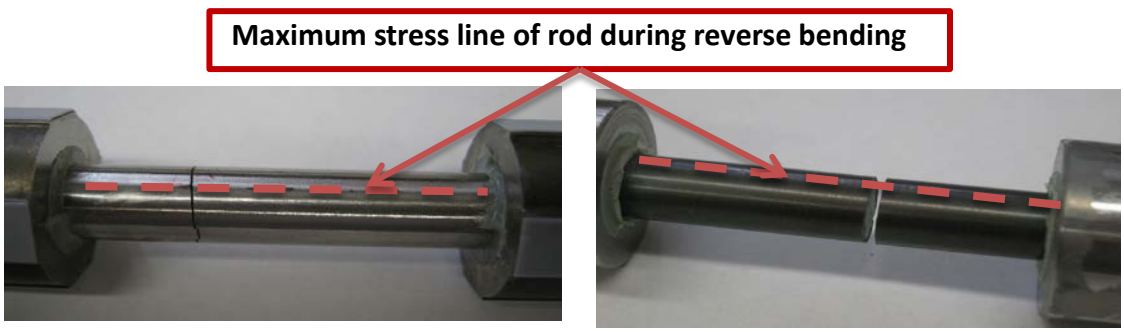

Fig. 24 SS tube with cast epoxy performed much better than that of S tube as well as SSAP02 surrogate rod. ZrE01 with filled cast epoxy also performed well.

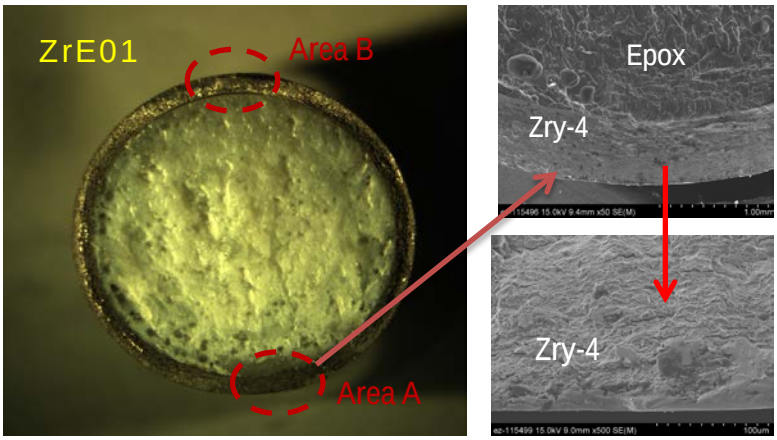

Fig. 25 Fracture Surface of Hydrided Zry-4 surrogate Rod, ZrE01. Fracture surface around area *A* (highest bending moment location) revealed striations resulting from cyclic crack propagation.

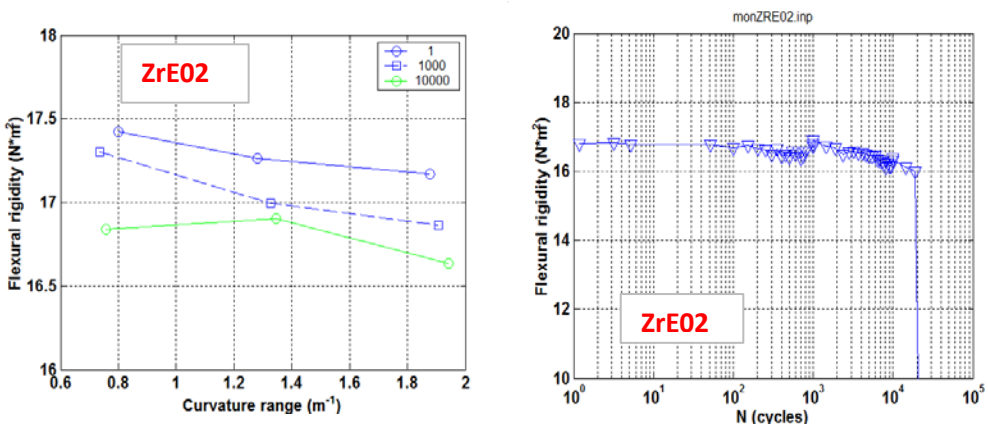

Fig. 26 Rod ZrE02 was made of pre-hydrided Zry-4 cladding + cast epoxy. Specimen had been cycled with amplitudes ±4 and ±6mm before applying 8-mm amplitude loading. Static measurements were conducted at three intervals, no significant degradation of flexural rigidity was observed. On-line monitoring demonstrated an equivalent decrease (5%) in flexural rigidity prior to rod failure.

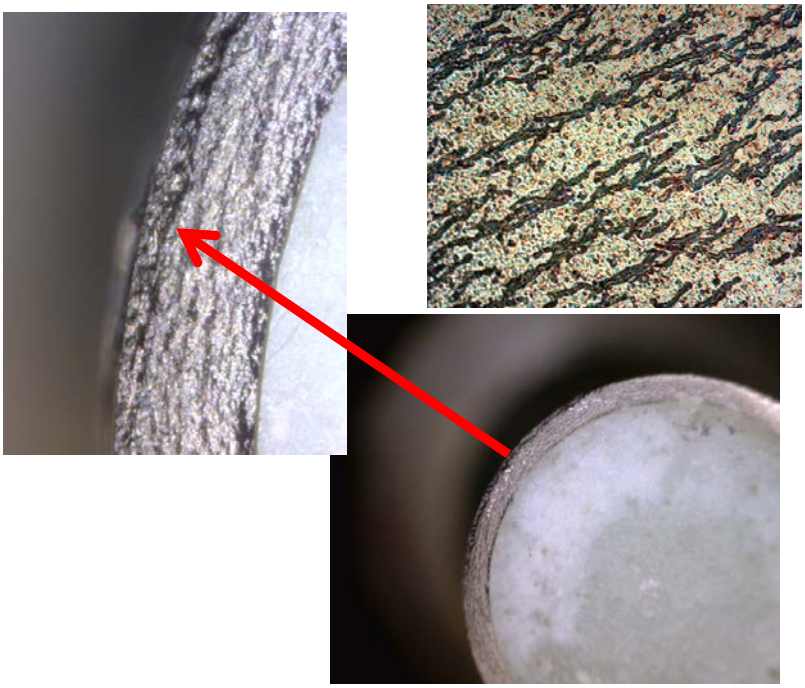

Fig. 27 Optical image of the cross section of tested pre-hydrided Zry-4 sample ZrE02. The delamination of Zr-4 and cast-epoxy at highest bending moment location was observed. The potential circumferential hydride delamination also indicated, shown to the left of Fig. 27, at the outer hydride ring region; the cyclic shear stress induced by the bending loading in the pre-hydride clad could be the root cause, in addition to the flexural normal stress fields. In reversal bending mode, the surrogate rod will experience both flexural normal tensile/compressive stress as well as more or less uniform shear stress across the cross-section of the rod system. The potential of such combined mixed-mode loadings induced mixed-modes failure to SNF vibration integrity deserves our special attention.

IX. FUTURE INITIATIVES ON SNF VIBRATION INTEGRITY STUDY

The developed reversal U-bent tester is currently under final stage of upgrading for hot-cell operation. The device is scheduled to be installed into the hot-cell during the summer of 2013 to start with reversal bending fatigue testing on the high burn-up SNF. Three proposed follow-on research topics regarding the continuing development of the SNF vibration integrity initiative are described below.

1. Developing semi-empirical characterization protocol for evaluating the fuel clad interaction and the impact of pellet-clad bonding to the effective lifetime of fuel-clad structure bending fatigue performance.
2. Collecting and evaluating the generated SNF vibration experimental data through statistical analyses tools to effectively understand the aging properties of clad, fuel and their cohesion bond, and the overall relation of clad-fuel structural response to individual component mechanical property evolutions.
3. Developing the accumulated damage index in assisting SNF effective lifetime evaluation under normal transportation vibration mode through using the target amplitude ranges and testing cycles based on transportation vibration time history data.

The developed reversal U-bent tester is designed to simulate the normal transportation related vibration, however, for periodic transient shocks experienced by rail or truck transportation and normal handling drop impact, a higher loading-rate device would be required. Thus, based on the developed U-bent concept, to build an integrated high loading-rate U-bent tester to simulate transient shock or handling-drop impact is also of interest.

Due to higher stiffness/rigidity (low fracture toughness and low ductility) of oxide fuel compared to that of Zr clad, the fused fuel pellets of high burn-up SNF will have a higher probability to fail or fracture than that of Zr clad under shock impact loading (i.e., the pellet damage loading threshold is lower than that of Zr-clad). Based on the surrogate data, it clearly indicates that due to higher stiffness of fuel pellet it can carry more moment resistance than clad if pellets and pellet-pellet/pellet-clad interface bonding remain intact. However, the oxide fracture toughness can degrade significantly under high-rate loading, if the fuel pellet fracture/debond threshold was reached under transient shock loading, the majority of moment resistance capacity will then shift to clad accordingly. This will result in an accelerated degradation of fuel clad under continuing vibration loading as demonstrated in Fig. 22. Thus, in order to have a more realistic and accurate SNF vibration reliability evaluation, the investigation on the impact of high rate loading, such as transient shock or handling drop loading, to the accumulated damage of SNF system under normal transportation will be essential.

X. CONCLUSIONS

The test system can be used to test and characterize static bending stiffness as well as the vibration integrity of spent nuclear fuel. The reversal bending is conducted utilizing a U-frame setup with the push-pull motion applied at the force loading point. The U-frame setup can be integrated into a test machine in either a vertical or horizontal position. The deformation of a rod specimen is measured using three-point deflection, and from that data, the curvature of a deformed rod specimen can be estimated.

A U-frame assisted bending fatigue test system has been proposed and developed in this study. Modifications and upgrades occurred during the process in order to obtain a reversal pure bending condition and at the same time, to make the setup friendly for hot-cell testing. The current version of the test system features a horizontal layout of the U-frame that is integrated in a Bose dual linear motor TestBench. The LRB sets are embedded in the rigid arms and pre-loaded to enable the reversal pure

bending of the U-frame without any concern over the backlash. The adapted horizontal layout also eliminates the effect of the weight of the U-frame components on the deformation of the rod specimen that would exist should a vertical layout setup be used. In addition, loads on both sides of the U-frame enabled by Bose dual linear motors are critical to deliver a symmetrical loading to the setup in a dynamic loading condition. The single-side loading can create serious concern over the stress state applied to the rod specimen because the time is required for stress waves to propagate from the loading end to the un-loading end of the rod specimen. Moreover, the electromagnetic force-based test system is found to be more reliable and compact than a conventional servo-hydraulic system.

The three-point deflection measurement implemented in this study focuses on the deformation of the rod specimen instead of the total deformation that would occur in a single-point deflection measurement. The curvature of the deformed rod specimen can be calculated and the flexural rigidity can be defined readily. The flexural rigidity could depend on the level of curvature applied. However, this doesn't prevent it from characterizing the property of the rod specimen in a cycle test. In the cyclic fatigue test, the variation of flexural rigidity under a defined moment or curvature is the focus of the data collection, and the variation with increased cycles indicates the degradation of rod property.

The relationship of total strain or bending moment versus the number of cycles to failure exhibits a defined trend. Under a displacement or load control mode, it is observed that the lifetime of the rod in the cycle tests decreased with the increase in the total strain or load applied. It is also revealed that the clad-pellet bonding may play a certain role in the fatigue of the rod. This finding suggests an important effect of the cladding-pellet interaction on the fatigue response of spent fuel and remains to be investigated.

ACKNOWLEDGMENTS

Authors would like thank Ting Tan, Hao Jiang, Thomas Cox, Chuck Baldwin, and Yong Yan for their supports, and John Scaglione and Edgar Lara-Curzio for reviewing this paper. Authors also want to thank Gordon Bjorkman and Bob Einziger for providing valuable comments during the program development. The project is sponsored by Nuclear Regulatory Research, U.S. Nuclear Regulatory Commission under DOE contract DE-AC05-00OR22725 with UT-Battelle, LLC.

REFERENCES

1. Wang, J.-A. J., Wang, H., Yan, Y., Howard, R., and Bevard, B., High burn-up spent fuel vibration integrity study progress letter report (out-of-cell fatigue testing development – Task 2.1), ORNL/ TM-2010/288, Jan 2011
2. Wang, J.-A. J., Wang, H., Tan, T., Jiang, H., Cox, T., Yan, Y., Progress letter report on U-frame test setup and bending fatigue test for vibration integrity study (out-of-cell fatigue testing development – Task 2.2), ORNL/TM- 2011/531, January, 2012.
3. Wang, J.-A. J., Wang, H., Cox, T., Yan, Y., Progress letter report on U-frame test setup and bending fatigue test for vibration integrity study (out-of-cell fatigue testing development – Task 2.3), ORNL/TM-2012/417, August, 2012.
4. Hong Wang, Jy-An John Wang, Ting Tan, Hao Jiang, Thomas S. Cox, Rob L. Howard, Bruce B. Bevard, and Michelle Flanagan, "Development of U-frame bending system for studying the vibration integrity of spent nuclear fuel," *Journal of Nuclear Materials*, 440 (2013) 201-213.

WM2014 Conference, March 2 – 6, 2014, Phoenix, Arizona, USA

Potential Impact of Interfacial Bonding Efficiency on High-Burnup Spent Nuclear Fuel Vibration Integrity during Normal Transportation – 14502

Hao Jiang, Jy-An Wang[1], Hong Wang
Oak Ridge National Laboratory
[1]Corresponding author: email: wangja@ornl.gov

ASTRACT
Finite element analysis (FEA) was used to investigate the impacts of interfacial bonding efficiency at pellet–pellet and pellet–clad interfaces on spent nuclear fuel (SNF) vibration integrity. The FEA simulation results were also validated and benchmarked with reversible bending fatigue test results on surrogate rods consisting of stainless steel (SS) tubes with alumina-pellet inserts. Bending moments (*M*) are applied to the FEA models to evaluate the system responses of the surrogate rods. From the induced curvature, κ, the flexural rigidity *EI* can be estimated as $EI = M/\kappa$. The impacts of interfacial bonding efficiency on SNF vibration integrity include the moment carrying capacity distribution between pellets and clad and the impact of cohesion on the flexural rigidity of the surrogate rod system. The result also indicates that the immediate consequences of interfacial de-bonding are a load carrying capacity shift from the fuel pellets to the clad and a reduction of the composite rod flexural rigidity. Therefore, the flexural rigidity of the surrogate rod and the bending moment bearing capacity between the clad and fuel pellets are strongly dependent on the efficiency of interfacial bonding at the pellet–pellet and pellet–clad interfaces.

INTRODUCTION
For high-burnup SNF, the fuel pellets and clad can be fused together to form an integrated SNF system. To understand the underlying mechanism of pellet–pellet and pellet–clad interface dynamics in a transportation environment, it is essential to accurately evaluate the mechanical properties of the integrated SNF system. Prior to conducting physical experimentation on high-burnup SNF, a series of FEA protocols has been developed to investigate SNF vibration integrity using a surrogate rod system that resembles a SNF composite rod system.

It is important to understand and to quantify the bonding efficiency at the pellet–pellet and pellet–clad interfaces of the high-burnup SNF system under normal transportation conditions including normal handling drops and transient shocks. FEA methods have been used to develop simulation protocols, in addition to experimental calibration and verification efforts, to establish qualitative as well as quantitative assessments of SNF rod system performance under normal SNF transportation conditions. This paper describes the methodology used to evaluate the effect of pellet–pellet and pellet–clad interactions with consideration of the interfacial bonding efficiency on SNF vibration integrity. This methodology provides a solid roadmap for further protocol development with respect to effective lifetime prediction of a SNF system under normal transportation vibration. The proposed methodology that couples FEA simulations and experimental exploration efforts is also under development. The current methodology is focused on assessing the influence of interfacial bonding at the pellet–pellet and the pellet–clad interfaces on SNF vibration integrity.

The FEA models of a surrogate rod system use alumina pellets and SS tubing with the appropriate boundary conditions, including bonded epoxy at the clad/pellet interfaces. The model consists of a surrogate rod with 3D representation of fuel pellets, clad, and possible combinations of the gaps at the pellet–pellet and pellet–clad interfaces. The ABAQUS code was used in the FEA, and the surrogate rod was represented by the beam element with the associated effective

stiffness. This approach was used to obtain the beam element properties that would be most effective as input for further development of the detailed SNF assembly model. The approach is also designed to estimate the damping properties of the beam elements due to frictional resistance between the clad and embedded pellets. This pellet–clad interaction modeling uses a "contact element" algorithm and can be further implemented into other embedded boundary conditions, such as internal pressure and residual stress, etc.

This study provides detailed explanations on the effects of pellet–pellet and pellet–clad interactions, including pellet fracture and pellet–clad bonding efficiency, on clad performance reliability under normal transportation considerations. The FEA simulation results were also calibrated and benchmarked with the fatigue aging data [2, 3] obtained from reversible bending fatigue testing.

The objective of this paper is to investigate the potential impact of interfacial bonding efficiency at pellet–pellet and pellet–clad interfaces on SNF vibration integrity. The FEA simulation results are validated and calibrated by use of reversible bending fatigue testing on the surrogate SS rod with alumina-pellet inserts.

The FEA models, with a 50.8 mm (2 in.) gauge section that covered the SS clad and alumina pellets and with epoxy layers supplying cohesion, were developed with the ABAQUS code. In order to estimate the surrogate rod system responses including the stress profile and the associated curvature, κ, the bending moments (*M)* were applied to both ends of the surrogate rod. From the FEA results, the flexural rigidity (*EI*) of the simulation cases is estimated as $EI = M/\kappa$. Detailed discussions and comparisons of the simulation cases are organized as follows.

1. The section model with good interfacial bonding and without pellet fracture
2. The section model with good bonding at pellet–clad interfaces and de-bonding at pellet–pellet interfaces
3. The section model with de-bonding both at pellet–clad and pellet–pellet interfaces

The simulation results indicate that the system response and the associated flexural rigidity are strongly dependent on the interfacial bonding efficiency.

ANALYSIS OF INTERFACIAL BONDING EFFICIENCY OF SURROGATE RODS

Structural analysis and an interfacial bonding evaluation of the surrogate rods used in the bending fatigue testing system [2–4] were performed with the ABAQUS code. The reversible bending fatigue testing system used surrogate rods to calibrate and improve the test setup in an out-of-cell environment. To validate simulation results with out-of-cell surrogate data, the surrogate rod materials used in FEA are the same as those used in the out-of-cell testing. High-density alumina was selected as the pellet material, and SS 304 was used as the clad material. Epoxy was used as the interfacial bonding material. Material properties of the surrogate rod are listed in Table 1.

Table 1. Material properties of surrogate rod

Material	Young's Modulus (psi)	Poisson's Ratio	Yield Strength (psi)	Density (lb/in^3)
Stainless Steel[a]	2.800×10^7	0.300	4.206×10^4	0.2901
Al_2O_3[b,c]	5.395×10^7	0.220	3.626×10^5	0.1416
Epoxy[d,e]	5.076×10^5	0.370	1.001×10^4	0.0452

[a]Product Data Bulletin, 304/304L stainless steel, AK Steel Corporation, http://www.aksteel.com
[b]Ceramic Properties Standard, CoorsTek, Inc., http://www.coorstek.com
[c]The mean flexural strength of the Al_2O_3 is around 48 ksi from the vendor McMaster-Carr.
[d]More about Glass, Ceramics, Carbon; More About Stainless Steel Alloys, Mechanical and Physical Properties, http://www.mcmaster.com
[e]http://www.engineeringtoolbox.com/material-properties-t_24.html

1. Rods with Good Interfacial Bonding

Fig. 1 shows the geometry of a U-frame bending fatigue testing system with a co-planar configuration for the surrogate rod. The 2-in. gauge section is highlighted in black. A finite element model was established to represent the 2-in. gauge section of the test specimen, referred to as the Clad-Epoxy-Pellet section model. **Fig. 2** shows the cross-sectional and longitudinal cut views of the 2-in. surrogate rod. The inside and outside diameters (ID and OD) of the clad are 0.382 and 0.436 in., respectively. The alumina pellet OD is 0.372 in. The 2-in. gauge section of the surrogate rod contains two 0.6 in. pellets in the middle and two 0.4 in. pellets at the ends. The gap between the clad and the pellet was sized 0.005 in. and filled with a cast epoxy layer. The extent of epoxy filling and bonding apparently depends on the casting and the subsequent loading. However, the relevant data were not available. In our modeling study, three conditions will be studied: 1) pellet–clad and pellet–pellet interfaces are bonded, 2) pellet–clad interfaces are bonded and pellet–pellet interfaces are de-bonded, and 3) pellet–clad and pellet–pellet interfaces are both de-bonded.

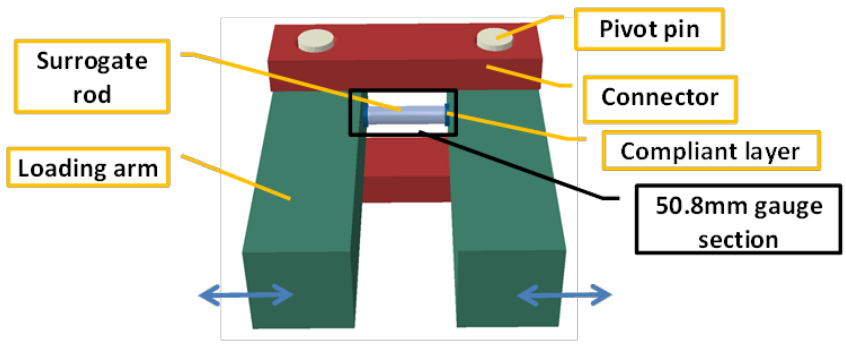

Fig. 2. Geometry of horizontal U-frame bending fatigue testing system with co-planar configuration of the rod.

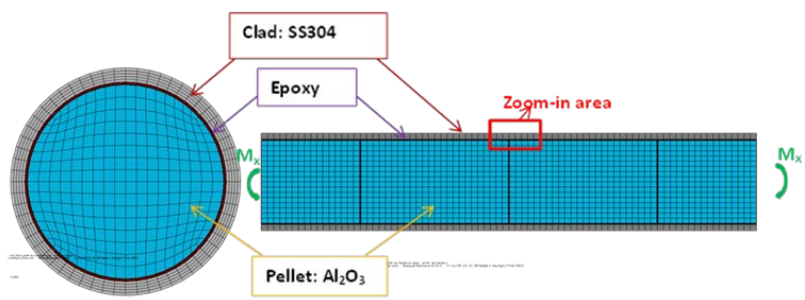

(a) Cross-sectional view **(b) Longitudinal cut view**

Fig. 1. Geometry of Clad-Epoxy-Pellet section model with four pellets.

The Clad-Epoxy-Pellet section model with four pellets is shown in **Fig. 2**. Bending moments were applied on both ends of the surrogate rod rotating along the *x*-axis, as shown in **Fig. 2**(b). According to the out-of-cell surrogate data, the bending moments ranged from 20 to 30 N·m; the bending moment M_x was selected as 25 N·m. Both loading surfaces of the surrogate rod were constrained with rotation along *y*- and *z*-axes and translation along the *x* direction. In the following finite element models, the global mesh is 0.02 in. Some local meshes are as small as 0.0025 in.

The quasi-static procedure used in FEA is from the ABAQUS code. The original surrogate rod was, in fact, 6 in. long with 10 alumina pellets [3–4]. The contact between neighboring pellets generally depends on the casting process. Gaps may exist between the pellets and may be filled with epoxy. The modeling study in the report considered the following aspects:

1. gaps were filled with epoxy layers in which pellet–epoxy and epoxy–pellet interfaces were tied or bonded,
2. gaps existed and were not filled with epoxy layers, and
3. no gap existed between neighboring pellets and pellet–pellet interfaces were de-bonded.

The configuration of the perfectly bonded case is shown in **Fig. 3** . Thin epoxy layers are tied to the gap surfaces at the pellet–clad interfaces and at the pellet–pellet interfaces to simulate cohesive bonding.

This model has three 0.0014-in. gaps filled with epoxy at the pellet–pellet interfaces. The resultant stress distribution and curvature are shown in Fig. 4. The resultant curvature is 0.157 m^{-1}, too small to be noticeable, as illustrated in Fig. 4(a). From the resultant stress distribution shown in Fig. 4, the maximum stress occurs at the outer surface of the alumina rod, and the resultant forces also indicate that the alumina pellets carry a larger portion of the moment resistance than the clad. The clad did not yield under a 25 N·m bending moment, nor did the alumina pellet, which has a much higher yield strength than the SS clad. This indicates that the surrogate rod in a perfectly bonded condition will remain within the linear elastic range under the target loading.

The curvature and flexure rigidity for this case is summarized in Table 2. In this case, a load control procedure was used, the bending moment *M* was applied to both ends of the surrogate rod, and the bending curvature κ was estimated from the FEA result within the gage section. Furthermore, the flexural rigidity *EI* (the product of Young's modulus *E* and moment of inertia *I*) of a surrogate rod can be estimated from the applied moment *M* and the resultant curvature κ as described in Eq. 1.

$$EI = M/\kappa \ . \qquad (1)$$

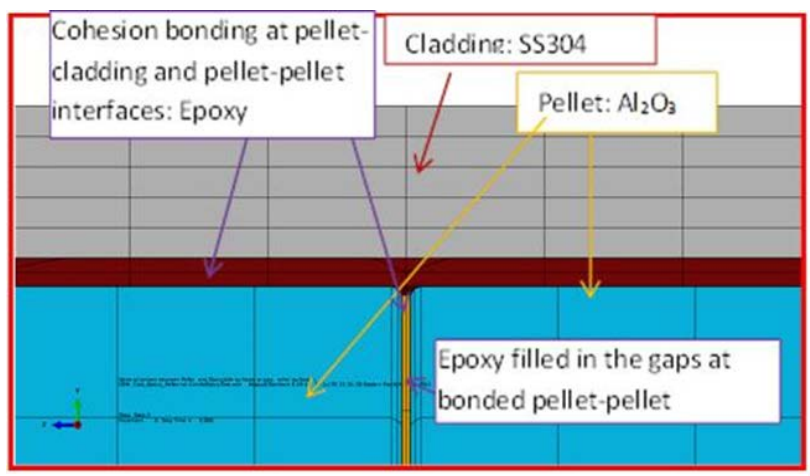

Fig. 3. Zoomed-in area of Fig. 4 for the case of epoxy filling in the gaps at bonded pellet–pellet interfaces.

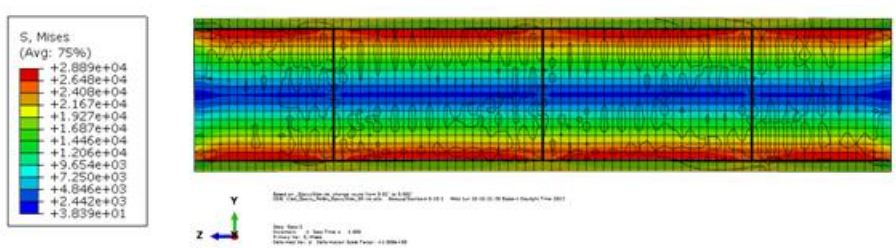

(a) Longitudinal cut view of resultant curvature and von Mises stress

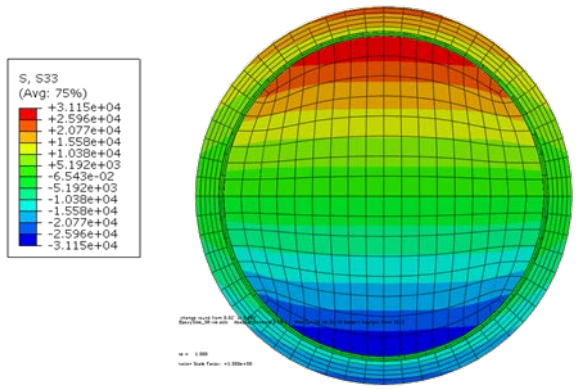

(b) Cross-sectional view of resultant σ_{zz} at a pellet–pellet interface

Fig. 4. Normal stress distribution and curvature resulting from Clad-Epoxy-Pellet section model with four pellets and epoxy-filled gaps at pellet–pellet interfaces.

Table 2. Curvature and flexural rigidity for the perfect interfacial bonding simulation

Designation	Curvature, κ (1/m)	Bending moment, *M* (N·m)	Flexural rigidity, *EI* (N·m^2)	Note
Clad-Epoxy-Pellet4-Tie-Pellet-Epoxy-Tie-at Gap	0.163	25	153	Gaps between neighboring pellets filled with epoxy; pellet–epoxy and epoxy–pellet interfaces bonded

In surrogate rod SSAP05 [3], alumina pellets were bonded to the SS tube and to each other using epoxy. The SSAP05 specimen was tested up to the 25 N·m bending moment. High flexural rigidity was observed, as shown in Fig. 5. The initial (first cycle) test data, which has the highest flexural rigidity on the left side, indicates that the bonds at the pellet–clad and pellet–pellet interfaces should remain intact at the corresponding curvature level. The flexural rigidity of the first test data is very close to the FEA estimation of 153 N·m^2.

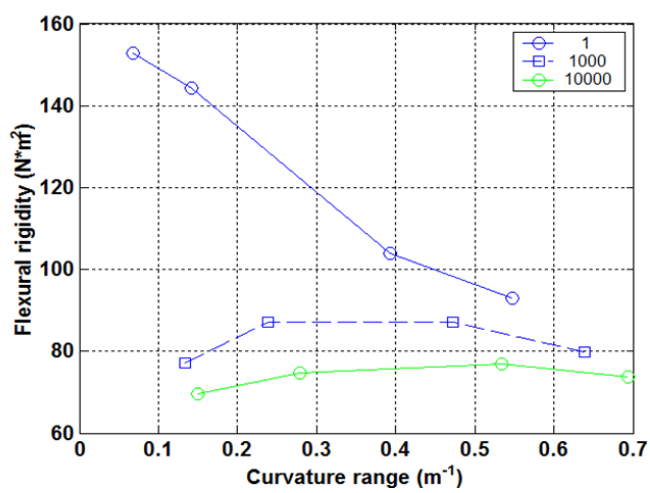

Fig. 5. ORNL SSAP05 specimen test data, flexural rigidity vs. curvature measured at various cycle numbers during a bending cycle test [3].

With good interfacial bonding, the alumina rod can carry most of the bending moment under normal transportation vibration because the Young's modulus of the alumina rod is twice that of the clad (Table 1). Due to the high yield strength of the alumina pellets, the surrogate rod can work within the linear elastic range to a large extent. The high flexural rigidity estimated from FEA

(Table 2) is in good agreement with that estimated from bending fatigue testing data. Thus, the epoxy layers fully bonded to the surfaces of gaps in both clad–pellet and pellet–pellet directions would capture the earlier elastic behavior of the surrogate rod, and the structural integrity of interfaces should be maintained.

Symmetrical reversible output force was obtained for the composite rod (SS tube + alumina rod) using a U-frame bending fatigue testing system, as shown in Fig. 6. Displacement control was used for bending tests with amplitudes of 0.118 to 0.512 in. (3 to 13 mm) with a frequency of 0.1 Hz, and the deflection was measured at the midpoint of the rod. The composite rod bending test results indicate that before the inserted alumina rod fracture, the composite rod responded linearly and most of the bending load carrying capacity resided on the alumina rod due to a Young's modulus that was twice that of the SS clad. Upon the alumina insert fracture, sudden load transfer occurred and the SS tube started to carry the majority of the bending moment, which resulted in plastic deformation of SS clad, as will be demonstrated in the following simulation cases.

2. Effect of Pellet–Pellet Interfacial Bonding Efficiency

Before being transported, the SNF system exhibits inherited stress fields, such as axial tensile stress and tangential tensile stress due to pellet–clad mechanical interaction, or due to oxide volume expansion, as well as radial compressive stress due to hydride compaction and tangential shear stress due to hydride volume expansion. Vibration during transportation will induce reversible bending in a SNF assembly. Repeated expansion and contraction in both the axial and tangential directions of the SNF rod due to reversible bending flexural deformation, combined with stress concentration, can degrade the interfacial bonding at fuel pellet–clad interfaces and pellet–pellet interfaces, as shown in Fig. 7. While the shear stress is small relative to the normal stress due to bending, it does not mean that it can be neglected. In particular, in a composite rod or SNF rods, excessive shear due to material mismatch can be a cause of failure for interfacial bonding.

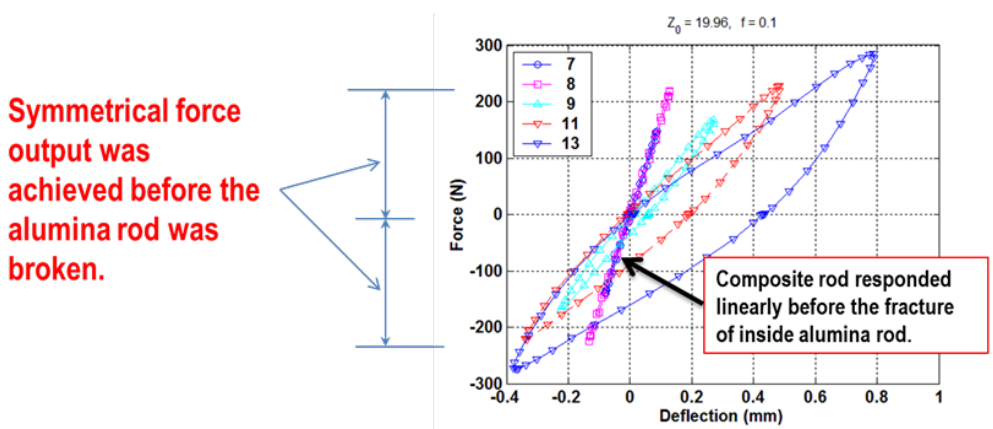

Fig. 6. Symmetrical reversible output force obtained for a composite rod (stainless steel tube + alumina rod) using a U-frame bending fatigue testing system with displacement input of 0.1 Hz and amplitude 0.118 to 0.512 in. [2, 3].

At pellet–pellet interfaces, interfacial bonding fails mainly from normal stress due to reversible bending flexural deformation, combined with relatively less shear stress, as shown in Fig. 7; at pellet–clad interfaces, localized high shear stress will also arise to compensate for the material mismatch under flexural deformation. As mentioned above, the shear stress is small relative to

the normal stress; thus, it is likely that the interfacial bonding failure at pellet–pellet interfaces will occur before the de-bonding at pellet–clad interfaces. Observation of the ORNL reversible bending fatigue of the surrogate SS rod with alumina pellets verified this hypothesis. In this section, the Clad-Epoxy-Pellet section model with four pellets was used to investigate the surrogate rod bending response with perfect bonding at pellet–clad interfaces, but various de-bonded states at pellet–pellet interfaces were the focus. The material properties, geometry, and loading and boundary conditions are the same as those used in the previous FEA simulation.

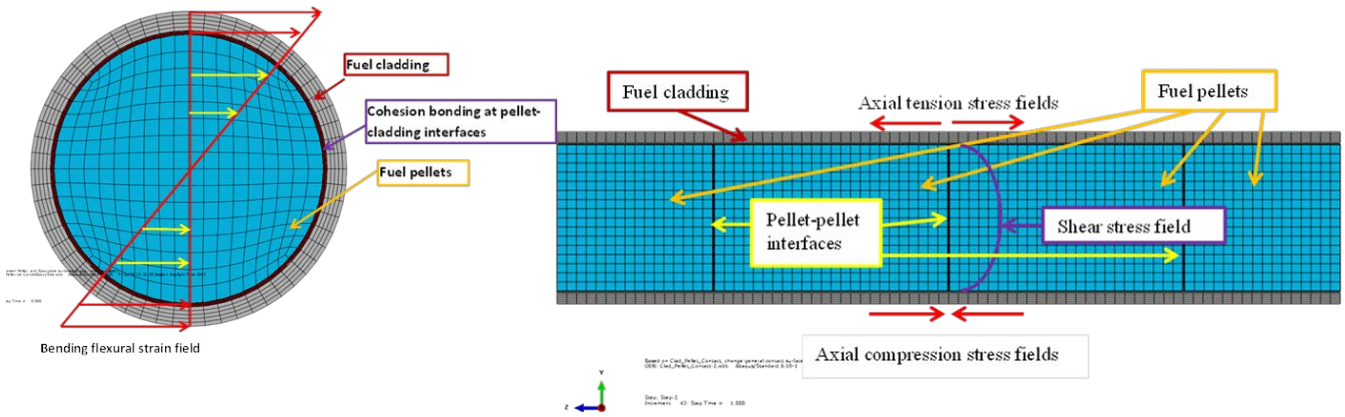

(a) **(b)**

Fig. 7. Transportation-induced reversible bending stress fields in a SNF system.

The first case study of pellet–pellet interfacial de-bonding was dedicated to gaps at pellet–pellet interfaces without epoxy, while a thin epoxy layer still existed at pellet–clad interfaces and was tied to the adjacent surfaces to provide perfect cohesion.

The stress and curvature responses to the bending moment are illustrated in Fig. 8. Compared to the results shown in Fig. 4, there are significant differences in the stress distribution between the case of pellet–pellet interfacial bonding and the case of pellet-pellet interfacial de-bonding, where perfect bonding remains for both pellet–clad interface cases. For instance, for the pellet–pellet interface of the de-bonded case, the maximum tensile stress, which reaches the yield strength of clad at 42 ksi, occurs at the clad and is located at both the top and bottom sides near the pellet–pellet interface regions. The curvature profile enlarged 10 times in Fig. 8(b) shows a lateral contraction and lateral expansion at the compression and tension sides of the clad, respectively. Particularly, a localized clad buckle developed near the pellet–pellet gaps, likely due to the lack of internal support. On the compression side, the clad deforms continuously when the pellet–pellet surfaces are being driven together until the gaps are closed. No stress concentrations are observed at pellet–pellet contact corners. Resultant σ_{zz} clearly indicates that the intensely stressed clad takes over more bending moment resistance than that of the pellets at the de-bonded pellet–pellet interfaces.

At the de-bonded pellet–pellet interfaces, the pellets can only transfer load via hard contact, so the load carrying capacity shifts significantly from pellets to the clad. The SS tube starts to carry the majority of bending moment at the tension-side near the pellet–pellet interface region, which results in a significant localized plastic deformation at the SS clad. Over most of the gauge section, the pellets still provide sufficient internal support to the clad due to good cohesion at the

pellet–clad interfaces and will carry most of the bending load; therefore, there is no yielding at most regions of the SS clad. The results are contrary to the results of the perfectly bonded case in Fig. 4, which shows that the pellets carry significant bending moment resistance; the maximum stress resides at the pellets, and there is no yielding at either the pellets or the clad.

It is also interesting to note that the von Mises stress distribution in the de-bonded pellets case appears to be in a dog-bone shape due to contact pressure at pellet–pellet interfaces. This also differs from the results of the bonded pellet–pellet interface case. The third discrepancy lies in the induced curvature. In the de-bonded case, the resultant curvature is 0.669 m^{-1}, which is four times that of the perfectly bonded case shown in Fig. 4.

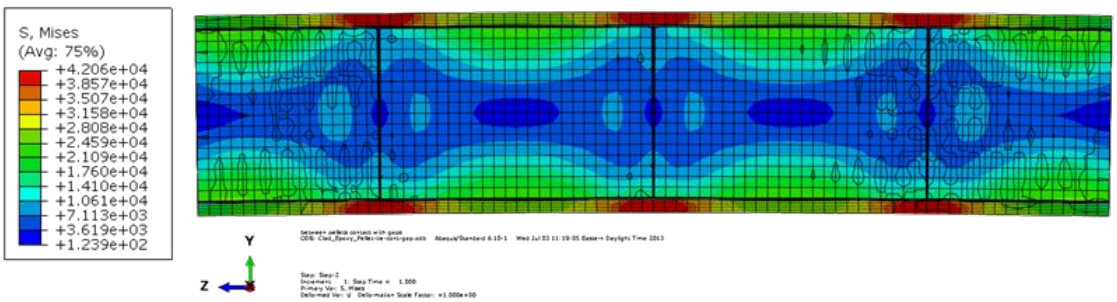

(a) Longitudinal cut view of resultant curvature and von Mises stress

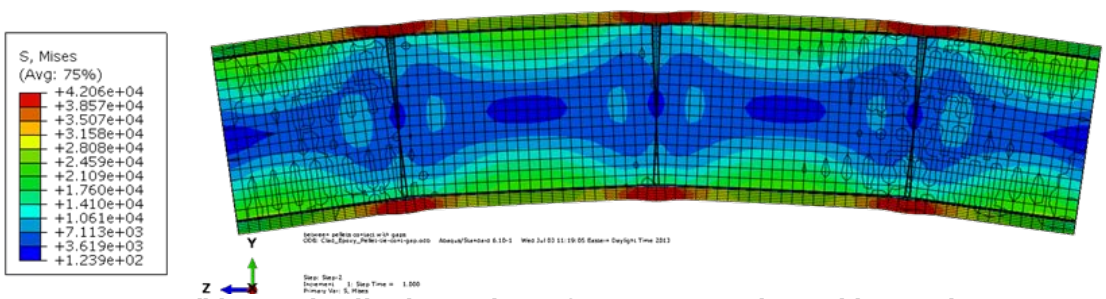

(b) Longitudinal cut view of curvature enlarged by 10 times

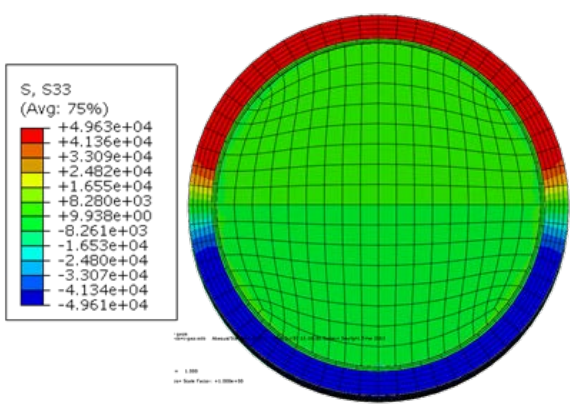

(c) Cross-sectional view of resultant σ_{zz} at a pellet–pellet interface

Fig. 8. Stress distribution and curvature resulting from Clad-Epoxy-Pellet section model with four pellets with gaps at de-bonded pellet–pellet interfaces.

The second case on the de-bonded pellet–pellet interface is no gap at pellet–pellet interfaces before applying a bending load. As in previous cases, a thin epoxy layer is applied and tied to surfaces at pellet–clad interfaces to simulate good cohesive bonding.

As illustrated in Fig. 9, the stress distribution of this case appears to be similar to that with gaps between the de-bonded pellet–pellet interfaces. The SS clad also yields at the top tensile side near the pellet–pellet interface regions; however, on the compression side, the maximum stress occurs at the pellets instead of clad. Nevertheless, the pellet is within the linear elastic range overall due to its high yield strength. From the curvature profile, no clad buckling is observed at the bottom (compression) region. This is because of the absence of gaps at the pellet–pellet interface region; thus, the compacted pellets provide good internal support to the clad tubing structure. Furthermore, pellets seem to carry a significant portion of bending moment resistance via pellet–pellet interaction (pinching at pellet corners), which significantly mitigates the stress level of the clad at the bottom (compression) region.

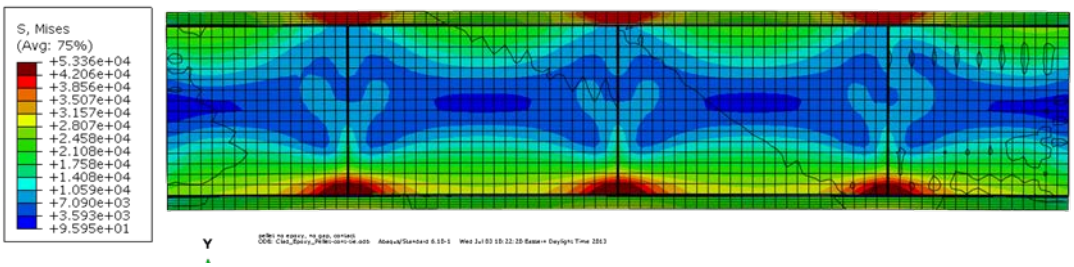

(a) Longitudinal cut view of resultant curvature and von Mises stress

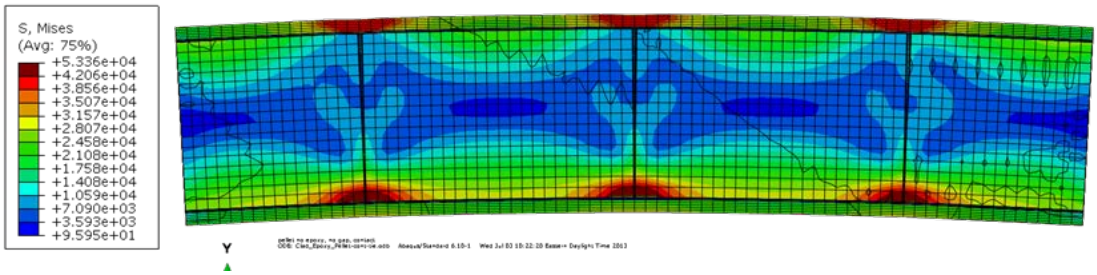

(b) Longitudinal cut view of curvature enlarged by 10 times

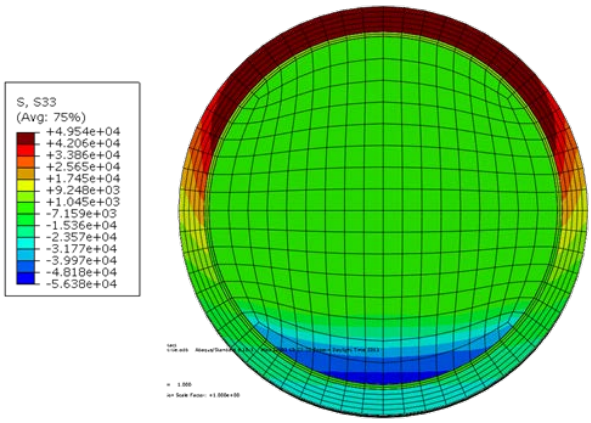

(c) Cross-sectional view of resultant σ_{zz} at a pellet–pellet interface

Fig. 9. Stress distribution and curvature resulting from Clad-Epoxy-Pellet section model with four pellets with no gaps at de-bonded pellet–pellet interfaces.

The pellet stress profiles also show a dog-bone shape due to contact pressure at the pellet–pellet interfaces. The resultant σ_{zz} profile with no gaps at the pellet–pellet interface indicates that these pellets can carry more bending moment resistance than pellets with gaps, as shown in Fig. 8. The induced curvature of this pellet–pellet interface de-bonding with gaps case is 0.241m^{-1}, much smaller than that of previous cases.

Table 3 summarizes the estimated curvature and the flexural rigidity based on the two pellet–pellet interface cases discussed in this section. The comparison between results in Tables 2 and 3 suggests that the immediate consequence of the de-bonded pellet–pellet interface is a significant increase in curvature, and this, in turn, results in a significant reduction in the estimated flexural rigidity. This phenomenon is primarily due to the load carrying capacity shifting from the pellets to the clad.

Table 3. Curvature and flexural rigidity for the bonded pellet–clad and de-bonded pellet–pellet cases

Designation	Curvature, κ (1/m)	Bending moment, M (N·m)	Flexural rigidity, EI (N·m^2)	Note
Clad-Epox-Pellet4-Tie-Pellet-Contact-Gap	0.669	25	37	Gaps between neighboring pellets had no epoxy filling
Clad-Epoxy-Pellet4-Tie-Pellet-Contact-No Gap	0.241	25	104	No gap between neighboring pellets; pellet–pellet interfaces were de-bonded

Table 3 shows that the gaps at pellet–pellet interfaces play a critical role in estimating the flexural rigidity of the surrogate rod. The induced curvature of 0.669 m^{-1} for the case of gaps is four times that of the perfectly bonded interface case. The curvature increase corresponds to a 76% reduction in flexural rigidity, from 153 N·m^2 for the perfectly bonded interface case to 37 N·m^2 for the case of empty gaps. When the gaps are eliminated, the flexural rigidity value can go as high as 104 N·m^2. The above indicates that the gap-induced large plastic deformations of SS clad at the pellet–pellet interface region can lead to significant reduction in the bending stiffness, or, the flexural rigidity (EI) of the surrogate rod system. If there are no gaps at the pellet–pellet interfaces, the pellets can carry a significant portion of bending moment resistance via direct pellet–pellet contact (interaction) to mitigate the potential yield of the clad.

3. Effect of Gaps Between Pellets with De-Bonded Pellet–Clad Interfaces

Under a flexural deformation, high shear stress will arise at pellet–clad interfaces to compensate for the material mismatch, in addition to the flexural shear stress in the SNF system. Thus, under a reversible bending load during normal transportation, both cyclic normal stress and shear stress can further degrade the interfacial bonding at fuel pellet–clad interfaces. In this section, de-bonded pellet–clad interfaces and de-bonded pellet–pellet interfaces cases are investigated

using a Clad-Epoxy-Pellet section model with four pellets. The surrogate rod consisting of SS clad and alumina pellet inserts is used to study the system response to bending moment with de-bonded interfaces. Loading and boundary conditions are the same as those of the previous cases, and the assigned bending moment is 25 N·m.

The first simulation case of interfacial de-bonding is at both pellet–clad and pellet–pellet interfaces. There are empty gaps at the de-bonded pellet–pellet interfaces and a thin epoxy layer at the de-bonded pellet–clad interfaces.

The resultant stress distribution shown in Fig. 10 indicates that the yielded SS clad almost extends throughout the whole gauge section, when the interfacial de-bonding occurs at both pellet–clad and pellet–pellet interfaces. This is in great contrast to the results shown in Fig. 8, where the SS tube only locally yields at pellet–pellet interface regions and the maximum stress resides at pellets on the compression side of pellet–pellet interfaces. The pellets were all below yield at the maximum stress level due to high yield strength. The pellet stress contours also show a dog-bone shape due to pellet–pellet contact interaction. The induced curvature of 0.727 m^{-1} is large enough to be visualized from the longitudinal cut view without increasing the scale. It suggests that due to the interfacial de-bonding both at pellet–clad and pellet–pellet interfaces, the contained pellet inserts and the SS clad can only make contact at the pellet–pellet and pellet–clad interface regions, and the pellets cannot provide direct internal support to the clad. Therefore, the load shifts significantly from pellets to the clad over the entire gauge section; the results also indicate that the SS clad carries the majority of the bending moment. The bending deformation in the de-bonded pellet–clad region will likely result in further pinching action at pellet–clad interfaces, which may also result in an accelerated aging of the clad tubing.

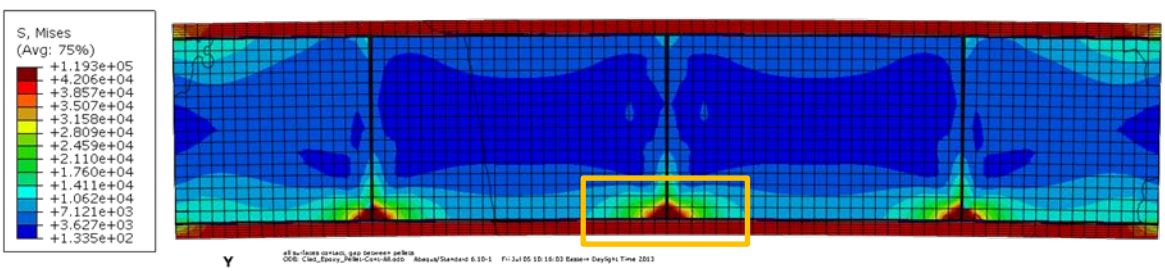

(a) Longitudinal cut view of resultant curvature and von Mises stress

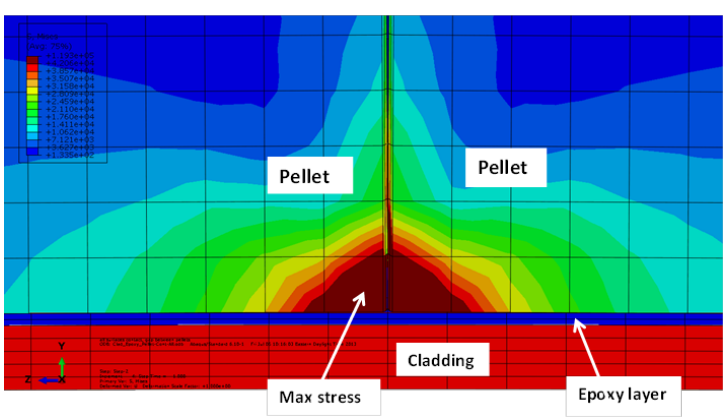

(b) Zoomed-in view of stress distribution at pellet–clad pinning region

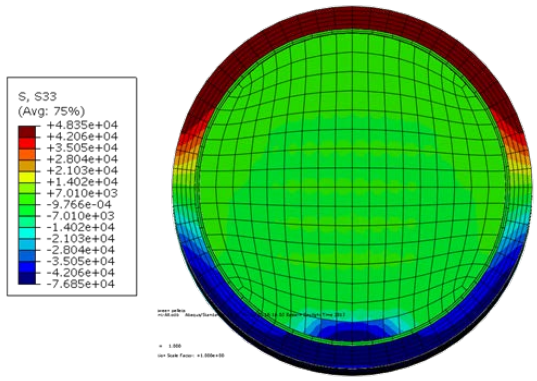

(c) Cross-sectional view of resultant σ_{zz} at a pellet–pellet interface

Fig. 10. Stress distribution and curvature resulting from Clad-Epoxy-Pellet section model with four pellets with gaps at de-bonded pellet–pellet interfaces and an epoxy layer at de-bonded pellet–clad interfaces.

The second case in this section is where a thin epoxy layer is filled at de-bonded pellet–clad interfaces and the pellets are all in direct contact with each other with no gaps at the pellet–pellet interfaces. The loading and boundary conditions as well as material properties are the same as those of the previous cases. Fig. 11 illustrates the surrogate rod responses to the bending moment upon interfacial de-bonding without gaps at the pellet–pellet interfaces. The longitudinal cut view shows that the SS clad yields at the top (tension) region throughout the gauge section but remains elastic at the bottom (compression) region. The maximum stress still occurs on the compression side of the pellet region where the pellets are pinching each other. Fig. 11 shows interfacial results similar to those observed in Fig. 9 for the bonded pellet–clad interfaces and de-bonded pellet–pellet interfaces without gaps. The pellets carry a large portion of the bending moment resistance via pinching pellet corners and reduce the stress intensity of the bottom (compression) portion of the clad. The major difference from the results in Fig. 9 is the extensive plastic deformation observed at the top region of the SS tube throughout the entire gauge section, instead of the localized yielding observed at the interface region in Fig. 9. Due to the lack of a direct load transferring mechanism from pellet to clad or vice versa because of de-bonded pellet–clad interfaces, the clad takes over the majority of the bending moment resistance.

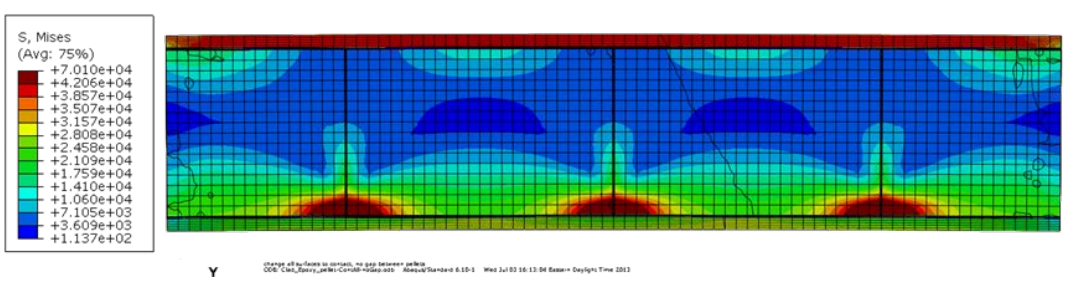

(a) Longitudinal cut view of resultant curvature and von Mises stress

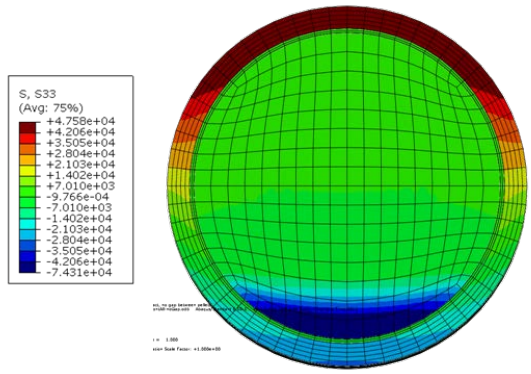

(b) Cross-sectional view of the resultant normal stress, σ_{zz}, at a pellet–pellet interface

Fig. 11. Stress distribution and curvature resulting from Clad-Epoxy-Pellet section model with four pellets with no gaps at de-bonded pellet–pellet interfaces and with an epoxy layer at de-bonded pellet–clad interfaces.

The results of the evaluated curvature and flexural rigidity for the cases of de-bonding at pellet–clad and pellet–pellet interfaces are listed in Table 4. Compared to the results of the de-bonded pellet–pellet interface case listed in Table 3, the flexural rigidities are further decreased by 8% (from 37 N·m^2 to 34 N·m^2) for pellets with gap cases and by 19% (from 104 N·m^2 to 84 N·m^2) for pellets with no gap cases. This result further validates the earlier hypothesis in the case of pellet–clad interfaces, that interfacial bonding efficiency can significantly affect the flexural rigidity of the surrogate composite rod.

Table 4. Curvature and flexural rigidity for de-bonded pellet–clad and pellet–pellet interfaces

Designation	Curvature, κ (1/m)	Bending moment, M (N·m)	Flexural rigidity, EI (N·m^2)	Note
Clad-Epox-Pellet4-Contact-Pellet-Contact-Gap	0.727	25	34	Gaps between neighboring pellets had no epoxy filling
Clad-Epoxy-Pellet4-Contact-Pellet-Contact-No Gap	0.298	25	84	No gap between neighboring pellets; pellet–pellet interfaces were de-bonded

In Table 4, the flexural rigidity of the case with no gaps at pellet–pellet interfaces is 2.5 times that of the case with gaps. In Table 3, the same comparison of flexural rigidity results in a similar ratio of 2.8. The reason for the large increase in flexural rigidity is the direct contact of the pellets at the pellet–pellet interfaces on the compression side. The direct pellet–pellet contact provides a significant increase in bending moment resistance, resulting in much less curvature deformation, as shown in Table 4.

CONCLUSION

Based on the FEA simulation results and further verification from ORNL surrogate rod bending test results, the impacts of interfacial bonding efficiency at pellet–pellet and pellet–clad interfaces on surrogate rod system performance can be summarized as follows.

First, with good interfacial bonding and without fuel pellet and clad fracture, the pellets in the surrogate rod will carry more bending moment resistance than the clad under normal transportation vibration. The maximum stress resides at the pellets, and the stresses at the clad and pellet are both below the yield condition; therefore, the system is in a linear elastic state under the target bending loads.

Upon fuel pellet failure including de-bonding at the pellet–pellet interfaces, the load carrying capacity shifts from fuel pellets to the clad, and the clad starts to carry the majority of the bending moment at the pellet–pellet interface region, which results in localized plastic deformation of the clad. With good cohesion at the pellet–clad interfaces, the pellets can still provide support to the clad and carry a sufficient portion of the bending moment resistance, so that a major portion of the clad at the gauge section remains in the linear elastic range.

Upon further de-bonding at the pellet–clad interfaces, the embedded pellets can no longer provide effective structural support to the clad as well as assist the load transfer within the surrogate rod system. Thus, the majority of the load carrying capacity shifts to the clad throughout the entire gauge section. That leads to the clad yielding in the entire gauge section instead of at localized pellet–pellet interface regions. When the pellets contact and pinch each other, the pellets seem to take over a significant portion of the bending load resistance, especially for cases where there are no gaps at the pellet–pellet interfaces. This pellet pinning action certainly mitigates and avoids the clad yielding, and the maximum stress resides at the pellet region and below the yield.

Table 5. Comparison of flexural rigidity between different bonding and de-bonding cases

	Flexural rigidity, *EI* ($N \cdot m^2$)	**Reduction from perfect bonding (%)**	**Increase from with gaps to without gaps (%)**
Perfectly bonded	153		
De-bonded pellet–pellet interfaces with gaps	37	76	
De-bonded pellet–pellet and pellet–clad interfaces with gaps	34	78	
De-bonded pellet–pellet interfaces without gaps	104	32	64
De-bonded pellet–pellet and pellet–clad interfaces without gaps	84	45	60

The immediate consequence of interfacial de-bonding is the load carrying capacity shift from fuel to clad, as well as the reduction of flexural rigidity, as shown in Table 5. Compared to the flexural rigidity of 153 $N \cdot m^2$ for a perfect bond, the flexural rigidity for the de-bonding at pellet–pellet interfaces alone is reduced by 76% (to 37 $N \cdot m^2$) in the case with gaps at the pellet–pellet

interfaces and by 32% (to 104 $N \cdot m^2$) for the case with no gaps. Upon further de-bonding at the pellet–clad interfaces, the flexural rigidity is further reduced by 8% and 19% for the cases with gaps and without gaps, respectively. The overall reductions from the perfectly bonded case to the de-bonded case at all interfaces are about 78% and 45%, respectively, for the cases with gaps and without gaps.

More reductions in flexural rigidity are due to de-bonding at pellet–pellet interfaces than due to de-bonding at pellet–clad interfaces. Table 5 shows about a 60% increase in the flexural rigidity from the case with gaps to the case without gaps, which indicates a significant increase in system stiffness for the surrogate rod without gaps. Therefore, gaps at the interfaces of the surrogate rod system can have a significant impact on system reliability, especially at pellet–pellet interfaces.

The flexural rigidity and bending moment resistance capacity of the surrogate rod system (which is designed to resemble the SNF system) are strongly dependent on the efficiency of interfacial bonding at pellet–clad and pellet–pellet interfaces. This discovery was also validated by reversible bending fatigue test results performed on the surrogate SS rod with alumina pellets inserts.

REFERENCES

1. US Department of Energy, Used Fuel Disposition Campaign, *Used Nuclear Fuel Loading and Structural Performance under Normal Conditions of Transport – Modeling, Simulation and Experimental Integration RD&D Plan*, FCRD-UFD-2013-000135, April 1, 2013.

2. J.-A.J. Wang, H. Wang, Y. Yan, R. Howard, B. Bevard, *High Burn-up Spent Fuel Vibration Integrity Study Progress Letter Report (Out-of-Cell Fatigue Testing Development – Task 2.1)*, ORNL/TM-2010/288, Oak Ridge National Laboratory, Oak Ridge, TN, 2011.

3. J.-A.J. Wang, H. Wang, T. Tan, H. Jiang, T. Cox, Y. Yan, *Progress Letter Report on U-frame Test Setup and Bending Fatigue Test for Vibration Integrity Study (Out-of-Cell Fatigue Testing Development – Task 2.2)*, ORNL/TM-2011/531, Oak Ridge National Laboratory, Oak Ridge, TN, 2012

4. H. Wang, J.-A.J. Wang, T. Tan, H. Jiang, T. Cox, R. Howard, B. Bevard, M. Flanagan, “Development of U-Frame Bending System for Studying the Vibration Integrity of Spent Nuclear Fuel,” *Journal of Nuclear Material* **440**, 201–213, 2013.

ACKNOWLEDGEMENTS

This research was sponsored by DOE UFDC and was conducted at Oak Ridge National Laboratory under contract DE-AC05-00OR22725 with UT-Battelle, LLC. The authors would like to thank Program Managers Harold Adkins, Bruce Bevard, and Rob Howard for providing guidance and support to this project.

Proceedings of the ASME 2014 Pressure Vessels & Piping Conference
PVP2014
July 20-24, 2014, Anaheim, California, USA

PVP2014-29117

REVERSIBLE BENDING FATIGUE TESTING SYSTEM DESIGN CONCEPTS FOR SPENT FUEL VIBRATION INTEGRITY STUDY

Hao Jiang, Jy-An John Wang*, Hong Wang

Materials Science and Technology Division
Oak Ridge National Laboratory
One Bethel Valley Road, Oak Ridge, Tennessee 37831
*Correspondence author: Tel: 1-865-574-2274; email: wangja@ornl.gov

ABSTRACT

The dynamic analyses of a reversible bending fatigue testing system designed for the spent nuclear fuel (SNF) vibration integrity study was presented in this paper. Different design concepts were evaluated to assist the U-bent tester development. A finite element analysis (FEA) based on the vertical test setup was established to simulate the U-bent test system dynamic performances. The FEA results provided general guideline on predicting the dynamic behaviors of U-frame bending fatigue system for testing SNF. The initial vertical test setup design concepts were investigated in detail and the associated deficiencies were also discussed in the paper. The horizontal test setup was also evaluated using FEA. Based on dynamic analysis results, the horizontal test setup with symmetric loading profile was recommended for developing a reversible U-frame bending fatigue testing system.

INTRODUCTION

The vibration in a SNF transportation environment is created by the interaction between the vehicle and ground, and then transmitted into the shipping package. The displacement imposed on the grips of fuel rods will be ultimately transformed as mechanical loading on the fuel rods due to the inertial effect, which is characterized as reversible cyclic bending. Because of the sustaining loading, the spent fuel rods in the transportation are experiencing with the potential fatigue aging, especially for the high burnup SNF that features the increased surface cracks, oxidation layers and subsurface hydrides, etc. Transportation packages for spent fuel must meet safety requirements under normal and accident conditions, as specified by federal regulations. It is required that the licensee assure that there will be no loss or dispersal of spent fuel, no significant increase in external surface radiation levels, and no substantial reduction in the effectiveness of the spent fuel package. As a result, the likelihood of the SNF remaining undamaged after storage and subsequent transportation needs to be evaluated.

However, no such testing system is available currently. This is mainly because of technical challenges associated with testing the SNF in a hot cell environment. The test method should be adaptable to a hot cell environment in which radiation dominates the test plan and all the handling is carried out by manipulator whose operation is limited. In addition, it is required that pure and reversible bending be implemented simultaneously in order to simulate the vibration loads that the spent fuel is subjected to in transportation.

Bending fatigue testing system has been developed for decades. There are vast literatures focusing on three-point bending and four-point bending [1], [2], reversal bending[3], as well as pure bending [4]. However, these methods are incapable of meeting the challenges discussed above and cannot be used in testing SNF rods and characterizing the vibration integrity. Recently, Wang et al. [5] has developed a U-frame-assisted bending fatigue system dedicated to the vibration integrity of spent fuel rod in the hot-cell. The system mainly consists of two rigid loading arms and an axially-loaded third member. The latter may act as a flexure, depending on the joint design of the corners. Two testing setup plans have been proposed; namely, horizontal setup and vertical setup.

The finite element analysis (FEA) was used in studying the responses of the U-frame setup. It has been found out that the location of the rod specimen in the plane of U-frame setup is critical. The conversion efficiency of loading at the rigid

Notice: This submission was sponsored by a contractor of the United States Government under contract DE-AC05-00OR22725 with the United States Department of Energy. The United States Government retains, and the publisher, by accepting this submission for publication, acknowledges that the United States Government retains, a nonexclusive, paid-up, irrevocable, worldwide license to publish or reproduce the published form of this submission, or allow others to do so, for United States Government purposes.

 Copyright © 20xx by ASME

arms into the stress in the gage section of rod specimen can be increased substantially if a co-planar design is used. Further design optimization of the test system requires a thorough dynamic analysis, especially considering that the system is targeting a transportation environment in which the dynamic road-vehicle interaction is involved. A detail finite element model of testing system has been developed to investigate the dynamic responses. Based on the required system performance, design options were evaluated and recommendations formed for the design optimization. FEA simulation saved time and effort significantly in development process, and reduced costs of fabrication tremendously due to unnecessary design iterations by testing along. The FEA results serve as general guideline in predicating dynamic behaviors of U-frame bending fatigue system for hot-cell spent fuel testing.

VERTICAL U-FRAME DESIGN CONCEPT EVALUATION

Initial vertical design concept

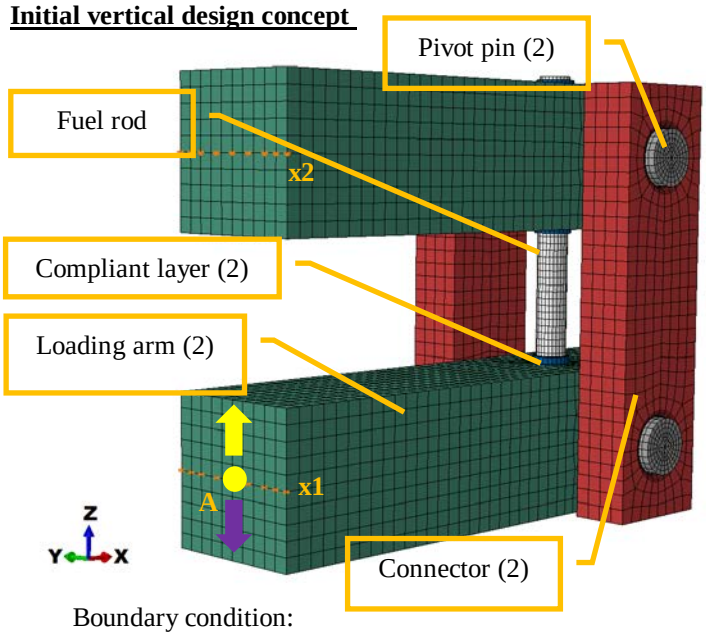

Boundary condition:
(1) x2: UX=UY=UZ=URX=URZ=0
(2) x1: UX=UY=URX=URZ=0

Figure 1. Boundary and loading conditions of vertical U-frame bending fatigue testing system

A larger variety of commercial universal testing machines are set up vertically, such as MTS 810 servo-hydraulic tester [5], and the use of the machines has accumulated extensive experience. Therefore the first generation design is focused on the integration of the proposed vertical design concept into these testing machines.

A FEA model has been developed in ABAQUS based on vertical design concept in Figure 1. The U-frame testing system was comprised of two rigid arms, which were connected by two connectors through two pivot pins. The rigid arms featured a cross section 2 × 2 and length 203.2 mm (8 in.). The connectors had a width of 40.6 mm (1.6 in.), thickness of 20.3mm (0.8 in.) and length of 152.4 mm (6 in.). The pivot pins had a diameter of 20.3 mm (0.8in.) and length of 106.7 mm (4.2 in.). The holes for the fuel rod were oriented vertically and located 152.4 mm (6 in.) away from the loading ends. A 152.4 mm (6 in.) section of fuel rod was used in this study with cladding ID 9.449 mm (0.372 in.) and OD 11.074 mm (0.436 in.). To simplify the analysis, the inside fuel pellets were modeled by using a single equivalent pellet whose diameter and length were same as the ID and length of the cladding. The compliant layers were used between the fuel rod and the wall of specimen holes in order to control and eliminate the contact damage. Two polycarbonate covers with ID 11.074 mm (0.436 in.), OD 13.614mm (0.536 in.) and length 55.9 mm (2.2 in.) were used as these layers.

The boundary and loading conditions of the U-frame system are also illustrated in Figure 1 . The local horizontal axis of the end surface of the upper loading arm was constrained in all DOFs except the rotational DOF around the Y-axis. The implemented boundary conditions simulate the constrained pivot link between the upper rigid arm and the universal test machine, for example, MTS 810 servo-hydraulic tester. The local horizontal axis of the end surface of the lower rigid arm was constrained similarly but with additional DOF relaxed in the Z-axis to allow the external loading. A sinusoidal force was applied at the center point of the lower rigid arm to simulate the single side driving. The loading arm length is 152.4 mm (6 in.). The sinusoidal force was expressed as follows, $F = A\sin(2\pi ft + \phi)$,where F is the load applied to lower loading arm and measured in N, A is amplitude that takes 177.9, 266.9, 355.9 N, respectively, f is frequency defined in 0.1~100 Hz, and ϕ is phase angle.

The fuel rod was an assembly of pellet made of material UO_2 and cladding of Zry-4. As mentioned above, Polycarbonate was selected for the compliant layers as a cover for the fuel cladding in two specimen holding areas. Rest of the system including the rigid arms, the connectors and the pivot pins were made of stainless steel. All materials were assumed to have a perfect-plastic behavior. The material properties of components of the U-frame system used in FEA simulation were summarized in Table 1.

Figure 2 shows the von Mises stress distribution in fuel rod as dynamic responses for the vertical design concept. Two stress concentration areas emerged with the maximum stress occurring in the lower area. Obviously, the fuel rod experienced asymmetric bending. Two issues might be involved with the distorted deformation. First, the weights of components, especially those of the rigid arms, have been shown to have a significant impact on the performance of vertical U-frame setup. Due to the gravity, the fuel rod actually underwent a combinational loading contributed by

Copyright © 20xx by ASME

external moment and self-weight-induced moment from components, which would produce an asymmetric bending motion. Second, the single side loading in the vertical setup might cause asymmetry dynamic loading to the system.

Table 1. Mechanical properties of component materials of U-frame setup.

Name	Young's Modulus (GPa)	Poisson's Ratio	Yield Strength (MPa)	Density (kg/m^3)
Stainless Steel[a]	193	0.300	290	8030
Polycarbonate[b]	7	0.350	69	12105
UO_2[c]	201	0.318	2146	10,970
Zry-4[d]	91	0.326	906	6560

[a] Ref. [6], [b] Ref. [7], [c] Ref. [8], [d] Ref. [9].

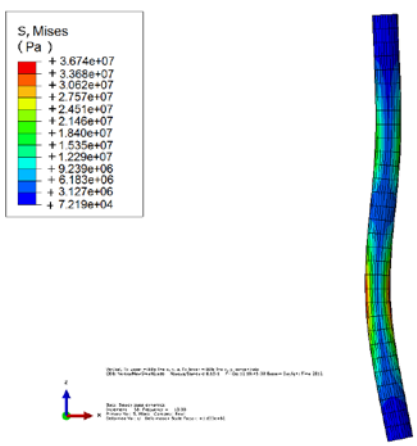

Figure 2. Von Mises stress distribution in fuel rod for the vertical design concept at 10Hz under 177.9 N loading with the arms at the extreme opening position.

Vertical design concept with counterweights

The counterweights were considered to balance the effect of self-weights. As shown in Figure 3, each counterweight consists of two parts. Part 1 was an extended portion of the loading arm whose bottom was modified into a 30° slope to avoid interference of the loading arms in the extreme closing position. Part 2 was a block added to the end face of Part 1. The counterweights used the same material as in the rigid arm (Table 1). The size of the part 2 depends on the requirement of moment equilibrium with respect to the pivot located on end surface of the loading arm (Figure 1). The above calculation resulted in part 2 with dimensions 174.5×50.8× 58.4 mm (6.87 × 2 × 2.3in.).

The FEA model in Figure 1 was modified with the counterweight added to each rigid arm. The dynamic response

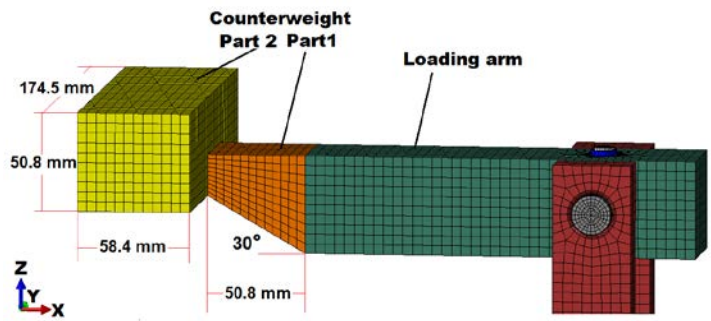

Figure 2. Counterweight to balance the effect of self-weight for the vertical design

of the U-frame is improved significantly, but asymmetric vibration motion persists. Figure 4 shows the Mises stress distribution in fuel rod for the vertical design with counterweights under 177.9 N loading at 10Hz and 0.1Hz respectively. The stress distribution in Figure 4(a) at 10Hz is much closer to the pure bending than that in for the system without counterweights. However, the location of maximum stress is still off the middle of the fuel rod. These results indicate that, even the counterweights canceled the self-weight-induced moment; the asymmetric dynamic responses still exist. While, the von Mises stress distribution in Figure 4(b) reveals that the maximum stress located at the middle section of the fuel rod as a result of symmetric pure bending at 0.1Hz.

The resultant phase angles of dynamic response at a middle point of the fuel rod were investigated. The phase angles of displacement with respect to 10Hz and 0.1Hz excitations of vertical design with counterweights were compared in Table 2. The 10Hz response demonstrates more phase delay, especially in horizontal X and vertical Z directions. This is because of more significant inertia effect on the system response at higher frequency. When the larger delay occurs at higher frequency, the single side loading will cause asymmetry dynamic loading to the system. Dynamic responses at 10Hz in Figure 4(a) confirm the speculation. On contrary, the 0.1Hz response shows merely a slightly phase shift to the loading. While dynamic responses at 0.1Hz in Figure 4 indicate that counterweights are able to balance off self-weight-induced moments and help the vertical setup to achieve symmetric pure bend state.

Experiment validation of vertical test setup with counterweights

A prototype of the U-frame was made based on the developed firstly for the vertical design due to the availability of driving system. The counterweights need to be included into the setup. In the engineering process, all of the design aspects studied by FEA have been implemented but with some modifications, including the use of ball bearings instead of pins in the pivots between the side connecting plates and the

Copyright © 20xx by ASME

rigid arms [5]. The third generation (3G) U-frame setup that is integrated into a MTS 810 servo-hydraulic tester is shown in Figure 5(a).

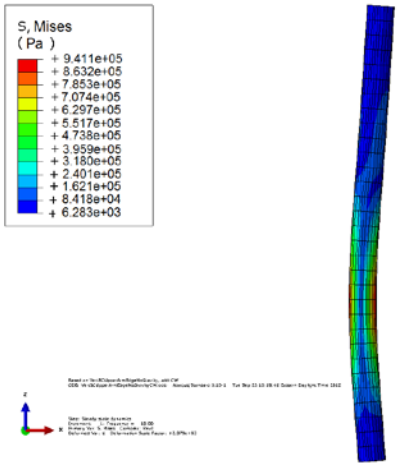

(a) 10Hz

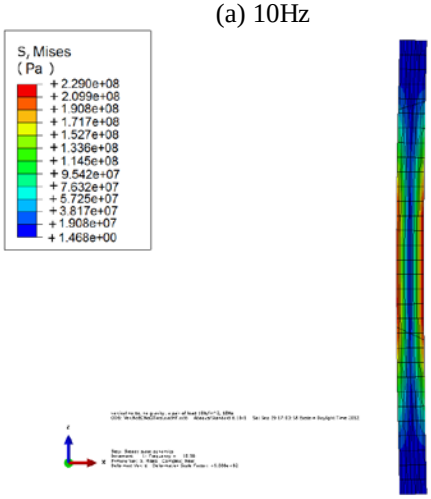

(b) 0.1Hz

Figure 3.Von Mises stress distribution in the fuel rod for the vertical design concept with counterweights under 177.9 N loading.

Table 1. Phase angle comparison between 10 Hz and 0.1 Hz response at a middle point of the fuel rod

PHASE ANGLE (DEGREES)	ϕX	ϕY	ϕZ
FORCE INPUT AT END SURFACE OF LOWER LOADING ARM	**0**	**0**	**0**
10HZ RESPONSE AT MIDDLE POINT OF FUEL ROD	**-179**	**-10**	**-179.9**
0.1HZ RESPONSE AT MIDDLE POINT OF FUEL ROD	**-0.651**	**-1.2**	**-0.842**

* X,Y,Z corresponding to Figure 4

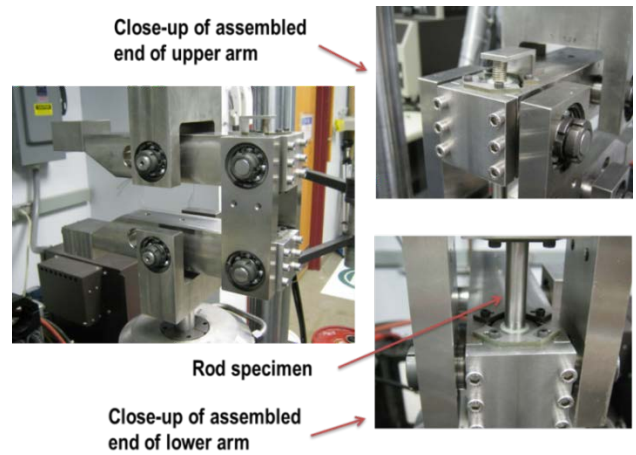

(a)

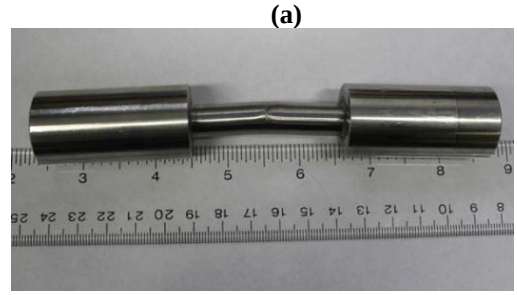

(b)

Figure 4. (a) 3G U-frame setup integrated on a MTS 810 servo-hydraulic tester; the U-frame is driven at the lower end. (b) A tested composite rod (stainless tube + alumina rod) showing a symmetrical failure mode.

The composite rod is made of Stainless Steel (SS) and high density alumina to simulate the fuel cladding and rod bases on their similar mechanical properties. A symmetrical fracture was observed with counterweights added at frequency 0.1Hz as shown in Figure 5(b). This test observation verified the FEA result at 0.1Hz in section 2.2.

FINAL DESIGN--HORIZONTAL U-FRAM DESIGN CONCEPT EVALUATION

Dynamic responses

To mitigate the deficiency inherent in vertical design and to improve the system performance, the horizontal design concept was evaluated and a horizontal test setup was developed. Figure 6 shows a horizontal concept with co-planar configuration of the rod, in which U-frame structure is set on a horizontal plane. All the geometries of the U-frame components in the horizontal design remained the same as in the vertical design, including the 152.4 mm (6 in.) loading arm (Figure 1). The materials used in the model and meshing as well as the contact conditions were also unchanged (Table 1). However, the boundary and loading conditions were different from the vertical design as shown in Figure 6. The local vertical axis of frontal surfaces of the two loading arms was only allowed translational movement in horizontal

Copyright © 20xx by ASME

direction Z and rotation vertically around the Y axis to simulate the pivot pins used in the linkage to universal testing machine. The external forces were applied in horizontal direction to the two middle points of frontal surfaces of the two rigid arms in Figure 6. The two forces were designed to be out of phase. As a result, the symmetric loadings applied to the rigid arms were finally transferred into a horizontal in-plane reverse bending motion in the rod.

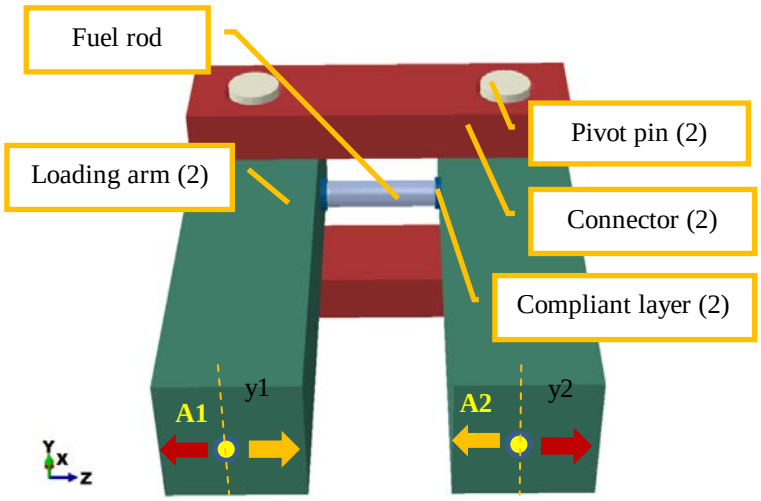

Boundary conditions:
Local vertical axes y1 and y2: UX=UY=URX=URZ=0

Figure 5. Geometry of horizontal U-frame bending fatigue testing system with co-planar configuration of the rod

Dynamic responses of U-frame system for the frequency range from 10 to 100 Hz under three amplitudes 177.9, 266.9, and 355.9 N are summarized in Figure 7 in terms of displacement of U-frame and maximum stress at middle of fuel rod. Figure 7(a) shows that the displacements increase when load increases as expected, but decrease significantly when frequency increases. The displacement amplitude of U-frame is ranging from 0.002 to 0.457 mm (8.3×10-5 to 0.018 in.), corresponding to 177.9 N at 100Hz and 355.9 N at 10 Hz, respectively. Figure 7(b) shows that the maximum stress decreases correspond well with the concurrent decrease in the displacement response.

The stress distribution of U-frame bending fatigue testing system at frequency 10 Hz of 355.9 N loading is illustrated in Figure 8. Maximum Mises stress 30.9MPa occurs at fuel rod (pellet and cladding assembly). It is further revealed that maximum stress 30.9MPa actually locates at the middle surface of pellet. From the Mises stress distribution at fuel rod, it can be seen that the Mises stresses are distributed symmetrically across the rod neutral axis [Figure 8], representing a pure bending behavior of the rod as validated in the static analysis [5]. Resultant maximum stresses 16.5MPa at cladding, 2.9MPa at polycarbonate covers, and a 30.9MPa at pellet, are all under yield strengths listed in Table 1.

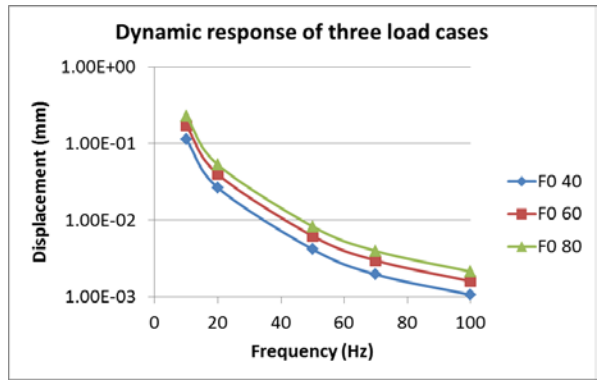

(a)

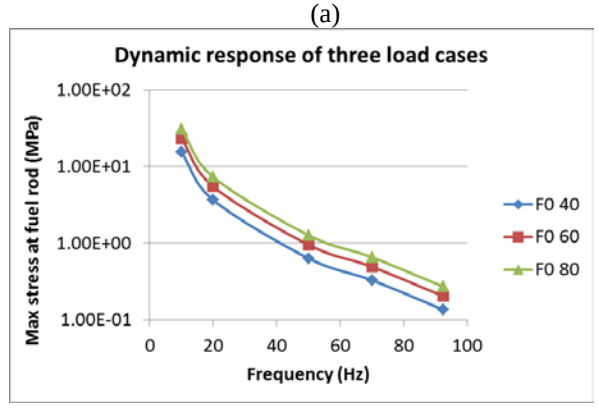

(b)

Figure 6. Dynamic responses of U-frame system under three loadings: (a) displacement of loading arm; (b) maximum stress at middle of fuel rod

<u>Advantage of horizontal design concept compared to vertical design concept</u>

When the dynamic responses of horizontal design are compared to those of vertical design under the same loading condition, the major differences can be revealed. Displacements and maximum stresses of the vertical design with counterweights are one order magnitude smaller than those of horizontal design without counterweights for various loading arm lengths and loading conditions. For example, the maximum stress decreased from 15.0MPa for horizontal design with 152.4 mm loading arm to 0.79MPa for vertical design with counterweights under the same load input, ±177.9 N at 10 Hz, in Fig. 9. Under the same condition, the displacement amplitude decreased from 0.110mm (4.32×10^{-3} in.) for horizontal design to 0.005 mm (2.06×10^{-4} in.) for vertical design with counterweights. These results indicate that counterweights have a negative impact on system dynamic responses due to extra mass added to the system.

Dynamic analyses of U-frame system with loading arm lengths 152.4 mm (6 in.) and 101.6 mm (4 in.) were both performed by FEA. Dynamic responses of system with different arm lengths are also compared in Figure 10. With the 177.9 N amplitude, the displacement of loading arms increases

Copyright © 20xx by ASME

around 30% overall due to the reduction of the arm from 152.4 mm to 101.6 mm. Therefore, the system with shorter loading arms is more efficient in transferring external loading to bending at the fuel rod.

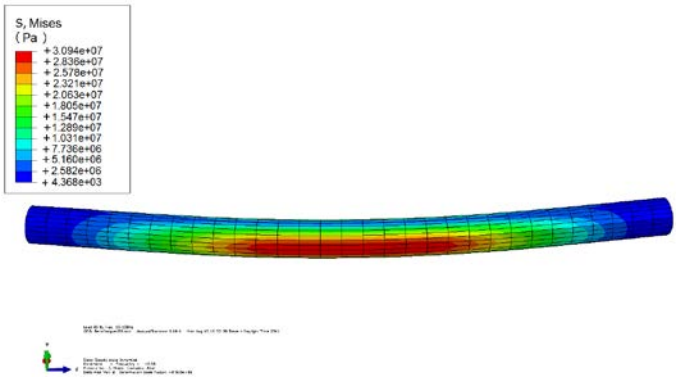

Figure 7. Von Mises stress distribution of fuel clad in U-frame system when the arms are in the extreme pulling position; the force input was 355.9N amplitude, 10 Hz

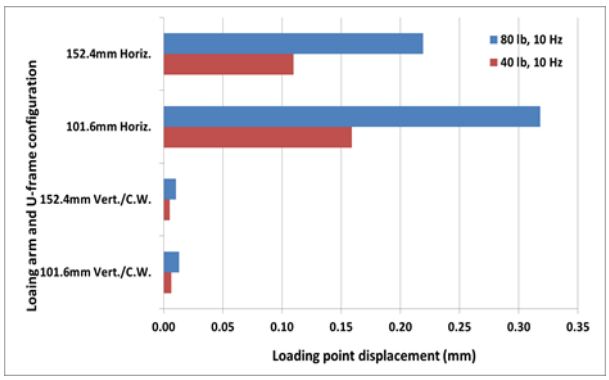

(a)

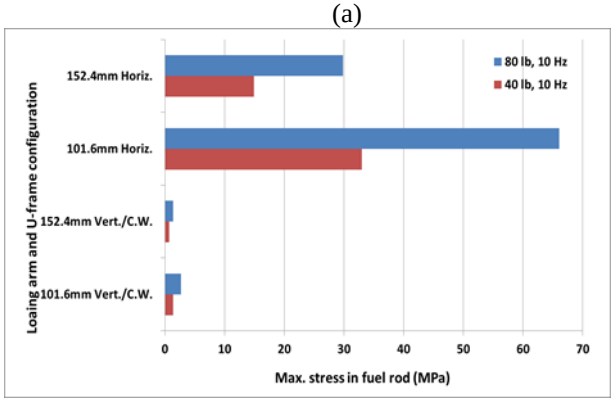

(b)

Figure 9. Dynamic response comparison in terms of (a) displacement and (b) stress between horizontal design and vertical design with counterweights under the symmetric loading at 10Hz.

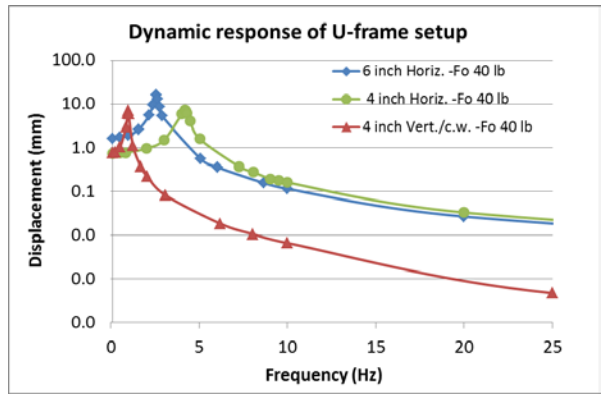

Figure 80. Dynamic responses of horizontal design and vertical design with counterweights

Dynamic responses over frequency range from 0.1Hz to 100Hz of the vertical design with 101.6 mm loading arm and counterweights are compared to the horizontal design concept with 152.4 mm and 101.6 mm loading arms in Figure 10. Overall, the resonant frequency of vertical design with counterweights is relatively lower (0.98 Hz) than those of horizontal design and the attainable loading arm displacement of the vertical design with counterweights above the resonant frequency is also significantly lower than those of the horizontal design. On the other hand, shortening of the loading arm from 152.4 to 101.6 mm drove the resonant frequency up from 2.56 Hz to 4.19 Hz in horizontal design. These results further reveal that the horizontal design has a much better dynamic performance than the vertical design with counterweights.

Experimental validation of horizontal test setup with symmetric loading

The prototype of horizontal U-frame setup has been constructed recently and integrated into Bose dual LM2 TB as demonstrated in Figure 11. The main components are similar to those of horizontal setup on the MTS 810 tester but with modification. Particularly, the inside roller bearing houses are designed to be detachable to facilitate the repair or replacement of roller bearing sets should the damage occur in hot-cell testing [5]. The dual motors are used in driving the U-frame at the two loading points so that the symmetrical loading is obtained. The symmetrical loading and the high frequency capability offered by the Bose system enable the pure bending cyclic test in a relative wide frequency range. Moreover, the electromagnetic force –based linear motor technique appears to be favorable to the hot cell environment because no oil is involved as in a servo-hydraulic system.

The surrogate rod SSAP14 that were composed of SS cladding tube and 10 alumina pellets was used in the test. The cycle test was performed under load control: ±250N, 5Hz.

Copyright © 20xx by ASME

SSAP14 surrogate rod fractured near 1.48×10^4 cycles .The fracture as shown in Figure 12 indicates that the failure was again the pure bending as targeted. Distributed fractures over the gage section validate FEA simulation result of the horizontal design concept, that is, the maximum stress always locates at the middle of fuel rod.

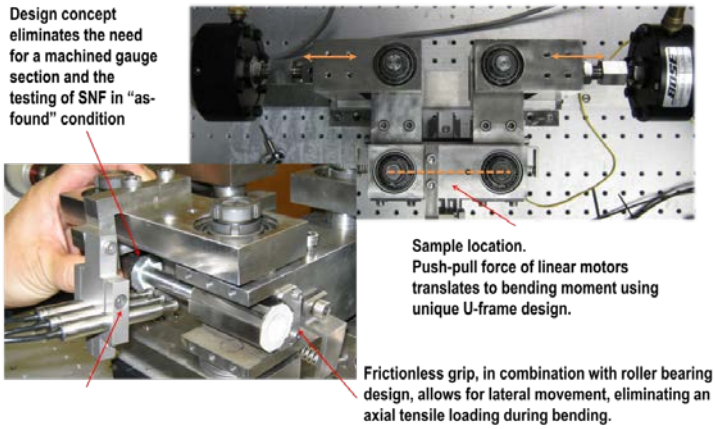

Figure 91. Horizontal U-frame test setup integrated to Bose dual LM2 TB; U-frame is driven at two ends.

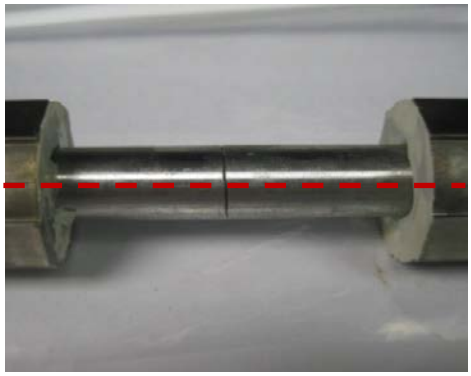

Figure 12. Fractured surrogate rod SSAP14made of SS cladding and alumina pellets.

CONCLUSION AND RECOMMENDATION

The purpose of this investigation was to analyze the dynamic performance of the U-frame design concepts for bending fatigue testing system development. FEA simulation has significantly reduced the design iterations and system development cost. The conclusion and recommendation from this study are made.

The FEA results provided insight of dynamic behaviors of U-frame bending fatigue system for testing SNF rod. For vertical U-frame set-up, the asymmetric bending mode, induced by the U-frame self-weight and the system asymmetric loading condition, need to be corrected with appropriate counter-weight system. However, the counter-weight approach also has negative impact on system dynamic responses. U-frame system resonance occurred at low frequencies. The decrease in the loading arm length drove the resonant frequency up in horizontal design, thus, provides better dynamic performance for the horizontal U-frame system; but resonant frequency goes down significantly when the counterweights are included in vertical design concept. Pure bending stress state of the fuel rod has been achieved by using horizontal design concept Test data from the vertical test setup with counterweights at low frequency and from the horizontal test setup with symmetric loading validate pure bending as predicted in FEA and U-frame system can be performed effectively at the higher frequency operation. The horizontal test setup with symmetric loading is recommended for U-frame bending fatigue testing system design.

ACKNOWLEDGMENTS

The research was sponsored by NRC RES under DOE contract DE-AC05-00OR22725 with UT-Battelle, LLC. The authors gratefully acknowledge Program Manager Michelle Flanagan of the Office of Nuclear Regulatory Research, U.S. Nuclear Regulatory Commission, for providing the support; Authors also want to thank Dr. Tianlei Li for reviewing this manuscript.

REFERENCES

[1] W. D. Bowman, 1989. End constraint and alignment effects in three and four point tension-compression bending tests, in Factors That Affect the Precision of Mechanical Tests, ASTM STP 1025, Eds. R. Papirno and H. C. Weiss, ASTM, Philadelphia, pp. 174-184.

[2] J. X. Li, T. Zhai, M. D. Garratt, and G. H. Bray, 2005. Four-point-bend fatigue of AA 2026 aluminum alloys, Metal Mater. Trans. A - Phys. Metal Mater. Sci., 36A, 2529-2539.

[3] P. Yavari, T. G. Langdon, 1983. Simple reverse bending machine for low cycle fatigue at elevate temperatures. Rev Sci Instrum 54(3):353-356.

[4] T. B. Zineb, A. Sedrakian, and J. L. Billoet, 2003. An original pure bending device with large displacements and rotations for static and fatigue tests of composite structures, Composites Part B: Engineering, 34, 447-458.

[5] J.-A. J. Wang, H. Wang, T. Tan, H. Jiang, T. Cox, Y. Yan, 2012. Progress letter report on U-frame test setup and bending fatigue test for vibration integrity study (out-of-cell fatigue testing development – Task 2.3), ORNL/TM- 2012/417, August.

[6]http://www.eaglesteel.com/download/techdocs/304_Stainless_Steel.pdf

[7]http://www.eplastics.com/Plastic/Lexan_Polycarbonate_Sheet

[8] Bhabha Atomic Research Centre (BARC) Highlights, Nuclear Fuel Cycle, Chapter 4, pp. 35-39 (2007). http://www.barc.ernet.in/publications/eb/golden/nfc/toc/Chapter%204/4.6.pdf

[9] K. J. Geelhood, C. E. Beyer, and W. G. Luscher, 2008. PNNL Stress/Strain Correlation for Zircaloy, PNNL-17700, July.

Copyright © 20xx by ASME